NACA

RESEARCH MEMORANDUM

A STUDY OF THE USE OF CONTROLS AND THE RESULTING AIRPLANE RESPONSE DURING SERVICE TRAINING OPERATIONS OF FOUR JET FIGHTER AIRPLANES

By John P. Mayer, Harold A. Hamer, and Carl R. Huss

Langley Aeronautical Laboratory
Langley Field, Va.

NATIONAL ADVISORY COMMITTEE
FOR AERONAUTICS

WASHINGTON

June 22, 1954

CONTENTS

[redacted]

NATIONAL ADVISORY COMMITTEE FOR AERONAUTICS

RESEARCH MEMORANDUM

A STUDY OF THE USE OF CONTROLS AND THE RESULTING AIRPLANE RESPONSE DURING SERVICE TRAINING OPERATIONS OF FOUR JET FIGHTER AIRPLANES

By John P. Mayer, Harold A. Hamer, and Carl R. Huss

SUMMARY

Results from a limited flight program to obtain information on the airplane response and actual rates and amounts of control motion used by service pilots in performance of squadron operational training missions with four jet fighter airplanes are presented. The results are presented in the form of envelopes of maximum measured values and in terms of frequencies and probabilities of occurrence, and flight times before a given value is exceeded.

Whenever feasible the results have been compared with present design requirements, methods of computation, and other test results. Comparisons indicate that the maximum tail loads encountered in these tests were less than those specified by the present requirements. When compared on a probability basis, the results are roughly the same for each of the test airplanes and are also about the same as those of other operational training tests. When compared on a time-to-exceed basis, it is shown that the data of these tests and of the other tests represent the same manner of utilization and that the data of the present tests are representative of many more hours of flight time than were actually recorded.

INTRODUCTION

In the present methods for determining airplane design loads, the maximum loads are calculated by specifying what are believed to be the critical motions of the controls or by specifying the critical airplane response. For the most part these critical motions are based on the maximum amounts and rates of control physically possible. In operational flight, however, the actual maximum control motions and airplane response may differ appreciably from the specified variations.

[redacted]

In order to obtain some information on the airplane response and the actual amounts and rates of control used by service pilots in the performance of operational training missions, the NACA with the cooperation of the U. S. Air Force and the Bureau of Aeronautics, Navy Department, has been conducting a flight program with several jet-propelled fighter airplanes. Information of this type is needed in order to determine more realistic design-load criteria and to provide information for use in designing airplane control-boost systems. In addition, this information is needed to determine the important quantities and ranges of measurement to be used in the design of instruments for statistical loads measurements.

This paper is a summary of the information obtained with all the test airplanes of references 1 to 6 in addition to other data analyzed since the issuance of those papers. The data are presented, for the most part, as envelopes of maximum values of the measured quantities and, where feasible, the data are compared with present design requirements or methods. A limited statistical analysis is also presented for some of the measured quantities. The paper is organized in a manner such that data pertaining to specific quantities, which are listed in the "Contents," may be used without reference to the entire paper.

SYMBOLS

b	wing span, ft
c	wing mean aerodynamic chord, ft
C_{L_α}	wing lift-curve slope, per radian
$C_{L_{\alpha_t}}$	horizontal-tail lift-curve slope, per radian
$\left(dC_m/dC_L\right)_A$	rate of change of pitching-moment coefficient with lift coefficient for complete airplane
C_{m_o}	zero-lift wing-fuselage pitching-moment coefficient
$C_{m_{WF}}$	wing-fuselage pitching-moment coefficient
$C_{N_{WF}}$	wing-fuselage normal-force coefficient
d	distance from airplane center of gravity to aerodynamic center of wing-fuselage combination, ft

[redacted]

g	acceleration due to gravity, 32.2 ft/sec^2
H_p	pressure altitude, ft
I_Y	moment of inertia about lateral axis, slug-ft^2
K	empirical constant denoting ratio of damping moment of complete airplane to damping moment produced by tail
K_1, K_2, K_3	dimensional constants appearing in longitudinal equation of motion
k_Y	pitching radius of gyration, $\sqrt{\frac{I_Y}{m}}$, ft
L_T	horizontal-tail load, lb
M	Mach number
m	airplane mass, W/g, slugs
n_L	longitudinal load factor
n_T	transverse or lateral load factor
n_V	normal load factor
n_{V_a}	maximum allowable positive normal load factor as defined by service V-n diagram
n_{V_L}	limit design positive normal load factor
n_{V_m}	maximum positive normal load factor as defined by design V-n diagram
n_{V_S}	service limit positive normal load factor
n_{V_U}	actual ultimate normal load factor
q	dynamic pressure, $\frac{1}{2}\rho V^2$, lb/sq ft
q_c	impact pressure, lb/sq ft

q_t	dynamic pressure in vicinity of tail, lb/sq ft
S	total wing area, sq ft
S_t	total horizontal-tail area, sq ft
T_{90}	time to roll 90°, sec
V	true airspeed, ft/sec
V_i	indicated airspeed, knots
$V_{i_{max}}$	maximum allowable indicated airspeed as defined by V-n diagram, knots
W	airplane gross weight, lb
x_t	distance from airplane center of gravity to aerodynamic center of horizontal tail, ft
α	airplane angle of attack, deg
$\dot{\alpha}$	time rate of change of angle of attack, radians/sec
$\ddot{\alpha}$	second derivative of α with respect to time, radians/sec^2
$d\alpha_t/d\delta_E$	rate of change of horizontal-tail angle of attack with elevator deflection
β	airplane angle of sideslip, deg
Δ	increment
δ_A	aileron deflection (one aileron), deg
δ_{A_a}	maximum available aileron deflection (one aileron), deg
$\dot{\delta}_A$	aileron deflection rate (one aileron), radians/sec
δ_E	elevator deflection, deg
δ_{E_a}	maximum available elevator deflection, deg
$\dot{\delta}_E$	elevator deflection rate, radians/sec
$\dot{\delta}_{E_{max}}$	maximum calculated elevator deflection rate, radians/sec

[redacted]

δ_R	rudder deflection, deg
δ_{R_a}	maximum available rudder deflection, deg
$\dot{\delta}_R$	rudder deflection rate, radians/sec
η_t	horizontal-tail efficiency factor, q_t/q
$\dot{\theta}$	pitching angular velocity, radians/sec
$\dot{\theta}_{max}$	maximum calculated pitching angular velocity, radians/sec
$\ddot{\theta}$	pitching angular acceleration, radians/sec^2
$\ddot{\theta}_{max}$	maximum calculated pitching angular acceleration, radians/sec^2
λ	time to reach positive peak normal load factor, sec
ρ	mass density of air, slugs/cu ft
$\dot{\phi}$	rolling angular velocity, radians/sec
$\ddot{\phi}$	rolling angular acceleration, radians/sec^2
$\dot{\psi}$	yawing angular velocity, radians/sec
$\ddot{\psi}$	yawing angular acceleration, radians/sec^2

Statistical Symbols

a	symbol represents measured quantity (i.e., $\dot{\delta}_E$, θ, n_V, etc.)
$\bar{a}$	bar over symbol represents average value of frequency distribution
f	frequency of occurrence or number of cycles of normal load factor
N	total number of observations for a particular quantity
p	number of normal-load-factor peaks per hour of flying time

P probability

T total recorded flight time, hr

t average flight time required to equal or exceed a given value, hr

α_3 coefficient of skewness of frequency distribution, $\frac{1}{\sigma^3}\frac{\Sigma(a - \bar{a})^3}{N}$

α_4 coefficient of kurtosis of frequency distribution, $\frac{1}{\sigma^4}\frac{\Sigma(a - \bar{a})^4}{N}$

σ standard deviation of frequency distribution, $\left[\frac{\Sigma(a - \bar{a})^2}{N}\right]^{1/2}$

TEST AIRPLANES

The airplanes used in this program were standard service airplanes. They were the North American F-86A, McDonnell F2H-2, Republic F-84G, and the Lockheed F-94B airplanes.

The F-86A-5-NA is a single-place, swept low-wing, single-engine jet-propelled fighter. The airplane has automatic full-span leading-edge slats and partial-span slotted flaps and incorporates speed brakes located on both sides of the rear fuselage section. The longitudinal control system includes an adjustable stabilizer (used for control at high Mach numbers as well as for control-force trim) and a hydraulically boosted elevator. A rate restrictor is incorporated in the elevator control system which restricts the elevator rate to about 45 degrees per second. The aileron control forces are augmented by a hydraulic booster mechanism. It was necessary to use two F-86A's during this program because one was damaged during landing.

The F2H-2 is a single-place, straight low-wing, two-engine jet-propelled fighter. A hydraulic boost is incorporated in the aileron control system. Speed brakes are located in the upper and lower wing surfaces inboard of the aileron and just ahead of the partial-span flaps.

[redacted]

The F-84G-1-RE is a single-place, straight low-wing, single-engine jet-propelled fighter-bomber airplane. The airplane is equipped with a hydraulic aileron boost with a manually adjustable boost ratio. A speed brake is installed in the bottom of the fuselage.

The F-94B-1-LO is a two-place, straight low-wing, single-engine (equipped with afterburner) jet-propelled interceptor. The aileron control forces are augmented by a hydraulic booster mechanism. Hydraulically operated speed brakes are incorporated in the bottom of the fuselage.

Neither the external appearance nor the weight and balance of the airplanes was altered by the addition of the NACA instrumentation. Three-view drawings of all the airplanes are presented in figure 1. Physical characteristics and dimensions of the airplanes are given in table I. The moments of inertia given in table I are estimated from the latest information available.

INSTRUMENTATION

Standard NACA photographically recording instruments were used to measure (1) the quantities defining the flight conditions - that is, airspeed, altitude, speed-brake position, and, in the F-86A, slat position, (2) the imposed control motions, and (3) the response of the airplane in terms of load factors, angular velocities, angle of sideslip, and, in the case of the F-84G and F-94B, angular accelerations and angle of attack. The recorders were synchronized at 1-second intervals by means of a common timing circuit.

In order to relieve the pilot of any recording-instrument switching procedure and thus assist in obtaining normal operation, a pressure switch was employed to operate the recording instruments at airspeeds above the indicated stalling airspeed. In the F-84G and F-94B a nose-wheel-door microswitch, which was actuated when the door closed, was used in parallel with the pressure switch to insure continuous operation of the recorders at airspeeds below the indicated stalling airspeed.

A standard two-cell pressure recorder connected to the airplane service system was used to measure the pressure altitude and indicated airspeed. The service systems were of the usual total-pressure-tube and flush static-pressure-orifice type. The location of the total-pressure tubes and static-pressure orifices for the four airplanes tested are indicated in figure 1.

A microswitch, incorporated into the cockpit speed-brake control handle in the F-84G and the first F-86A and attached in the immediate

proximity of the speed brake in the F2H-2, F-94B, and the second F-86A, was used to indicate whether the speed brake was in the open or closed position. The open or closed position of the slat on the F-86A was also indicated by a microswitch.

The control-surface deflections were measured with respect to the chord line of the component to which the control surface was attached by a control-position recorder having remote recording electrical transmitters installed near the surface. The elevator, rudder, and stabilizer (for the F-86A) transmitters were installed inside the fairings in order to take measurements at the inner hinge. The aileron transmitter was located at approximately the right-aileron midspan, with the exception of the F-84G. In this airplane the transmitter was located at the link arm connecting the right-aileron push-pull rod.

Normal load factors were measured by an NACA air-damped, single-component recording accelerometer in the F-84G and F-94B and by an NACA air-damped, three-component accelerometer in the F-86A and F2H-2. Transverse and longitudinal load factors were measured by an NACA air-damped, three-component accelerometer in all the airplanes. The locations of the accelerometers are given in references 1 to 5. It should be noted that the accelerometers were not located on the average "in flight" center of gravity. Angular velocities and angular accelerations were recorded by angular-velocity and angular-acceleration recorders. Load factors, angular velocities, and angular accelerations were recorded about three mutually perpendicular axes in which the longitudinal reference axis is the one commonly used for leveling the airplane. (See fig. 1.)

Sideslip angles were measured by a flow-direction recorder in combination with a vane mounted on a boom extending in front of the left wing on the F-86A and in front of the nose of the F2H-2, F-84G, and F-94B. (See fig. 1.) An angle-of-attack vane was also mounted on the boom for the F-84G and F-94B airplanes. The angle of attack is defined as the angle between the longitudinal axis and the projection of the relative wind in the vertical plane of the airplane. The angle of sideslip is defined herein as the angle between the longitudinal axis and the projection of the relative wind in the horizontal plane of the airplane.

All recording instruments were damped to about 0.65 of critical damping. The natural frequencies of the elements in all the instruments were selected to give the best compromise value which would minimize the magnitude of extraneous airplane vibrations and still give correct response to the maneuver.

[redacted]

The maximum errors for the measured quantities for all the airplanes are as follows:

Control-surface angle, deg	±0.7
Normal load factor	±0.1
Longitudinal and transverse load factors	±0.03
Pitching angular velocity, radians/sec	±0.03
Pitching angular acceleration, radians/sec^2	±0.1
Rolling angular velocity, radians/sec	±0.15
Rolling angular acceleration, radians/sec^2	±0.5
Yawing angular velocity, radians/sec	±0.02
Yawing angular acceleration, radians/sec^2	±0.06
Angles of attack and sideslip, deg	±0.7

Complete information on accuracies, instruments used, and natural frequencies of the instruments for the individual airplanes is given in references 1 to 5.

TESTS

All the flights obtained during this program were performed in conjunction with the regular squadron operational training. Data were recorded only during those flights in which the primary mission was acrobatics, ground gunnery, aerial gunnery, or dive-bombing. The maneuvers performed during these tests include most of the tactical maneuvers that were within the capabilities of the individual airplanes. These maneuvers were performed from ground level to altitudes of approximately 35,000 feet and at airspeeds varying from the stalling airspeed to the maximum service limit airspeed. Although not requested, most of the maneuvers were performed in smooth air; however, in some cases gusts were encountered. Other than to request that the airplanes be used in as many types of missions as were normally carried out by the squadron, no attempt was made to specify the type or severity of maneuvers.

Approximately 60 hours of flight time were recorded during these tests and approximately 18 hours of this recorded time have been presented as maneuvering time in time-history form in references 1 to 5. This ratio of recorded time to maneuver time of 3.33 is not representative of normal operation because the pilots were requested to perform as many maneuvers as practical during each flight in order to minimize the time required to complete the program.

The F-86A and, with the exception of one flight, the F-94B were flown without external fuel tanks, whereas the F2H-2 and, with the exception

of 2 flights, the F-84G were flown with external fuel tanks. In the case of the F2H-2, however, all maneuvers were performed with the external tanks empty.

A total of 42 service pilots participated in these tests: 8 in both the F-86A and F-94B, 12 in the F2H-2, and 14 in the F-84G. No pilot accounted for more than 20 percent of the maneuver time obtained during the particular program in which he participated. During these tests, anti-gravity suits were worn by most of the pilots. Although the pilots were aware of the instrumentation, it was stressed that this was not to restrict their normal handling of the airplane since they would not be personally identified with the test results.

METHODS OF ANALYSIS

In this paper the measured quantities are presented, as indicated in the "Contents," in an order beginning with the pilot-imposed control motions and following with the airplane response to these control motions. The results are given, for the most part, in three forms: (1) basic data and envelopes for each test airplane, (2) combination of the envelopes for all the test airplanes, and (3) statistical curves.

Basic data and envelopes for each test airplane.- The basic results are presented as plots of the maximum measured quantities and show how the envelopes were determined for each airplane. Only those maximum values which helped establish the envelopes are shown. In a few of the figures it may be noted that some of the high test points are not used to establish the envelope. In these cases it was believed that the inclusion of the isolated points within the envelope might misrepresent the mass of the data. The maximum values obtained as a result of stalled maneuvers are indicated only at the lower airspeeds since in most cases the boundaries at the higher speeds were not materially affected by stalls. The maximum values obtained in take-offs and landings were taken only when the airplane was completely airborne. No corrections have been made to the indicated airspeeds for position error.

Combination of the envelopes for all the test airplanes.- In a few cases, the envelopes for each of the test airplanes are compared; however, for the most part, the data for all the test airplanes have been combined and an overall envelope has been obtained to represent the boundary for all the airplanes. The overall envelope consists of a number of superimposed envelopes representing certain types of flight conditions which are defined as operational maneuvers, stalls, and lateral oscillations. In a few of these figures the high values obtained during snap rolls at the higher airspeeds with the F-84G airplane, which are indicated in the basic-data figures, are not included within the envelope of operational maneuvers since in this type of maneuver the airplane is partially stalled. The envelopes labeled "stalls" include values

obtained during stalls, spins, take-offs, and landings. The isolated points, which were not used to establish the envelopes in the basic-data figures, are shown in the overall envelope plots. Where possible, comparisons are made with design requirements or computing methods.

Statistical analysis.- In analyzing the data of this paper, standard statistical procedures such as described in references 7 and 8 were used. The frequency distributions for the pertinent quantities are presented in tables II to VII. Also given in the tables are the total number of measurements counted N, the total flight time in hours represented by the data T, the average value of the given quantity $\bar{a}$, the standard deviation σ, the coefficient of skewness α_3, and the coefficient of kurtosis α_4.

Frequency distributions were used to represent the data in the form of a percentage of the total number of occurrences of a given quantity occurring in a given interval. The probability or relative cumulative frequency distributions are the summation of the frequency distributions and are given as the percentage of the total number of occurrences which equal or exceed a given value of the measured quantity. The experimental distributions were fitted with a Pearson type III probability curve and in this paper the term "probability curve" will refer to a Pearson type III curve.

RESULTS AND DISCUSSION

Control Deflections

Elevator.- The maximum elevator control angles for each airplane plotted against indicated airspeed are given in figure 2 and the ratios of the maximum angles used to the maximum available angles are shown in figure 3. The largest elevator angles used were obtained in stalls, take-offs, and landings. The maximum up elevator control limits were approached in stalls for the F-86A and F-84G airplanes. The maximum down elevator used did not vary appreciably with airspeed at airspeeds above the stall except for the F-86A airplane. For the F-86A the maximum down elevator angle was reached at an airspeed of 400 knots. Since the F-86A has a movable stabilizer, the elevator angles shown are associated with various stabilizer settings. The large down elevator angles at relatively high speeds for the F-86A are associated with the particular stabilizer settings used for trim at those speeds.

Aileron.- The maximum aileron control angles (right aileron only) for each airplane plotted against indicated airspeed are given in figure 4. The ratios of maximum aileron angles used to the maximum available aileron angles are shown in figure 5. For the F-84G airplane almost full aileron was used in stalls and rolls at low speeds. Except for the F-84G airplane the aileron angles used did not approach the

control limits. The point shown above the boundary for the F-84G airplane was obtained in a maneuver during a flight in which the fuel failed to drain from one of the wing-tip tanks. The point shown above the boundary for the F-94B airplane was obtained during a very abrupt turn.

Rudder.- The maximum rudder control angles for each airplane plotted against indicated airspeed are given in figure 6 and the ratios of the maximum rudder angles used to the maximum available rudder angles are shown in figure 7. The highest rudder angles were obtained, for the most part, in stalls, take-offs, and landings. The control limits were reached with the F-84G airplane and approached with the F-86A airplane in low-speed stalls. Throughout these tests rudder control was rarely used with any of the airplanes while maneuvering.

Control Rates

Elevator.- The maximum elevator control rates for each airplane plotted against indicated airspeed are given in figure 8 and the envelope of the maximum rates for all the airplanes is shown in figure 9. The maximum elevator rates used decreased with airspeed and the highest rates were obtained in stalls and landings. The rates for all the airplanes were about the same except for the F2H-2 airplane. The elevator rates used with the F2H-2 airplane were considerably lower than for the other airplanes as was also the case for the elevator angles. This was partly a result of the rearward center-of-gravity position and partly a result of the large value of elevator effectiveness for this airplane. The negative rates were about equal to the positive rates for all the airplanes. The highest rates were obtained with the F-94B airplane in landings where elevator rates as high as 2.2 radians per second were measured. At the low speeds these rates were generally associated with short-duration impulses of large deflection which did not affect the airplane motion appreciably. The limits of control rate for the F-86A as imposed by the rate restrictor were reached at the lowest airspeeds. It may be noted again that only the F-86A airplane was equipped with elevator boost. The point shown above the boundary for the F-84G airplane was measured in a very abrupt pull-up. The point shown above the boundary for the F-94B airplane was measured in the very abrupt turn previously mentioned in the aileron-angle discussion.

The probability values and the fitted curves for elevator rates greater than 0.2 radian per second for the F-86A, F-84G, and F-94B airplanes and greater than 0.1 radian per second for the F2H-2 airplane are shown in figure 10 for combined positive and negative elevator rates. The frequency distribution for elevator rates and the statistical parameters on which the probabilities are based are given in table II. It was found that the probabilities for positive and negative elevator rates

are about equal. (See table II.) In figure 10 it may be seen that the probabilities for the combined positive and negative elevator rates for the F-94B are greater than those for the other airplanes. Since it was found that most of the high elevator rates for the F-94B airplane were obtained in landings, an analysis was made for speeds less than 150 knots, speeds greater than 150 knots, and for all speeds. The probability curves for these speed ranges are shown in figure 11; it may be seen that the probabilities for a given elevator rate for speeds above 150 knots were considerably less than those for speeds below 150 knots. For the other airplanes it was found that the speed range did not affect the probability curves appreciably. A comparison of probabilities for all the test airplanes is shown in figure 12 for all speeds except for the F-94B where the data are given for speeds less than 150 knots and greater than 150 knots. In addition, since the data for the F2H-2 airplane were calculated from a lower initial level, these data were adjusted to the level of the other test airplanes for comparison. In figure 12 it can be seen that, except for the F-94B at low speeds, the probability of exceeding a given elevator rate is about the same for all the airplanes.

Aileron.- The maximum aileron control rates for each airplane plotted against indicated airspeed are given in figure 13 and the envelope of the maximum rates for all the airplanes is shown in figure 14. The maximum aileron rate used in these tests was about 1.46 radians per second with the F2H-2 airplane. The variation of the maximum aileron rate with indicated airspeed was not consistent among the airplanes and, except for the F-84G, the maximum rates were reached at speeds greater than 200 knots for all airplanes. For the F-84G the highest rates were reached in low-speed stalls. The highest rate for the F-94B airplane occurred near the maximum airspeed. This point, which is associated with the high aileron angle shown at 440 knots in figure 4, and the other point shown above the boundary for this airplane were obtained during very abrupt turns.

The probability values and the fitted curves for aileron rates greater than 0.2 radian per second for each airplane at all speeds are shown in figure 15. The frequency distribution for aileron rates and the statistical parameters on which the probabilities are based are given in table III. It may be seen that the probability curves for aileron rates are about the same for all the airplanes with the exception of the F2H-2, where the probabilities are considerably higher.

Rudder.- The maximum rudder control rates for each airplane plotted against indicated airspeed are given in figure 16 and the envelope of the maximum rudder rates for all the airplanes is shown in figure 17. The highest rate measured was 2.8 radians per second with the F-94B airplane in take-offs and landings. The two relatively high rates shown above the boundary for the F2H-2 airplane at 360 and 330 knots were measured during a small-amplitude rudder oscillation and during an abrupt turn, respectively.

[redacted]

The probability values and the fitted curves for rudder rates greater than 0.1 radian per second for all speeds, speeds greater than 150 knots, and speeds less than 150 knots for each of the test airplanes are shown in figure 18. The frequency distribution for rudder rates and the statistical parameters on which the probabilities are based are given in table IV. It may be noted that the probabilities of exceeding a given rudder rate are higher in the low-speed range. It can be seen that in comparing the four test airplanes for the entire speed range there is a wide scatter in the probabilities; however, when comparing the probabilities for speeds greater than 150 knots the scatter is somewhat reduced.

Airplane Angular Velocities

Pitch.- The maximum pitching velocities for each airplane plotted against indicated airspeed are given in figure 19 and the envelope of the maximum pitching velocities for all the airplanes is shown in figure 20. The highest pitching velocity measured during operational maneuvers in these tests was about 0.5 radian per second. One value of 0.8 radian per second was measured with the F-84G airplane in a low-speed stall. The positive pitching velocities reached a peak at about 300 knots for operational maneuvers. The highest negative pitching velocities were reached in low-speed stalls. Also shown in figure 20 are the maximum positive pitching velocities obtained by the method of reference 9. In reference 9 the maximum positive pitching velocity is given as

$$\dot{\theta}_{max} = 1.95 \frac{n_{V_m} - 1}{\lambda} \frac{W/S}{C_{L_\alpha} q} + 0.48 \frac{(n_{V_m} - 1) g}{V} \qquad (1)$$

In figure 20 the calculated maximum positive pitching velocities were computed by using a time to reach positive peak normal load factor λ of 0.93 second, which was found to have been the approximate minimum value for these tests. The calculated values are seen to be in fair agreement with the flight data.

Roll.- The maximum rolling velocities for each airplane plotted against indicated airspeed are given in figure 21 and the envelope of the maximum rolling velocities for all the airplanes is given in figure 22. The rolling velocities reached a peak at a speed of about 250 knots for operational maneuvers. The highest rolling velocity measured was about 3.5 radians per second with the F-84G airplane.

[redacted]

Helix angle $\dot{\phi}b/2V$: The maximum values of the wing-tip helix angle $\dot{\phi}b/2V$ for each airplane plotted against indicated airspeed are given in figures 23 and 24. The maximum value of $\dot{\phi}b/2V$ obtained was about 0.14 with the F-84G airplane in a stall. The value of $\dot{\phi}b/2V$ obtained with the other airplanes was about 0.08 at speeds up to 300 knots. Above this speed the values of $\dot{\phi}b/2V$ decreased with airspeed. Included in figure 24 is the present U. S. Air Force minimum-helix-angle requirement (ref. 10) applied to the F-86A airplane. Since the airplanes of this investigation were designed prior to the requirement of reference 10, the applicable helix-angle requirement (ref. 11) as determined for the F-86A airplane is also given in figure 24. It can be seen in this figure that the Air Force rolling requirement given in reference 11, for which these airplanes were designed, is reached for most of the airplanes above a speed of 300 knots. The present requirement (ref. 10) is not reached at the higher speeds.

Since Mach number is perhaps a more significant parameter, the envelopes of $\dot{\phi}b/2V$ are shown in figures 25 and 26 plotted against Mach number. It is shown in figure 25 that high values of $\dot{\phi}b/2V$ are obtained at the higher Mach numbers, whereas in figure 23 it is seen that few large values of $\dot{\phi}b/2V$ are obtained at the higher airspeeds. It may be seen in figure 26 that relatively high values of $\dot{\phi}b/2V$ are maintained to higher Mach numbers with the F-86A airplane than with the straight-wing airplanes.

Time to roll 90°: Recently it has been suggested that a more realistic rolling requirement than that presently used would be to specify that the airplane roll 90° in 1 second (ref. 12). The values of the minimum time to roll 90° from a steady-state condition for each airplane plotted against indicated airspeed are given in figure 27 and the envelope of the minimum time to roll 90° for all the airplanes is shown in figure 28. It can be seen that the minimum time used by the service pilots of these tests to roll 90° is about 1 second except at the lowest and highest airspeeds. The peak rolling velocities reached during 90° of roll for each airplane plotted against time to roll 90° are given in figures 29 and 30. Included in figure 30 is the limit boundary showing the lowest possible rolling velocity $\pi/2T_{90}$ to roll 90° in any given time. It may be seen that the maximum rolling velocities used in rolling 90° are fairly close to the limit boundary.

Rolling velocity and normal load factor: One of the critical maneuvers for design of the vertical tail is the rolling pullout type of maneuver which consists of a rolling maneuver combined with high normal load factor. The maximum rolling velocities for each airplane plotted against normal load factor are given in figure 31 and the envelope for

all the airplanes is shown in figure 32. It may be seen that the maximum rolling velocity reached a peak at a load factor of about 2 for operational maneuvers.

Yaw.- The maximum yawing velocities for each airplane plotted against indicated airspeed are given in figure 33 and the envelope for all the airplanes is given in figure 34. The maximum yawing velocity measured in these tests was greater than 0.56 radian per second (the limit of the recorder) with the F-84G airplane. For the other airplanes, the maximum yawing velocities obtained during operational maneuvers were about 0.3 radian per second. For the F-86A airplane values as high as 0.53 radian per second were reached in low-speed stalls. For the F-84G airplane all values above 0.35 radian per second at speeds greater than 200 knots were obtained in snap rolls. At the highest airspeeds the maximum yawing velocities for all the airplanes were the result of lateral oscillations.

Airplane Angular Accelerations

Pitch.- The maximum pitching accelerations for each airplane plotted against indicated airspeed are given in figure 35 and the envelope for all the airplanes is given in figure 36. The maximum pitching acceleration reached in these tests was -2.0 radians per second per second with the F-84G airplane. In general the maximum pitching acceleration for operational maneuvers increased with airspeed to about 300 knots, a point corresponding approximately to the upper left-hand corner of the V-n diagram, and then decreased with further increase in airspeed. The maximum positive and negative pitching accelerations are about equal, although there was a tendency in these tests toward higher negative pitching accelerations.

The probability values for combined positive and negative pitching accelerations over 0.2 radian per second per second for each airplane are shown in figure 37. The frequency distributions for pitching accelerations and the statistical parameters on which the probabilities are based are given in table V. In analyzing the pitching accelerations statistically, it was found that the probabilities of exceeding negative pitching accelerations were slightly higher than the probabilities of exceeding positive pitching accelerations. In figure 37 it may be seen that within the limits of the experimental data the probability of exceeding a given pitching acceleration is about the same for all the test airplanes. It is seen that in only about 2 out of 1,000 maneuvers (0.2 percent of all maneuvers), in which a pitching acceleration over 0.2 was reached, would the pitching acceleration exceed 2 radians per second per second.

Comparison of calculated or design pitching accelerations with test results: A comparison of the maximum pitching accelerations reached in these tests for all the airplanes (composite of positive and negative envelopes given in fig. 36) with calculated or design values determined

by six different methods is shown in figure 38. The six design curves shown in figure 38 were calculated for the F-86A airplane at sea level. The curves for the other airplanes used in these tests are similar to those shown for the F-86A. The curve depicting the Navy requirement (ref. 13) is obtained from the specifications which state, among other things, that the airplane should be designed for maximum pitching accelerations of -6, -3, and 6 radians per second per second at the airspeeds corresponding to the upper left-hand corner, upper right-hand corner, and lower left- and right-hand corners of the V-n diagram, respectively.

The curve illustrating a method of reference 14 is obtained from the empirical relation

$$\ddot{\theta}_{max} = \frac{125}{W^{1/2}} \left(n_{V_m} - 1\right) \tag{2}$$

Another empirical relation given in reference 14 is

$$\ddot{\theta}_{max} = \frac{40000}{W} \tag{3}$$

For the average weight of the test airplanes this relationship results in a value of maximum pitching acceleration of about 3 radians per second per second.

The curve which is established by Civil Aeronautics Administration design specifications (ref. 15) is obtained from the empirical relation.

$$\ddot{\theta}_{max} = \frac{45}{V} n_{V_L} \left(n_{V_L} - 1.5\right) \tag{4}$$

where V is true airspeed in miles per hour and equal to or greater than the value corresponding to the upper left-hand corner of the V-n diagram.

The method of reference 16 for estimating maximum pitching accelerations is based on the equation

$$\ddot{\theta}_{max} = 2.5 \left(\dot{\delta}_E \frac{C_{L_{\alpha_t}}}{C_{L_\alpha}} \frac{d\alpha_t}{d\delta_E} \frac{S_t x_t}{I_Y} n_{V_m} \frac{W}{S} \frac{1}{V_i} \right)^{1/2} \tag{5}$$

[redacted]

where 2.5 is an empirically derived constant. It should be noted that the units for $\dot{\delta}_E$ and V_i in this equation are degrees per second and miles per hour, respectively. The elevator rate used in figure 38 for the method of reference 16 is 3.5 radians per second (200 deg/sec) which is approximately the maximum elevator rate attainable.

The curve labeled Method A was obtained from the method given in an unpublished paper by Howard W. Smith of Boeing Airplane Company which is based on the assumptions that (1) the maximum negative pitching acceleration occurs at the instant the load factor is a maximum and that (2) the elevator has been restored to the level-flight trim position at this same instant. Thus, the fundamental equation of motion of an airplane in symmetrical pitching maneuvers

$$\ddot{\alpha} + K_1\dot{\alpha} + K_2\,\Delta\alpha = K3\,\Delta\delta_E \tag{6}$$

reduces to

$$\ddot{\alpha} + K_2\,\Delta\alpha = 0 \tag{7}$$

since $\dot{\alpha}$ and $\Delta\delta$ are 0. Furthermore

$$\ddot{\alpha} \approx \ddot{\theta} \tag{8}$$

so that

$$\ddot{\theta} = -K_2\,\Delta\alpha \tag{9}$$

where

$$\Delta\alpha = \frac{\Delta n_V\, W/S}{C_{L_\alpha} q} \tag{10}$$

[redacted]

and

$$K_2 = C_{L_\alpha} \frac{qSc}{mk_Y^2}\left[-\left(\frac{dC_M}{dC_L}\right)_A + C_{L_{\alpha_t}}\sqrt{\eta_t}\,\frac{\rho}{2}\,K\,\frac{S_t x_t^2}{mc}\right] \tag{11}$$

Substituting equations (10) and (11) for $\Delta\alpha$ and K_2 into the equation for maximum pitching acceleration yields

$$\ddot{\theta}_{max} = \frac{gc}{k_Y^2}\,\Delta n_{V_m}\left[\left(\frac{dC_M}{dC_L}\right)_A - C_{L_{\alpha_t}}\sqrt{\eta_t}\,\frac{\rho}{2}\,K\,\frac{S_t x_t^2}{mc}\right] \tag{12}$$

The curve showing maximum pitching accelerations obtained by the method of reference 9 is given by the equation

$$\ddot{\theta}_{max} = 6.5\,\frac{W/S}{C_{L_\alpha} q}\,\frac{n_{V_m} - 1}{\lambda^2} + 0.95\,\frac{g}{V}\,\frac{n_{V_m} - 1}{\lambda} \tag{13}$$

where V is true airspeed in feet per second. The maximum elevator rate associated with the above maximum pitching acceleration is given approximately by the equation

$$\dot{\delta}_{E_{max}} = \frac{\left(n_{V_m} - 1\right)\frac{W}{S}}{K_3 C_{L_\alpha}\, q}\left[\frac{36.3}{\lambda^3} + 2.96\,\frac{K_1}{\lambda^2} + 0.143\,\frac{K_2}{\lambda}\right] \tag{14}$$

In this method the shape of the load-factor variation with time and the minimum time required to reach the peak load factor are assumed, based on experimental data. For fighter-type airplanes, the minimum time to reach peak elevator deflection is given in reference 9 as 0.2 second, which corresponds approximately to a time to reach peak load factor of about 0.55 second. Thus, in figure 38 the calculations for the method of reference 9 are for a value of 0.55 second to reach maximum load factor, except where the elevator rates obtained by using this value would exceed 3.5 radians per second. In these cases the value of λ was adjusted so as not to exceed an elevator rate of 3.5 radians per second. The values of the constants in equation (14) are given only for

the maximum positive pitching acceleration. Because of the shape of the load-factor curve assumed in reference 9, the maximum positive pitching accelerations will be greater than the maximum negative pitching accelerations; however, this result is somewhat unrealistic since maximum negative pitching accelerations are probably at least equal to maximum positive pitching accelerations.

It may be seen in figure 38 that the maximum pitching accelerations reached in these tests are less than one-half of the calculated or design values. It should be emphasized that the design curves shown represent maximum values that could be obtained. A pitching acceleration of 5 radians per second per second is within the maximum capabilities of the pilot and the airplane for most of these airplanes; however, the test boundary represents what the service pilots used in the performance of their training missions in these tests.

Another comparison between experimental and calculated maximum pitching accelerations is presented in figure 39. As in the case of figure 38, the calculations are for the F-86A airplane at sea level. In this figure the calculated values are determined by the methods of references 16 and 9 for elevator motions which are more closely related to the elevator motions used in these tests. In the first case the maximum pitching acceleration is calculated by the method of reference 16 by using the maximum elevator rates obtained in these tests. In the second case the maximum pitching acceleration is calculated by the method of reference 9 by using a value of 0.5 second for the minimum time to reach peak elevator deflection, which corresponds to a minimum time of approximately 0.93 second required to reach peak load factor. Since the F-86A airplane is restricted to elevator rates of approximately 45 degrees per second, the maximum pitching acceleration is also calculated for an elevator rate of 45 degrees per second in figure 39 for both methods.

It may be seen in figure 39 that the maximum pitching accelerations calculated by the methods of references 16 and 9 by using elevator motions similar to those obtained in these tests compare fairly well with the test results. Both methods predict the actual pitching accelerations very well at speeds beyond the upper left-hand corner of the V-n diagram. At lower speeds it appears that the method of reference 9 is somewhat better. It can be seen that, when the elevator rate is restricted to 45 degrees per second (0.786 radian per second), both curves are lowered although they are still higher than the experimental data at low speeds.

The maximum elevator rates associated with the maximum pitching accelerations given in figures 38 and 39 for methods of references 16 and 9 are shown in figure 40. In this figure the two curves which reach maximum elevator rates of 3.5 radians per second correspond to the maximum pitching accelerations calculated by the two methods shown in figure 38. The other elevator-rate curves given in figure 40

correspond to the maximum pitching accelerations, also calculated by these two methods, shown in figure 39. The test boundary shown does not include the highest values measured during stalls, take-offs, or landings.

It may be seen in figure 40 that the actual elevator rates (composite of positive and negative envelopes given in fig. 9) are considerably below the maximum design rates throughout the speed range. For the case where the time to reach peak load factor was assumed to be 0.93 second in the method of reference 9, it may be seen that the elevator rates are in fair agreement with the actual rates; however, the calculated rates are lower than actual rates at speeds greater than 300 knots.

Of the various methods of calculating maximum pitching accelerations shown in figure 38 the methods of references 13, 14, and 15 are empirical; the method of reference 16 is semiempirical; and the method of reference 9 and that derived by Smith (denoted as method A) are based on theoretical considerations. It appears that any of these methods could be fitted to the present test data with fair accuracy. The methods of references 9 and 16, however, seem somewhat more realistic. Although the method of Smith is based on theoretical considerations, the assumption that the elevator angle has reached zero at the time of maximum pitching acceleration appears to be conservative on the basis of the present tests since the actual elevator motions were not so abrupt as would be indicated by this method.

In the method of reference 16, the maximum elevator rates must be assumed, the stability parameters C_{L_α}, $C_{L_{\alpha_t}}$, and $d\alpha_t/d\delta_E$ must be known, and an empirical constant must be determined. In the method of reference 9 the time to reach maximum load factor or peak elevator deflection must be assumed and the value of C_{L_α} must be known. Both methods are easy to use if the proper parameters are known; however, the method of reference 9 is somewhat simpler to use in that only one parameter must be assumed, namely the time to reach maximum load factor. In the method of reference 16, the variation of maximum elevator rate with speed must be assumed. From the results of these tests it appears that it is not sufficient to assume a constant elevator rate throughout the speed range. It is fortunate in the method of reference 9 that in assuming a time to reach maximum load factor the maximum elevator rates vary approximately the same as the results of these tests.

From the results of these tests, therefore, it appears that the methods of references 9 and 16 best fit the test data; however, it should be remembered that all the methods will result in pitching accelerations within the maximum capabilities of the pilot and airplane if the pilots control the airplane in the manner specified by the methods.

[redacted]

The results of these tests indicate, however, that the service pilots in performing their normal training missions did not approach these design limits of pitching acceleration.

Pitching acceleration and normal load factor: A relationship between pitching acceleration and normal load factor is of interest in the determination of horizontal-tail loads. If the normal load factor and pitching acceleration are known, the maneuvering horizontal-tail load may be determined. For subsonic speeds the maximum up maneuvering tail load will occur when maximum positive normal load factors are combined with maximum negative pitching accelerations. The maximum pitching accelerations plotted against normal load factors for each airplane are given in figure 41 and the envelope for all the airplanes is given in figure 42. The point shown outside the boundary for the F-94B airplane at a normal load factor of 7 was caused by a gust. It can be seen in figures 41 and 42 that, in general, the maximum negative pitching accelerations increase with normal load factor, whereas the maximum positive pitching accelerations decrease with normal load factor. Since the tests were in the subsonic speed range, these data indicate combinations of load factor and pitching acceleration for which maximum tail loads are obtained. The data indicate, however, that the maximum pitching accelerations are small at the highest normal load factor for each airplane.

Roll.- The maximum rolling accelerations for each airplane plotted against indicated airspeed are given in figure 43 and the envelope for all the airplanes is given in figure 44. The maximum rolling acceleration obtained in these tests was 7.5 radians per second per second with the F-86A airplane. The maximum rolling accelerations reached a peak at an airspeed of about 300 knots. A few relatively high rolling accelerations were measured with the F-94B and F-86A airplanes at high speeds, as shown by the points above the respective boundaries. The point for the F-86A airplane was measured during a rolling pullout type of maneuver. Of the three points for the F-94B airplane, the two points at 470 and 440 knots were measured during very abrupt turns and are associated with the high aileron rates at these speeds shown in figure 13. The other isolated point at 365 knots was caused by a gust. Although the highest rolling acceleration was obtained with the F-86A airplane, the highest rolling velocities were obtained with the F-84G airplane.

Yaw.- The maximum yawing accelerations for each airplane plotted against indicated airspeed are given in figure 45 and the envelope for all the airplanes is given in figure 46. The maximum yawing acceleration reached in these tests was 1.05 radians per second per second with the F-84G airplane. This point and the point at 305 knots which are shown above the boundary for the F-84G airplane were obtained during snap rolls. For the most part, the high yawing accelerations at high speeds were obtained in inadvertent lateral oscillations for all airplanes; however, the acceleration shown above the boundary at 370 knots for the F-94B airplane

[redacted]

was caused by a gust and the acceleration shown above the boundary at 455 knots for the F-86A airplane in figure 45 was obtained in the same rolling pullout maneuver previously mentioned under rolling acceleration. The point for the F-86A is shown below the lateral-oscillation boundary in figure 46 since it was obtained during an operational maneuver. The lateral oscillations were especially prominent for the F-94B and F-84G airplanes. When the yawing accelerations due to the inadvertent lateral oscillations are not included, it can be seen in figure 46 that the yawing accelerations decrease at speeds greater than about 300 knots.

Angle of Attack and Angle of Sideslip

Angle of attack.- As a matter of general interest the maximum angles of attack for the F-84G and F-94B airplanes plotted against indicated airspeed are given in figure 47. The largest angles of attack measured in these tests were greater than 40° and -24° for the F-84G airplane in spins. At these angles the limits of the recorder were exceeded. The maximum nose-up angles of attack measured varied from about 27° at 100 knots to about 1° at 500 knots. The maximum nose-down angles of attack varied from about -4° at 100 knots to about -1° at 500 knots. The point outside the boundary for the F-84G airplane was measured in an abrupt push-down.

Angle of sideslip.- The maximum angles of sideslip and corresponding indicated airspeeds obtained in these tests for each airplane are given in figure 48 and the envelope for all the airplanes is given in figure 49. The angle-of-sideslip measurements were insufficient to define an envelope for the F-86A airplane. The highest sideslip angle measured was over 32° with the F-84G airplane in spins. At this angle the limits of the recorder were exceeded. The maximum sideslip angles reached were about the same for the F-84G and F-94B airplanes at the higher airspeeds, whereas those reached with the F2H-2 were lower throughout the speed range in these tests. The maximum sideslip angles which define the operational-maneuver boundary in figure 49 were obtained in rolling pullouts, aileron rolls, sideslips, and rudder kicks. No one type of maneuver was more critical than another although there are more points along the boundary obtained from rolling maneuvers.

Airplane Load Factors

Normal load factor.- The maximum positive and negative normal load factors and corresponding indicated airspeeds for each airplane are given in figure 50. In this figure the operational V-n diagram for each airplane is included with the corresponding load-factor data for comparison of the test results with the operational limits. In order to compare the

results for all the test airplanes, the measured load factor divided by the maximum allowable load factor n_{V_a} as determined from the V-n diagram is shown in figure 51 plotted against the measured airspeed divided by the maximum allowable airspeed.

In comparing the maximum normal load factors reached with all the airplanes it may be seen that the positive service limit load factor was reached with all the airplanes over most of the speed range; however, the negative limit load factor was not reached at any speed. The highest negative load factor reached was -1.1 for the F-84G airplane (see fig. 50) and occurred at a value of $V_i/V_{i_{max}}$ of 0.43. (See fig. 51.) One contributing factor to the lack of negative load factors may be in the limitations of jet-engine operation at negative accelerations.

Comparisons of the maximum normal load factors obtained in these tests with maximum normal load factors obtained during other tests with F-86A airplanes (ref. 17) and unpublished V-G records from F2H-2 airplanes are shown in figures 52 and 53, respectively. The data of reference 17 for the F-86A airplanes represent about 1,150 hours of operational training and the unpublished data for the F2H-2 airplanes represent 3,821 hours of operational training.

In the comparison of the data obtained in the present tests for the F-86A airplane with those of reference 17 (fig. 52) it may be seen that in both cases the pilots reach the positive service limit load factor over almost the entire speed range; however, the negative limit load factor was not reached in either case. In the data of reference 17 the service limit load factor was exceeded 28 times, the design limit load factor 5 times, and the design ultimate load factor twice. For the airplane of the present tests, the service limit load factor was reached but not exceeded by an appreciable amount. In the negative load-factor region, there are very few points in both sets of data. In the data of reference 17 a load factor of -1.0 was reached once; whereas in the present test program with the F-86A the maximum negative load factor was about -0.3. It is interesting to note in figure 52 that, below the service limit, the two sets of data are very similar.

In the comparison of the data obtained in the present tests for the F2H-2 airplane with that of 3,821 hours of unpublished V-G records obtained during training (fig. 53) it may be seen that the 3,821 hours of V-G data resulted in positive and negative load factors larger than those obtained from the present tests over the entire speed range. The positive design and service limit load factor was reached once in the present tests; however, it was exceeded 31 times in the V-G data. The design ultimate load factor was not exceeded in either test program. Most of the large negative load factors from the V-G data were obtained from gusts.

[redacted]

Applicability of Pearson type I and type III curves to normal-load-factor data: The probabilities for normal load factor are shown for each airplane in figure 54 where Pearson type III curves have been fitted to the data as counted by method B of the appendix. In analyzing the normal-load-factor data it was found that the data fell more closely into the Pearson type I class. Therefore Pearson type I curves were fitted to the normal-load-factor data for each airplane. An example of this is shown in figure 55 for the F-86A airplane. For comparison, the type III curve is also shown. In this figure it may be seen that the Pearson type I curve does fit these data somewhat better than the Pearson type III curve for the F-86A airplane. (Similar fit was found for the other test airplanes.) It may be seen, however, that the limits of the type I curve are at load factors of about 0.8 and 9.2; that is, the probability would reach 1 at a load factor of 0.8 and would reach 0 at a load factor of 9.2. This extrapolation would be unrealistic since it indicates that a load factor of 9.2 would never be exceeded with the F-86A airplane. The maximum load-factor limits computed for the other test airplanes using Pearson type I curves were 13.1 for the F2H-2, 10.2 for the F-84G, and 12.7 for the F-94B. In view of the unrealistic limits for the F-86A airplane and the similarity in fit for the Pearson type I and type III curves, the Pearson type III curves were considered adequate for this analysis. The frequency distributions of normal load factor and the statistical parameters on which the probabilities and times to exceed are based for all the test airplanes are given in table VI.

Comparison of normal-load-factor statistical data for the test airplanes: In order to compare the probability of equaling or exceeding a given normal load factor for all of the test airplanes, the probabilities obtained by counting method B of the appendix are given in figure 56 plotted against normal load factor and in figure 57 plotted against a ratio of measured load factor to service limit load factor $\frac{n_V - 1}{n_{V_S} - 1}$. In figure 56 it may be seen that the probability of equaling or exceeding a given load factor in these tests is greater for the F-94B and F-84G airplanes than for the F-86A and F2H-2 airplanes. The greatest difference between the probabilities at a load factor of 6 is of the ratio of about 10 to 1. It will be noted in figure 50 that the service limit load factors for the F-86A and F2H-2 airplanes are lower than for the other test airplanes. In figure 57 it may be seen that when the data are compared on the basis of the service limit load factor the results are fairly close throughout the load-factor range.

In order to compare the probability of a load factor being less than a given value for each airplane, the probabilities were computed by using method A of the appendix and are shown in figure 58. It can be seen in this figure that the probabilities of load factors being less than zero are very low. For instance, for the F-84G airplane the probability that

a load factor less than 0 will be reached is about 0.005 or 1 maneuver in 200, and about 1 maneuver in 7,000 will result in load factors less than -1. It can be noted in figure 58 that the probabilities of a load factor being less than a given load factor are about the same for all the test airplanes.

Comparison of normal-load-factor statistical data with other test results: In order to obtain an indication of the applicability of the results obtained from these tests in which only a relatively few hours were flown with those of other tests where considerably more flight time was obtained, a comparison of load-factor data is given in figures 59 to 67. For these comparisons the positive-load-factor results for the test data are based on counting method B of the appendix. In the case of negative load factors, all values less than zero were read and classified in a manner similar to that used for the other test data.

In figure 59 a comparison between the probability curve obtained for the F-86A airplane of these tests and the probability curve and test points for 1,150 hours of operational training with F-86A airplanes (ref. 17) is shown for positive load factors. In this figure the probability curves are given for load factors greater than 2. A comparison of the flight time required to equal or exceed a given load factor for these cases is shown in figure 60. Also included in this figure is the faired curve for ground- and aerial-gunnery missions only, as obtained from reference 17.

Since there were very few negative load factors reached in both cases, a Pearson type probability curve was not computed for the negative-load-factor points. A comparison of the time required to exceed a given negative load factor is shown in figure 61 where the test points only are given. The test points represent the total recorded time divided by the number of occurrences greater than a given load factor.

For the F2H-2 airplane unpublished V-G records of 3,821 hours of operational training were used for a comparison. In figure 62 a comparison of the flight time required to exceed a given load factor is shown for the test airplane and the airplanes for which 3,821 hours of V-G data were available. Data are shown only for load factors greater than 5 for the 3,821 hours of data since individual load-factor peaks at the lower load factors are obscured due to the nature of V-G records. A comparison of the time required to exceed a given negative load factor for the test airplane and the 3,821 hours of data is shown in figure 63.

A comparison of the flight time required to equal or exceed a given value of positive load factor for the test F-84G airplane with that for F-84B and F-84E airplanes used in operational training is shown in figure 64. The curves shown for the F-84B and F-84E airplanes were obtained from the only data presently available (ref. 18) and are faired curves.

The data for the F-84B represent 270 hours of flight time and the data for the F-84E represent 235 hours of flight time. These data are probably not representative of normal training operations since the F-84B was restricted to a load factor of 5 because of a pitch-up tendency and the data for the F-84E were obtained mainly during high-altitude performance tests.

Data are not available for a direct comparison with the Lockheed F-94B test data; however, a comparison is made with 1,212 hours of operational training with the Lockheed F-80A and B airplanes (ref. 19) and with 1,044 hours of operational training with F-80A, B, and C airplanes (ref. 20). In figure 65 a comparison of the probability values obtained from these different sets of data is shown for positive load factors. Also included are values from 253 hours of dive-bombing and ground- and aerial-gunnery training with F-80A, B, and C airplanes (ref. 20). These data along with 220 hours of ground- and aerial-gunnery data with F-80A and B airplanes are compared on a time-to-exceed basis in figure 66.

In figure 67 a comparison of the time-to-exceed values obtained from these different sets of data is shown for negative load factors. Because of the lack of other F-84 negative-load-factor data, the data points for the F-84G test airplane are also presented in this figure.

The results shown in figures 59 to 67 indicate that up to the service limit normal load factor the probability of exceeding a given normal load factor for the test airplanes is about the same as that of other tests even though the data of the other tests represent considerably more flight time and different types of missions. The results also show that, in general, the average flight time required to equal or exceed a given normal load factor for the test airplanes of this program is less than that of the other tests, except when gunnery or dive-bombing only are considered for the other tests. In this case the results seem to merge, which would be expected, since the maneuvers of both sets of data are of similar nature. The time-to-exceed curves for this program are, for the most part, about parallel to those of the other tests; this parallelism indicates that both sets of data represent the same manner of utilization. It is indicated that the data of the present tests are representative of many more hours of flight time than were actually recorded.

Hypothetical case illustrating reversal of probability curve at high normal load factors: In many probability and time-to-exceed plots for normal load factor the experimental data show a tendency to diverge from a typical probability or time-to-exceed curve at high load factors as shown by the data for the F-86, F-84, and F-80 airplanes (figs. 59, 60, 64, and 66) and also for other airplanes (ref. 21). This type of reversal in the curves is similar to the results obtained when two frequency distributions are superimposed. In figure 68 two frequency curves are shown on a semilogarithmic scale. The data for the 1,150 hours of operational

training for the F-86A airplane (ref. 17) were used and the test frequencies were multiplied by 10 to approximate roughly the results for about 11,500 hours of flying.

The two assumed frequency distributions shown in figure 68 are defined as f_1 and f_2. The frequency distribution f_1 was faired through the test data. The frequency distribution f_2 was arbitrarily assumed to be a normal distribution centered at the design ultimate load factor of 11 and then fitted through the two experimental points. The square symbols indicate the assumed or calculated frequency and the circular symbols indicate the test frequencies multiplied by 10. In figure 69 the probability curves P_1 and P_2, corresponding to f_1 and f_2, are shown with the total probability curve P_T. The total probability curve is given by

$$P_T = \frac{P_1 N_1}{N_1 + N_2} + \frac{P_2 N_2}{N_1 + N_2} \tag{15}$$

Also shown in figure 69 are the experimental points from reference 17. In figure 70 the combined probability curve is shown on a time-to-exceed basis. It may be seen that the type of curve obtained by combining two distributions is similar to the curves found experimentally at high load factors.

A possible explanation of the two distributions is that the first distribution is the ordinary one to be expected up to the limit load factor, whereas the second distribution is one based on load factors reached inadvertently and in emergencies. For this reason none of the probability curves in this paper have been extended beyond the limits of the data.

It is believed that even though the data may be represented by combining two frequency distributions, enough data to determine the second or inadvertent distribution could not be obtained on fighter aircraft since many thousands of hours of flight time would probably be needed. It is therefore indicated that the loads to be expected could not be predicted by standard statistical methods.

Transverse load factor.- The maximum corrected transverse load factors plotted against the indicated airspeed for each airplane are given in figure 71 and the envelope for all the airplanes is shown in figure 72. In general, the maximum transverse load factors reached a peak at an airspeed of about 300 knots for operational maneuvers. The

maximum transverse load factor measured was 0.54 with the F-94B airplane. This point which is shown above the boundary for the F-94B airplane was obtained during an abrupt uncoordinated turn when entering the landing pattern. The design requirement of reference 13 states that the airplane shall be designed to withstand a transverse load factor of 2.

The probability points for transverse load factor and the fitted probability curves are shown in figure 73 for each airplane. The probabilities are given as the percentage of the total number of transverse-load-factor peaks that equal or exceed a given load factor if the load factor is above 0.05. The frequency distributions of transverse load factor and statistical parameters on which the probabilities are based are given in table VII. In figure 73 it may be noted that the probabilities of equaling or exceeding a given transverse load factor are about the same for all the test airplanes, except for the F-94B airplane for which the probabilities are considerably higher.

Vertical-tail load parameter βq_c.- In order to estimate the relative magnitudes of vertical-tail loads over the speed range, the maximum values of vertical-tail load parameter βq_c obtained in these tests for each airplane are plotted against indicated airspeed in figure 74 and the envelope for all the airplanes is given in figure 75. Angle-of-sideslip measurements for the F-86A airplane were insufficient to define an envelope. The product βq_c is plotted in these figures instead of βq, the usual vertical-tail load parameter, since at a given indicated airspeed the values of βq_c and βq are nearly the same. The maximum vertical-tail loads indicated in these tests by the value of βq_c were obtained at speeds which correspond roughly to the upper left-hand corner of the V-n diagram. The relatively high values of βq_c obtained at the highest speeds were obtained in inadvertent airplane lateral oscillations and were not the result of one of the critical maneuvers mentioned under the discussion of sideslip angle. These lateral oscillations were especially noticeable for the F-94B airplane. (See fig. 74.) It is interesting to note that stability deficiencies, such as uncontrolled lateral oscillations, may produce loads as high as those obtained in controlled maneuvers.

A comparison between the test results and the Navy rolling pullout requirement for βq_c that a full aileron roll be made at 0.8 of the design limit load factor is also shown in figure 75. It may be seen that the values of βq_c obtained from this requirement (calculated by the method of ref. 22) are greater than those obtained in these tests. Another design requirement which states that the airplane be designed for 5° of sideslip angle at limit diving speed results in a value of βq_c of about 5,000 which is more than twice the largest value obtained in these tests as shown in figure 75.

It would be of value to have a statistical instrument which would measure βq; however, since exterior equipment would be necessary to measure the sideslip angle, it has been suggested that the transverse load factor could be used in place of the angle of sideslip. In order to show the correlation of transverse load factor with sideslip angle, the corrected transverse load factors are shown plotted against the vertical-tail load parameter βq_c in figure 76. It can be seen that the correlation between the corrected transverse load factor and βq_c is fairly good. The scatter is caused partly by using q_c in place of q, partly because of reading inaccuracy of load factors and correction terms, and partly because of other variables entering into the side-force equations. Although the correlation between the corrected transverse load factor and the term βq_c is good, it has been found that the correlation between the transverse load factors uncorrected for angular-velocity and angular-acceleration effects and the term βq is very poor.

It is of interest to note in figure 76 that, for the F-84G airplane, all the large transverse load factors which are outside the mass of data were measured in snap rolls.

Longitudinal load factor.- The maximum longitudinal load factors for each airplane plotted against indicated airspeed are given in figure 77 and the envelope for all the airplanes is shown in figure 78. The highest longitudinal load factors reached in these tests were about 0.85 forward and about 0.55 rearward both with the F-86A airplane. In general, the maximum forward longitudinal load factor reached a peak at an airspeed of about 250 knots. The maximum forward load factors were due mostly to the time rate of change of flight-path angle in longitudinal pull-up type of maneuvers. The maximum rearward longitudinal load factors measured in these tests increased with airspeed up to the highest speeds. The maximum rearward load factors at the highest speeds were due mostly to the use of speed brakes in flight. Rearward load factors as large as 1.3 were measured in landing impacts. These data are not included in the figures.

Load-factor combination (n_T and n_V).- From the plots of transverse load factor against normal load factor in figures 79 and 80 it can be seen that relatively high values of transverse load factor may occur at high normal load factors as well as at low normal load factors. The highest transverse load factor measured in these tests (0.54) was obtained at a normal load factor of about 6 for the F-94B airplane. The points above the boundaries for the F2H-2 and F-94B airplanes, with the exception of the lateral-oscillation value, were obtained in abrupt turns when entering the landing pattern. These turns may be considered as rolling pullout type of maneuvers.

[redacted]

Airspeed and Altitude

The time spent in various altitude and airspeed ranges is shown in figures 81 and 82. The time is given in percent of the total maneuvering time which was approximately 3.6 hours for the F-86A, 2.5 hours for the F2H-2, 8.0 hours for the F-84G, and 3.9 hours for the F-94B airplane. In the airspeed frequency chart it is indicated that, in general, at least 65 percent of the maneuver flying time for all the test airplanes occurred at speeds between 200 and 350 knots. The maximum airspeeds reached for the straight-wing airplanes were about 500 knots and the maximum airspeed reached with the F-86A was about 600 knots. It may be seen in figure 82 that most of the maneuvering was done at altitudes less than 25,000 feet. Altitudes greater than 35,000 feet were seldom reached in these tests.

SOME APPLICATIONS OF RESULTS

Statistical Loads Instruments

One purpose of the present test program was to determine the important quantities and their ranges for use in designing instruments for statistical loads measurements.

In general, if accurate loads indications are desired, all the measurements made on these test airplanes would be necessary in addition to a knowledge of the stability derivatives for the airplanes. Since it would be impractical to obtain all these measurements with operational airplanes, some compromise must be made.

Wing loads.- Measurements of normal load factor, speed, and altitude are sufficient for determining overall wing loads. At the present time such measurements are being made by means of VGH recorders and flight analyzers. For statistical measurements the present tests indicate that a simple acceleration threshold counter would be adequate for most purposes. Such a counter, however, would not be satisfactory for obtaining time-to-exceed curves unless an empirical factor relating number of peaks to number of threshold points could be determined. From the results of this paper this factor is between 5 and 6 for a load factor interval of 0.5. (See table VI.)

Horizontal-tail loads.- The simplest form of the horizontal-tail-load equation is

$$L_T = C_{m_o} qS \frac{c}{x_t} + n_V W \frac{d}{x_t} - \frac{I_Y}{x_t} \ddot{\theta} \qquad (16)$$

or

$$L_T = C_{m_o} qS \frac{c}{x_t} + \frac{cn_V W}{x_t} \frac{C_{m_{WF}}}{C_{N_{WF}}} - \frac{I_Y}{x_t} \ddot{\theta} \tag{17}$$

Therefore, if the variation of the pitching moment of the wing-fuselage combination with lift coefficient and Mach number is known from other tests, the tail load is a direct function of airspeed, load factor, and pitching acceleration

$$L_T = \frac{\partial L_T}{\partial q} q + \frac{\partial L_T}{\partial n_V} n_V - \frac{\partial L_T}{\partial \ddot{\theta}} \ddot{\theta} \tag{18}$$

Thus, an instrument that measures airspeed, altitude, load factor, and pitching acceleration on a time scale would give a good measure of both the loads on the wing and the horizontal tail.

If only maximum loads were required, an instrument which would give envelopes of normal load factor against airspeed (V-G recorder), pitching acceleration against airspeed, and pitching acceleration against normal load factor could be used.

Vertical-tail loads.- Perhaps the simplest measurement that would indicate the magnitude of the vertical-tail load is the angle of sideslip in conjunction with the airspeed and altitude. The term βq is roughly proportional to the vertical-tail load and an instrument that could record this quantity would be of value.

Since the sideslip-angle measurement would have to be made externally, it would be convenient if some other means could be used to obtain this parameter. One way would be to measure transverse load factor; however, from the results of these and other tests, it has been determined that, in order to measure transverse load factor with any accuracy, the accelerometer must be located at the airplane center of gravity. Distances as close as 2 feet from the center of gravity result in large errors due to the angular motions of the airplane. Therefore, it is believed that an external measurement of the sideslip angle is necessary. Such measurements could be made with a unit that would not materially alter the exterior appearance of the airplane.

Thus, if a time recording of airspeed, altitude, normal load factor, pitching acceleration, and sideslip angle were made, a rough indication

of most of the air loads on the airplane could be obtained. The results from the present tests could be used as a guide to determine the ranges of the instruments.

Fatigue

Although the results obtained from these tests are not directly applicable to the fatigue problem for fighter-type airplanes, certain phases appear to be of some interest. For instance, in figure 57 it was shown that the probability curves for normal load factor are approximately the same for all four airplanes when based on the service limit load factor. Also in figures 59 and 65 it may be noted that the results from other tests of service airplanes are about the same at load factors up to the service limit load factor. Therefore, it would seem feasible to use a standard probability curve to represent the manner in which loads are imposed on fighter aircraft in order to arrive at a fatigue life. Such curves are shown in figures 83 and 84. In figure 83 the probability values for load factors greater than 2 are shown for the four test airplanes together with probability values for the F-86A and F-80 airplanes of references 17, 19, and 20. The probabilities are plotted against the ratio $\frac{n_V - 2}{n_{V_S} - 2}$ for comparison. It may be seen that all the combined data are approximately equal at load factors up to the limit load factor. Therefore, a curve was faired through the data and for purposes of illustration was extended linearly beyond the limit load factor. In figure 84 the standard probability curve is shown for load factors greater than 1 where the probabilities are plotted against the load-factor ratio $\frac{n_V - 1}{n_{V_S} - 1}$. In transferring the curve of figure 83 to figure 84, an average service limit load factor of 7 was used. Slightly different curves would be obtained for other service limit load factors; however, for fighter airplanes having service limit load factors from 5 to 8, either of the curves given in figures 83 and 84 would be satisfactory. The differences obtained in using either curve are within the scatter of the experimental data.

The number of cycles of load imposed on the airplane in any load-factor interval may be given as

$$f = PpT \tag{19}$$

where the probability of exceeding a given load factor P is obtained from curves such as shown in figures 83 and 84, and the number of hours of flight time T is specified. The term p is the average number of load-factor peaks per hour of flying time for the type of flying for which the airplane is used. This factor could be obtained from a statistical study of load factors on fighter airplanes in average operation. (The present test results should not be used since the maneuvers were somewhat more concentrated than average.) From the results of references 17, 19, and 20 it has been found that the value of p for those tests varies from about 13 to 29 load-factor peaks per hour above a load factor of 2 for all types of training missions. It is to be noted that a given maneuver will usually have several load-factor peaks. If gunnery training only were used to determine p, the value would be considerably greater (as high as 70); however, it is believed that the value of p should be obtained from data which present an overall representation of the manner in which the airplane is normally used. It was found from the present test results that the value of p for load factors greater than 1 is about two times the value of p for load factors greater than 2. Therefore, a tentative value of p would be about 30 for load factors counted above 2 and about 60 for load factors counted above 1. These correspond to the highest value found in references 17, 19, and 20 and are probably conservative.

In order to illustrate the possible use of the present results in determining the fatigue life of fighter airplanes, two examples of possible types of fatigue failure are shown in figure 85. In this figure the ratio of applied load to actual ultimate load n_V/n_{V_U} is plotted against the number of cycles f applied. The fatigue-failure curve shown is a typical curve for a fighter airplane (ref. 23) and is given for purpose of illustration only. It does not necessarily represent the failure curve for any of the test airplanes. It is assumed that, when a load-factor distribution curve reaches the failure curve, a fatigue failure will occur. The distribution curves shown in figure 85 were adjusted so as to reach the failure curve by changing the flight time T in equation (19).

Of the two cases presented in figure 85, the load-factor distribution used for curve A is that of figure 83. This curve represents a normal-strength airplane where the service-limit load factor is 7.33 and the actual ultimate load factor is 11. In this case a fatigue life of about 2,100 hours is obtained, based on the assumed failure curve. The load-factor distribution used for curve B is a case where a reversal at high load factor occurs. This curve represents an overstrength airplane where the service limit load factor is 6 and the actual ultimate load factor is assumed to be 14. This case is similar to that for the F-86A airplane and the probability curve used is that labeled P_T in figure 69. In this case, where the service limit is low and the ultimate is high, no fatigue

failure occurs; but the airplane fails when the ultimate load factor is reached on the average in about 1,850 hours.

In addition to a superimposed distribution caused by inadvertencies, a gust frequency could also be superimposed on the maneuver frequency distribution. This was not done in the present case since the data used to obtain the standard probability curves included load factors due to gusts as well as maneuvers. It is not known if the proportion of gusts encountered in these tests is representative of that obtained during normal service operations.

It should be remembered that the preceding discussion does not represent any particular airplane and that the fatigue lives given are for purposes of illustration only. Actual fatigue lives would depend upon the shape of the particular failure curve and load-distribution curve.

CONCLUDING REMARKS

From the results of the more than 2,000 maneuvers performed in the present tests of operational training with jet fighter airplanes, it has been determined that the service pilots utilized the positive V-n envelope but, in the flight time recorded in these tests, did not approach the negative V-n envelope. The maneuvers which are critical for horizontal- and vertical-tail loads appear to be less severe than any present design requirement. This observation does not mean that the present design requirements are overly conservative since these airplanes could reach the design limits if the pilots controlled the airplane in the manner specified by the requirements. The data presented do indicate, however, that in these tests, the service pilots in performing their operational training missions did not approach the design limits of the airplanes.

From the limited statistical analysis presented it is indicated that, for most of the measured quantities, the probability of exceeding a given value is roughly the same for all the test airplanes. In the case of normal load factor the probabilities of exceeding positive load factors for all the test airplanes were about the same when based on the airplane service limit normal load factor.

When compared with normal-load-factor data of other tests of operational airplanes representing considerably more flight time and different types of missions, the results indicate that up to the service limit normal load factor the probability of occurrence of a given normal load factor for the test airplanes is about the same as that of the other tests. When the two sets of data are compared on a time-to-exceed basis, it is indicated that both sets of data represent the same manner of utilization and that

the data of the present tests are representative of many more hours of flight time than were actually recorded.

It is indicated that the extrapolation of probability or time-to-exceed curves beyond the limits of the data is doubtful. For normal load factor it is shown that a possible reason for the change in shape of the probability curves at high load factors may be due to the combination of two separate frequency curves, one a regular distribution and the other caused by inadvertencies or emergencies.

Some possible applications of the results to the problem of fatigue and to the design of statistical loads instruments are also included.

Langley Aeronautical Laboratory,
National Advisory Committee for Aeronautics,
Langley Field, Va., December 7, 1953.

[redacted]

APPENDIX

COMPARISON OF METHODS OF COUNTING NORMAL LOAD FACTORS

In making a statistical analysis of the normal load factors obtained in these tests three different methods of counting the load factors were used. These methods are illustrated in figure 86. The solid symbols in the figure define the points counted in each method and the number of points counted at each interval is given in the table below the figure. In method A normal-load-factor thresholds were counted at intervals of 0.50. A count was made at every point at which a threshold value was intersected by the load factor. This method is similar to the simplest type of acceleration or load-factor counter. In method B only peak load factors were counted. For a peak to be counted by this method two criteria had to be fulfilled:

1. The load factor had to increase an amount equal to or greater than one-half of the amount that the load factor decreased following the previous peak counted.

2. The load factor had to decrease an amount equal to or greater than one-half of the amount the load factor increased following the previous peak counted.

This method is best shown by the illustration in figure 86.

The third method (method C) is one in which the load factor is assumed to be made up of several superimposed load-factor distributions. Increments of load factor are superimposed on the maximum load factor. In using this method only incremental values are read as shown in figure 86; therefore, in the figures and tables pertaining to this method a load factor of 1 has been added to the increments for purposes of comparison.

There are other methods of counting peaks and all are somewhat arbitrary. The three methods selected for this paper were chosen arbitrarily to show any differences in the frequency distribution due to different methods of counting.

The frequency distributions of normal load factor and the statistical parameters on which the probabilities are based for all the airplanes are given in table VI for methods A and B and also for the F2H-2 airplane by using method C. The thresholds used in method A are the first numbers in each of the intervals given in the table. Negative load factors were not counted by methods B and C.

A comparison of methods A and B is shown in figure 87 where the frequency of occurrence in percent of the total number of occurrences is plotted against normal load factor for each of the test airplanes. The symbols connected by straight lines represent method A and the rectangles represent method B. In this comparison (on a percentage basis) it may be seen that there are no appreciable differences in the results obtained by either method except near a load factor of 1. At load factors near 1, of course, an infinite number of points could be counted; therefore, the differences shown in figure 87 at load factors near 1 are not significant. (For this analysis the points given at a load factor of 1 were counted only when the load factor increment was greater than 0.25.) There appears to be some tendency at high load factors for the relative frequencies from method A to be somewhat lower than those from method B.

Probability curves for each airplane obtained by using methods A and B are shown in figure 88. In this figure the probability is given as the proportion of load factors exceeding a given load factor. For example, the probability curve for the F-84G airplane obtained by using method B indicates that in 1,000 maneuvers in which the peak load factor is greater than 1.0, one maneuver would have a load factor greater than 7.0. The probability curves based on methods A and B also compare reasonably well with each other as shown in figure 88. It must be remembered that at the highest load factor the difference of about 3 to 1 as shown for the F-86A, F2H-2, and F-84G airplanes is based on only one or two points at these high load factors and therefore is not a reliable basis for comparing the methods. On the other hand, at the lower load factors the probabilities are based on many points and the differences are more significant.

For the F2H-2 airplane all three methods of counting were used. The probability plots for all load factors above 1.5 for the three methods are shown in figure 89. It may be seen in this figure that there are no great differences in probability obtained from methods A, B, and C for the F2H-2 airplane.

For individual maneuvers such as shown in figure 86 the various methods will result in much different frequency counts (as shown in the table of fig. 86); however, when the mass of data is analyzed it appears that, although the three methods of counting are significantly different, the relative frequency distributions and probability curves obtained from all the methods are similar. Therefore, it is believed that the simplest method would be preferred in the design of statistical instruments.

[redacted]

REFERENCES

1. Hamer, Harold A., and Henderson, Campbell: Time Histories of Maneuvers Performed With an F-86A Airplane During Squadron Operations. NACA RM L51K30, 1952.

2. Huss, Carl R., Andrews, William H., and Hamer, Harold A.: Time-History Data of Maneuvers Performed by a McDonnell F2H-2 Airplane During Squadron Operational Training. NACA RM L52B29, 1952.

3. Henderson, Campbell, Thornton, James, and Mayo, Alton: Time-History Data of Maneuvers Performed by an F-86A Airplane During Squadron Operational Training. NACA RM L52C19, 1952.

4. Hamer, Harold A., and Mayo, Alton P.: Time-History Data of Maneuvers Performed by a Republic F-84G Airplane During Squadron Operational Training. NACA RM L53C27, 1953.

5. Huss, Carl R., Fisher, Raymond A., and Gainer, Patrick A.: Time-History Data of Maneuvers Performed by a Lockheed F-94B Airplane During Squadron Operational Training. NACA RM L53B27, 1953.

6. Mayer, John P., Huss, Carl R., and Hamer, Harold A.: Preliminary Results From a Limited Investigation of the Use of Controls During Service Operational Training With Fighter Airplanes. NACA RM L53D22, 1953.

7. Elderton, W. Palin: Frequency Curves and Correlation. Cambridge Univ. Press, 1938.

8. Kenney, John F.: Mathematics of Statistics. D. Van Nostrand Co., Inc. 1939.

9. Pearson, Henry A., McGowan, William A., and Donegan, James J.: Horizontal Tail Loads in Maneuvering Flight. NACA Rep. 1007, 1951. (Supersedes NACA TN 2078.)

10. Anon.: Flying Qualities of Piloted Airplanes. USAF Spec. No. 1815-B, June 1, 1948.

11. Anon.: Stress Analysis Criteria. AAF Spec. No. C-1803-E, Apr. 2, 1946.

12. Williams, W. C., and Crossfield, A. S.: Handling Qualities of High-Speed Airplanes. NACA RM L52A08, 1952.

[redacted]

13. Anon.: Airplane Strength and Rigidity. NAVAER SS-1C, Bur. Aero., Aug. 1, 1946.

14. Matheny, Cloyce E.: Maximum Pitching Angular Accelerations of Airplanes Measured in Flight. NACA TN 2103, 1950.

15. Anon.: Compilation of CAA Rules, Policies, and Interpretations Which Apply to Civil Air Regulation 3. Civil Aero. Manual 3, Supp. No. 5, CAA, U. S. Dept. Commerce. Mar. 8, 1950.

16. Bouton, Innes: Maneuvering Horizontal Tail Loads. Jour. Aero. Sci. (Readers' Forum), vol. 16, no. 7, July 1949, pp. 440-441.

17. Gray, Frank P.: Flight Load Data From Operational F-86A Aircraft. ATI 1588L3 (Memo. Rep. No. WCNSS3-4515-12-15), WADC, Aero. Div., U. S. Air Force, Jan. 15, 1952.

18. Gray, Frank P.: Advance Summaries of Flight Analyzer Data From Fighter Aircraft. Memo. Rep. No. MCREXA83-4515-12-9, Air Materiel Command, U. S. Air Force, June 29, 1950.

19. Gray, Frank P.: Analysis of Flight Analyzer Data Obtained From Operational F-80 Aircraft. Memo. Rep. No. MCREXA83-4515-12-10, Air Materiel Command, U. S. Air Force, Oct. 5, 1950.

20. Gray, Frank P.: Flight Load Data From F-80 Aircraft of the Air Training Command. Tech. Memo. Rep. WCLS 53-3, Air Research and Development Command, U. S. Air Force, Apr. 1, 1953.

21. Reynolds, Lawrence B.: A Summary of Flight Load Data Recorded in Tactical and Training Operations During the Period of World War II. Preprint No. 235, Inst. Aero. Sci., Inc., July 1949.

22. White, Maurice D., Lomax, Harvard, and Turner, Howard L.: Sideslip Angles and Vertical-Tail Loads in Rolling Pull-Out Maneuvers. NACA TN 1122, 1947.

23. Patching, C. A.: Interim Note on Repeated Load Testing of "Mustang" P-51D Wings. SM. Note 189, Aero. Res. Lab. (Melbourne), Sept. 1951.

TABLE I.- DIMENSIONS AND PHYSICAL CHARACTERISTICS OF THE TEST AIRPLANES

Component	Item	Unit	Airplane			
			F-86A	F2H-2	F-84G	F-94B
	Serial number		{USAF 48-227 USAF 49-1265}	Buaero number 125256	USAF 51-855	USAF 51-5380A
Wing	Total area (including portion covered by fuselage)	sq ft	287.9	294.1	261.0	258.0
	Span (without tip tanks)	in.	445.4	500.8	438.8	431.5
	Mean aerodynamic chord	in.	97.0	88.4	88.8	80.6
	Lateral location of mean aerodynamic chord normal to fuselage reference line	in.	98.7	111.0	98.3	92.0
	Vertical location of mean aerodynamic chord normal to and below fuselage reference line	in.	25.7	0.4	2.4	13.4
	Distance from nose to leading edge of mean aerodynamic chord	in.	164.3	197.0	169.6	210.9
	Aspect ratio		4.79	5.89	5.10	5.96
	Taper ratio, $\frac{\text{Tip chord}}{\text{Root chord}}$		0.51	0.52	0.57	0.38
	Sweepback of 25-percent-chord line	deg	35.2	-------	-------	-------
	Incidence of root chord	deg	1.0	-0.5	0.0	1.0
	Incidence of tip chord	deg	-1.0	-0.5	-2.0	-0.5
	Dihedral	deg	3.0	3.0	5.0	3.5
	Root airfoil section		NACA 0012-64 (modified)	NACA 65_1-212	NA,45-1512-.9 (12 percent thick)	NACA 65_{112}-213
	Tip airfoil section		NACA 0011-64 (modified)	NACA 65-209	NA,45-1512-.9 (12 percent thick)	NACA 65_{112}-213
Aileron	Total area (one)	sq ft	18.6	9.4	16.1	8.8
	Static limits of travel	deg	{Up 15 Down 15}	Up 20 Down 20	Up 17.2 Down 15.2	Up 20 Down 20
Horizontal tail	Total area (including portion covered by fuselage)	sq ft	35.0	69.8	48.4	47.8
	Span	in.	153.0	224.7	179.3	199.0
	Mean aerodynamic chord	in.	34.7	47.4	40.1	38.2
	Lateral location of mean aerodynamic chord normal to fuselage reference line	in.	38.5	49.6	41.5	38.5
	Vertical location of mean aerodynamic chord normal to and above fuselage reference line	in.	25.5	58.0	27.5	28.4
	Tail length (25 percent of wing M.A.C. to 25 percent of horizontal-tail M.A.C.)	in.	222.3	203.1	217.0	190.5
	Aspect ratio		4.65	4.65	4.65	5.75
	Taper ratio, $\frac{\text{Tip chord}}{\text{Root chord}}$		0.45	0.60	0.56	0.36
	Sweepback of 25-percent-chord line	deg	34.6	------	------	-------
	Incidence	deg	Adjustable	0.4	0.0	0.5
	Dihedral	deg	10.0	0.0	5.0	0.0
	Airfoil section		NACA 0010-64	NACA $65_{(10)}$-011	NA,40-010	NACA 65-010
Elevator	Total area (one)	sq ft	5.1	9.4	8.5	4.4
	Static limits	deg	{Up 35 Down 17.5}	Up 15 Down 15	Up 25 Down 10	Up 38 Down 17.5

[redacted]

TABLE I.- DIMENSIONS AND PHYSICAL CHARACTERISTICS OF THE TEST AIRPLANES - Concluded

Component	Item	Unit	Airplane			
			F-86A	F2H-2	F-84G	F-94B
Stabilizer	Leading-edge limits of travel	deg	{Up 1.3 Down 10}	Fixed	Fixed	Fixed
Vertical tail	Total area (including portion above fuselage and excluding dorsal or ventral area)	sq ft	33.4	38.9	30.9	22.5
	Span (from fuselage contour)	in.	90.2	86.0	86.0	77.0
	Mean aerodynamic chord	in.	57.5	67.3	63.0	48.3
	Vertical location of mean aerodynamic chord above fuselage contour	in.	38.5	37.6	28.3	23.5
	Vertical location of mean aerodynamic chord normal to and above fuselage reference line	in.	55.7	77.6	43.5	58.1
	Tail length (25 percent of wing M.A.C. to 25 percent of vertical-tail M.A.C.)	in.	201.3	205.4	218.3	193.5
	Aspect ratio		1.74	1.34	2.23	1.83
	Taper ratio, $\frac{\text{Tip chord}}{\text{Root chord}}$		0.36	0.45	0.39	0.40
	Sweepback of 25-percent-chord line	deg	35.0	------	------	------
	Airfoil section		NACA 0011-64	NACA $65_{(10)}$-011	RA,40-010	NACA 65-010
Rudder	Total area	sq ft	8.1	10.1	10.0	5.3
	Static limits	deg	{Right 27.5 Left 27.5}	Right 20 Left 20	Right 23.5 Left 23.5	Right 30 Left 30
Fuselage	Total length (excluding nose boom)	in.	412.4	481.8	461.4	481.3
	Maximum width	in.	60.0	46.9	49.9	56.0
	Frontal area (excluding canopy)	sq ft	20.0 (approx.)	15.7	17.0	17.0 (approx.)
Speed brakes	Total effective frontal area	sq ft	8.6	11.6 including cutouts	3.4	5.0
Tip tanks	Weight empty (one)	lb	----------	200	178	190
	Capacity (one)	gal	----------	200	230	230
Weight and location of center of gravity (full service)	Measured airplane weight	lb	[a]14,220	[b]17,940	[b]15,440	[a]13,160
	Center-of-gravity location corresponding to above weight	percent M.A.C.	20.8	26.8	23.8	27.5
Estimated moments of inertia for weight as given	Corresponding weight	lb	[a]12,600	[b]16,520	[b]15,440	[a]13,650
	I_X (roll)	slug-ft^2	6,700	19,000	18,600	11,900
	I_Y (pitch)	slug-ft^2	16,500	26,300	21,300	25,600
	I_Z (yaw)	slug-ft^2	21,700	42,700	38,900	37,800
Powerplant			General Electric J-47	Westinghouse (two) J-34-WE-34	Allison J-35-A-29	Allison J-33-A-33 with afterburner

[a]No external tanks.
[b]Tip tanks on but empty.

TABLE II.- FREQUENCY DISTRIBUTION OF ELEVATOR RATE

$\dot{\delta}_E$, radians/sec	Frequency													
	F-86A			F2H-2			F-84G			F-94B				
	Positive	Negative	Total	Positive	Negative	Total	Positive	Negative	Total	Positive	Negative	Total	$v_i < 150$	$v_i > 150$
0.1 to 0.19				13	18	31								
.2 to .29	21	21	42	5	3	8	71	105	176	50	45	95	23	72
.3 to .39				4	4	8								
.4 to .49	7	19	26	0	3	3	15	16	31	25	20	45	23	22
.5 to .59														
.6 to .79	3	6	9				8	3	11	13	13	26	17	9
.8 to .99	1	2	3				3	4	7	5	5	10	8	2
1.0 to 1.19	0	0	0				0	1	1	2	4	6	5	1
1.2 to 1.39	0	1	1				1	0	1	2	0	2	2	0
1.4 to 1.59							0	1	1	1	3	4	4	0
1.6 to 1.79										1	3	4	4	0
1.8 to 1.99										1	0	1	1	0
2.0 to 2.19										1	0	1	1	0
2.2 to 2.39										1	1	2	2	0
N	32	49	81	22	28	50	98	130	228	102	94	196	90	106
T	14.3	14.3	14.3	17.8	17.8	17.8	19.6	19.6	19.6	7.9	7.9	7.9	7.9	7.9
$\bar{\dot{\delta}}_E$	0.400	0.471	0.443	0.209	0.221	0.216	0.392	0.368	0.378	0.543	0.568	0.555	0.749	0.395
$\sigma_{\dot{\delta}_E}$	0.158	0.202	0.189	0.0778	0.106	0.0951	0.179	0.176	0.178	0.388	0.372	0.392	0.488	0.163
α_3	1.518	1.714	1.730	0.362	1.121	1.142	2.393	3.592	3.047	2.504	1.909	2.280	1.421	1.851
α_4	4.480	7.023	7.004	2.170	2.715	2.976	9.576	18.250	14.163	12.811	7.578	8.527	4.438	6.303

TABLE III.- FREQUENCY DISTRIBUTION

OF AILERON RATE

$\pm\dot{\delta}_A$, radians/sec	Frequency			
	F-86A	F2H-2	F-84G	F-94B
0.2 to 0.39	57	36	773	277
.4 to .59	11	10	151	44
.6 to .79	9	9	27	15
.8 to .99	1	4	12	5
1.0 to 1.19		2	3	1
1.2 to 1.39		3	1	1
1.4 to 1.59		1		
N	78	65	967	343
T	14.3	17.8	19.6	7.9
$\bar{\dot{\delta}}_A$	0.382	0.512	0.353	0.357
$\sigma_{\dot{\delta}_A}$	0.148	0.306	0.124	0.137
α_3	1.631	1.501	3.012	3.064
α_4	4.473	4.445	14.358	14.357

TABLE IV.- FREQUENCY DISTRIBUTION OF RUDDER RATE

$\pm\dot{\delta}_R$, radians/sec	Frequency											
	F-86A			F2H-2			F-84G			F-94B		
	$v_i < 150$	$v_i > 150$	Total	$v_i < 150$	$v_i > 150$	Total	$v_i < 150$	$v_i > 150$	Total	$v_i < 150$	$v_i > 150$	Total
0.1 to 0.19	3	22	25	4	30	34	56	186	222	43	62	105
.2 to .29	1	6	7	5	5	10	22	44	66	28	7	35
.3 to .39	2	2	4	0	1	1	16	10	26	22	9	31
.4 to .49	0	0	0	0	4	4	9	7	18	16	2	18
.5 to .59	1	0	1	0	5	5	2	2	4	12	4	16
.6 to .69	1	0	1	0	1	1	1	0	1	4	2	6
.7 to .79	1	0	1	0	0	0	1	1	2	5	0	5
.8 to .89	0	0	0	0	0	0	0	0	0	4	0	4
.9 to .99	0	0	0	1	0	1	0	0	0	4	1	5
1.0 to 1.09	0	0	0	0	0	0	0	0	0	4	0	4
1.1 to 1.19	0	0	0	0	0	0	0	0	0	0	0	0
1.2 to 1.29	3	0	3	1	0	1	0	0	0	1	0	1
1.3 to 1.39							1	0	1	1	0	1
1.4 to 1.49										1	0	1
1.5 to 1.59										1	0	1
1.6 to 1.69										0	0	0
1.7 to 1.79										0	0	0
1.8 to 1.89										1	0	1
1.9 to 1.99										0	0	0
2.0 to 2.09										0	0	0
2.1 to 2.19										0	0	0
2.2 to 2.29										1	0	1
2.3 to 2.39										0	0	0
2.4 to 2.49										0	0	0
2.5 to 2.59										0	0	0
2.6 to 2.69										0	0	0
2.7 to 2.79										1	0	1
2.8 to 2.89										1	0	1
N	12	30	42	11	46	57	108	250	340	150	87	237
T	14.3	14.3	14.3	17.8	17.8	17.8	19.6	19.6	19.6	7.9	7.9	7.9
$\bar{\dot{\delta}}_R$	0.592	0.183	0.300	0.368	0.246	0.269	0.254	0.190	0.214	0.433	0.225	0.369
$\sigma_{\dot{\delta}_R}$	0.423	0.0597	0.296	0.354	0.153	0.213	0.163	0.0839	0.121	0.439	0.148	0.377
α_3	0.521	1.602	2.416	1.711	3.413	2.521	3.356	2.935	3.741	3.010	2.441	3.556
α_4	1.815	4.454	7.782	4.241	8.868	10.251	20.428	13.931	27.196	13.705	9.505	19.640

TABLE V.- FREQUENCY DISTRIBUTION OF PITCHING ACCELERATION

$\ddot{\theta}$, radians/sec^2	Frequency											
	F-86A			F2H-2			F-84G			F-94B		
	Positive	Negative	Total	Positive	Negative	Total	Positive	Negative	Total	Positive	Negative	Total
0.20 to 0.29	75	101	176	27	35	62	129	182	311	58	65	123
.30 to .39	27	34	61	12	10	22	65	80	145	16	18	34
.40 to .49	14	21	35	8	6	14	34	53	87	9	11	20
.50 to .59	13	6	19	4	13	17	20	40	60	9	7	16
.60 to .69	3	5	8	6	0	6	19	14	33	1	10	11
.70 to .79	1	3	4	3	0	3	10	16	26	2	4	6
.80 to .89	1	1	2	0	2	2	3	6	9	0	3	3
.90 to .99	1	1	2	0	0	0	2	7	9			
1.00 to 1.09	0	0	0	0	1	1	2	4	6			
1.10 to 1.19	0	1	1	0	0	0	5	0	5			
1.20 to 1.29	1	0	1	0	1	1	1	1	2			
1.30 to 1.39	0	1	1	0	0	0	0	1	1			
1.40 to 1.49	0	0	0	0	1	1	0	0	0			
1.50 to 1.59	0	1	1				0	1	1			
1.60 to 1.69							0	0	0			
1.70 to 1.79							1	0	1			
1.80 to 1.89							0	0	0			
1.90 to 1.99							0	2	2			
N	136	175	311	60	69	129	291	407	698	95	118	213
T	14.3	14.3	14.3	17.8	17.8	17.8	19.6	19.6	19.6	7.9	7.9	7.9
$\bar{\ddot{\theta}}$	0.349	0.350	0.349	0.382	0.399	0.391	0.400	0.404	0.402	0.329	0.368	0.350
$\sigma_{\ddot{\theta}}$	0.155	0.186	0.173	0.157	0.254	0.202	0.215	0.227	0.222	0.121	0.167	0.150
a_3	2.517	3.420	3.183	0.980	2.451	2.301	2.318	2.827	3.361	1.576	1.321	1.505
a_4	11.970	18.057	16.954	2.717	9.889	10.846	10.304	15.253	13.497	4.821	3.610	4.369

TABLE VI.- FREQUENCY DISTRIBUTION OF NORMAL LOAD FACTOR

n_v	Frequency								
	F-86A		F2H-2			F-84G		F-94B	
	Counting method A	Counting method B	Counting method A	Counting method B	Counting method C	Counting method A	Counting method B	Counting method A	Counting method B
(-)1.0						2			
(-)0.5			2			12		1	
0 to 0.49	10		31			51		17	
.5 to .99	59		194			459		160	
1.0 to 1.49	928	412	815	256		3,016	845	1,186	311
1.5 to 1.99	1,321	207	1,065	180	168	2,959	444	1,289	173
2.0 to 2.49	1,178	190	893	135	131	2,375	306	1,182	158
2.5 to 2.99	896	96	598	106	85	1,844	204	952	116
3.0 to 3.49	528	71	379	85	74	1,416	179	700	100
3.5 to 3.99	334	41	205	43	30	965	150	472	77
4.0 to 4.49	190	34	105	22	22	631	110	305	51
4.5 to 4.99	82	9	59	12	15	311	74	195	35
5.0 to 5.49	49	12	26	10	9	150	28	114	17
5.5 to 5.99	17	8	3	1	1	78	15	68	12
6.0 to 6.49	3	2	2	1	1	45	12	37	5
6.5 to 6.99						15	3	19	4
7.0 to 7.49						6	3	14	3
N	5,555	1,082	4,377	829	536	14,339	2,373	6,689	1,062
T	14.3	14.3	17.8	17.8	17.8	19.6	19.6	7.9	7.9
$\overline{n}_v$	2.100	2.091	1.939	2.235		2.105	2.274	2.261	2.249
σ_{n_v}	0.934	0.987	0.922	0.963		1.086	1.159	1.167	1.217
a_3	0.880	1.442	0.777	1.031		0.885	1.199	0.990	1.087
a_4	3.646	4.954	3.642	3.710		3.652	3.907	3.943	3.858

TABLE VII.- FREQUENCY DISTRIBUTION OF TRANSVERSE LOAD FACTOR

$\pm n_T$	Frequency			
	F-86A	F2H-2	F-84G	F-94B
0.050 to 0.099	214	66	414	66
.100 to .149	79	9	163	67
.150 to .199	8	4	39	48
.200 to .249	4	2	7	31
.250 to .299	4		4	20
.300 to .349			3	12
.350 to .399				3
.400 to .449				0
.450 to .499				0
.500 to .549				1
N	309	81	630	248
T	14.3	17.8	19.6	7.9
$\bar{n}_T$	0.0949	0.0892	0.0983	0.160
σ_{n_T}	0.0362	0.0335	0.0391	0.0794
α_3	2.506	2.537	2.311	1.020
α_4	10.886	8.911	10.350	4.108

[redacted]

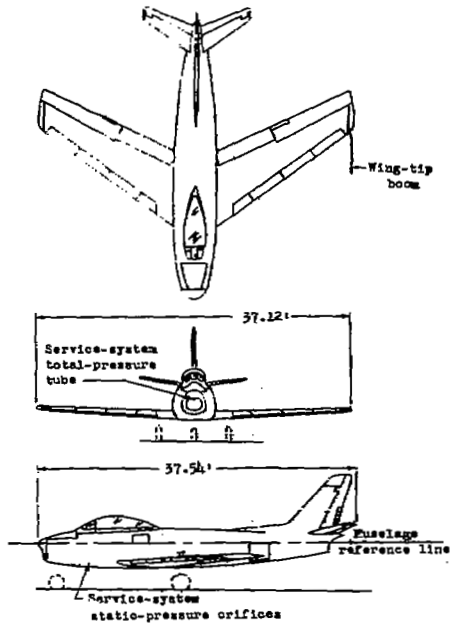

F-86A

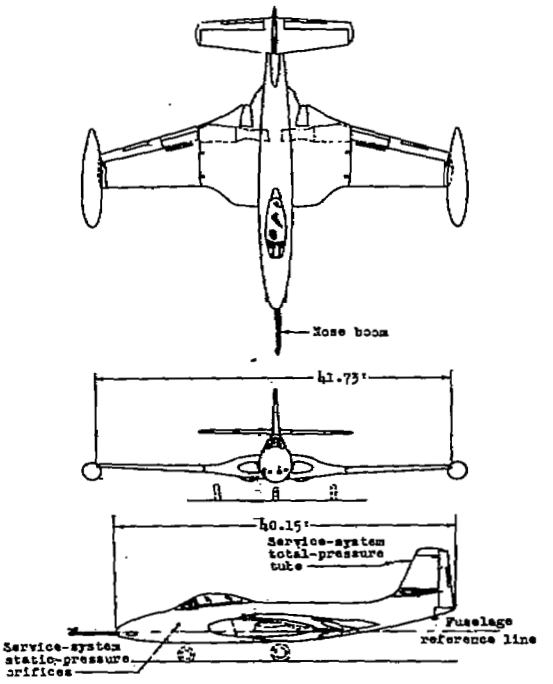

F2H-2

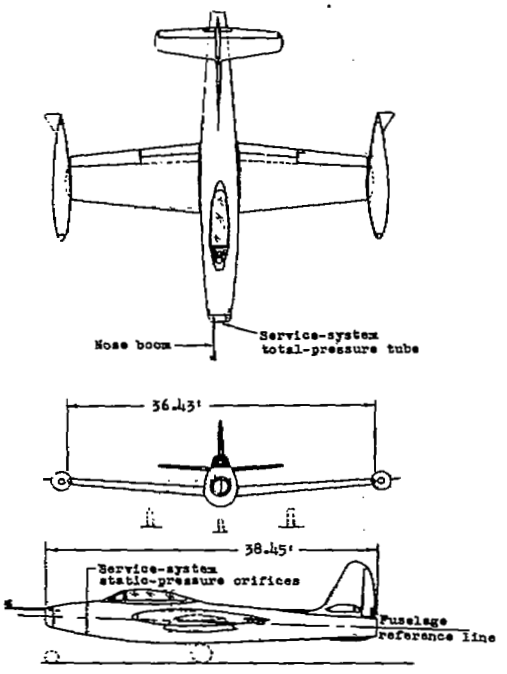

F-84G

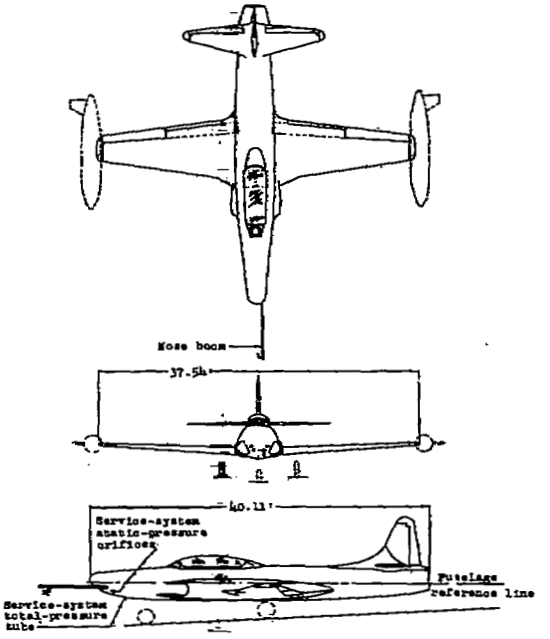

F-94B

Figure 1.- Three-view drawings of test airplanes.

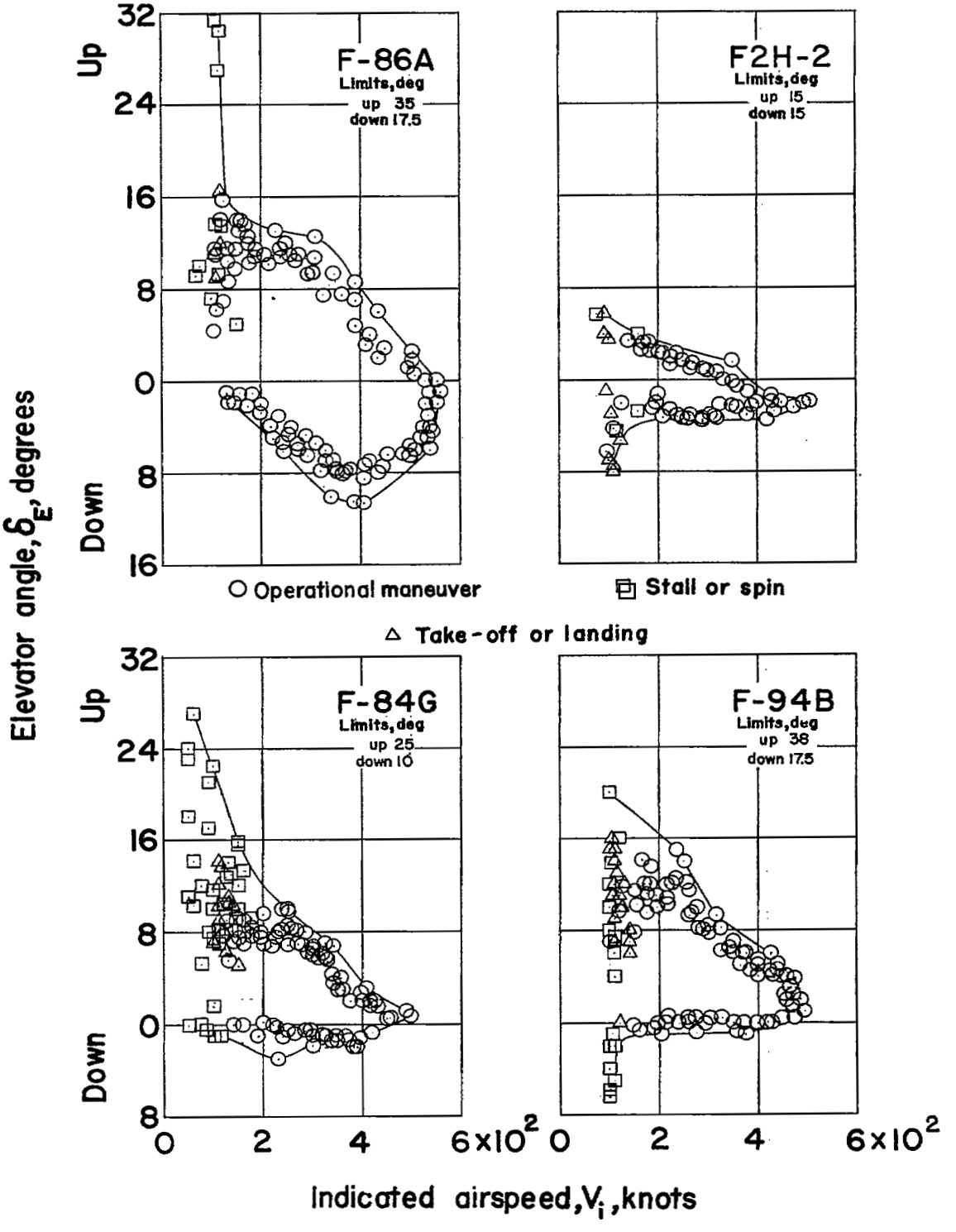

Figure 2.- Maximum elevator angles plotted against indicated airspeed.

[redacted]

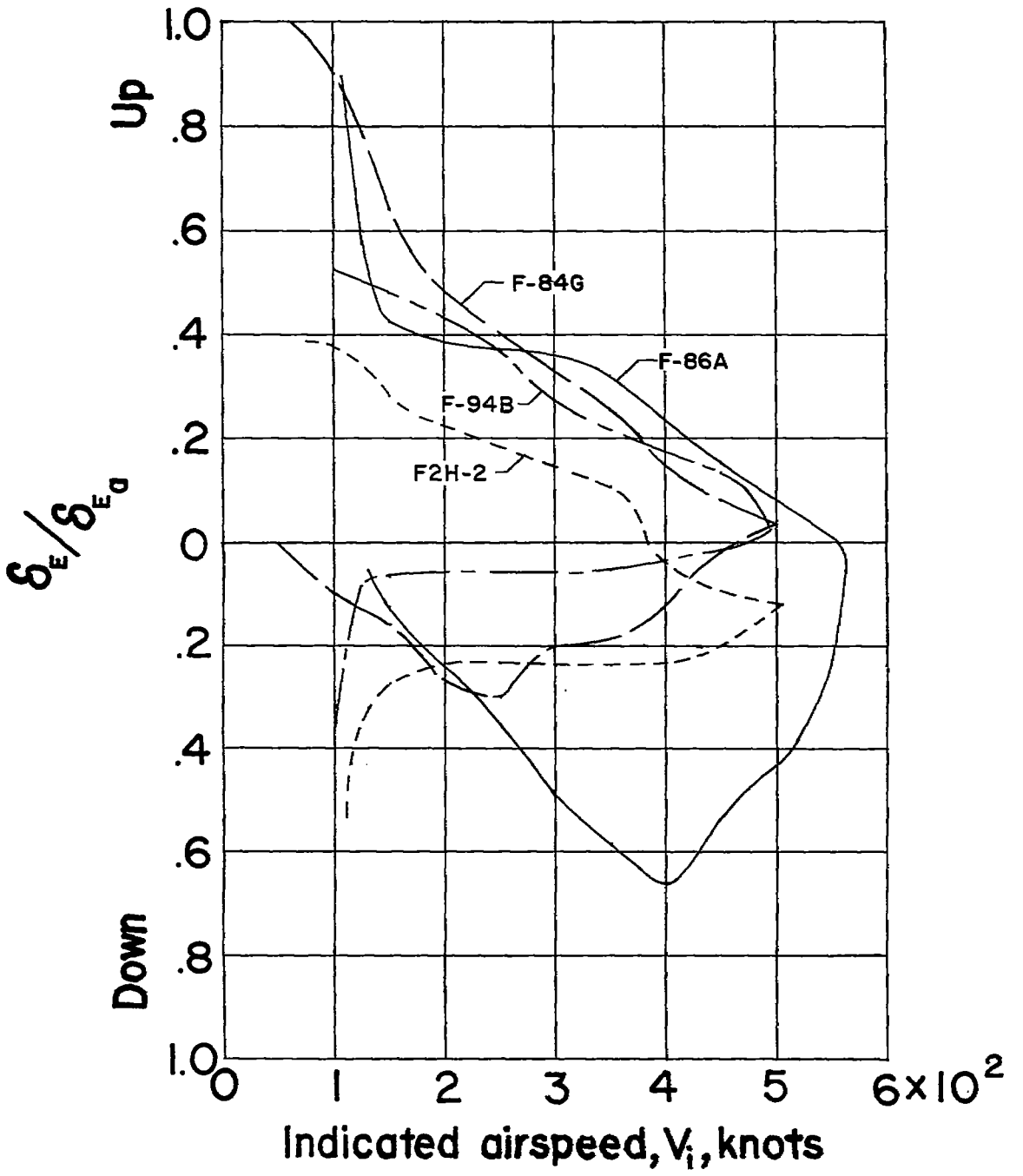

Figure 3.- Utilization of available elevator angles.

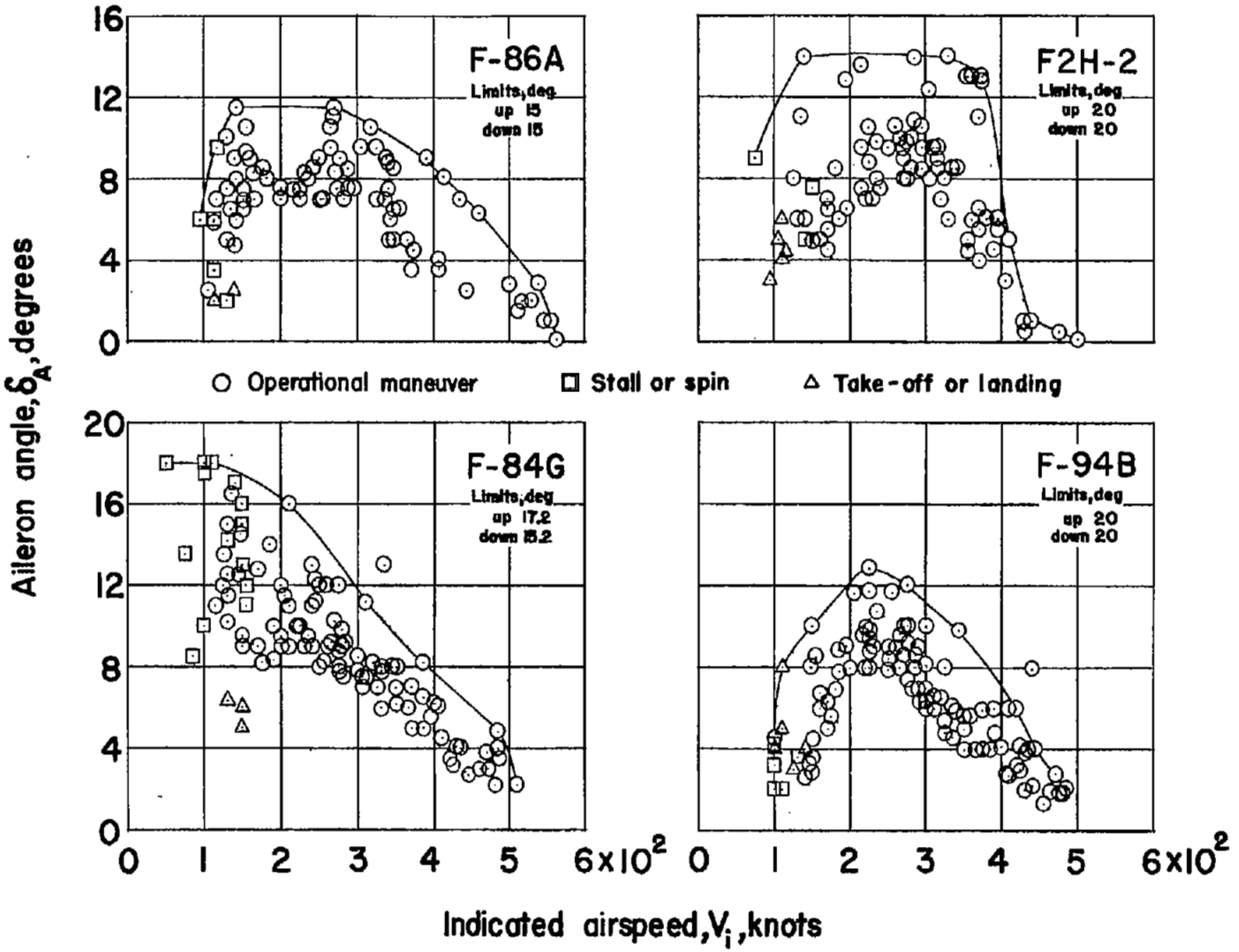

Figure 4.- Maximum up or down right aileron angles plotted against indicated airspeed.

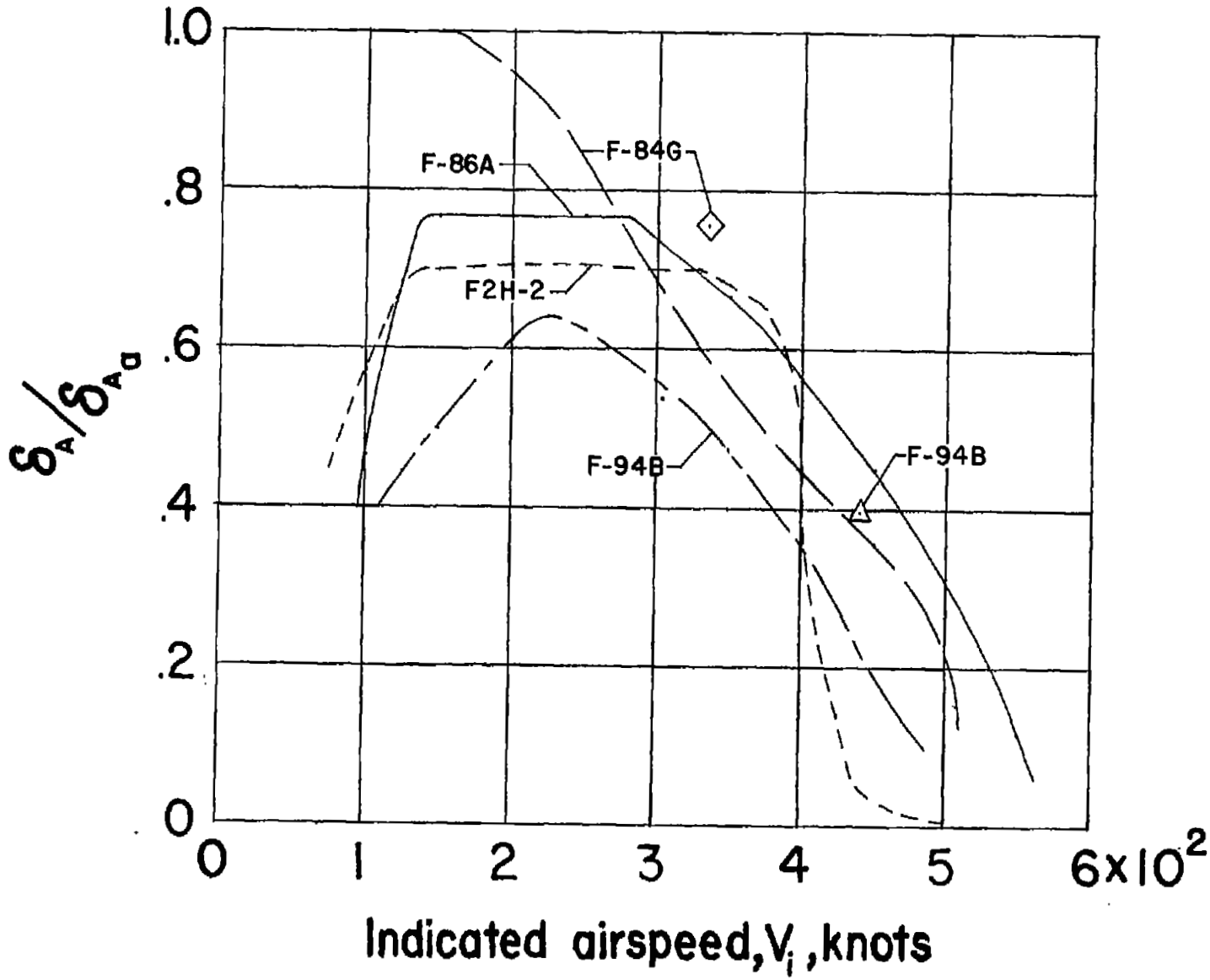

Figure 5.- Utilization of available up or down right aileron angles.

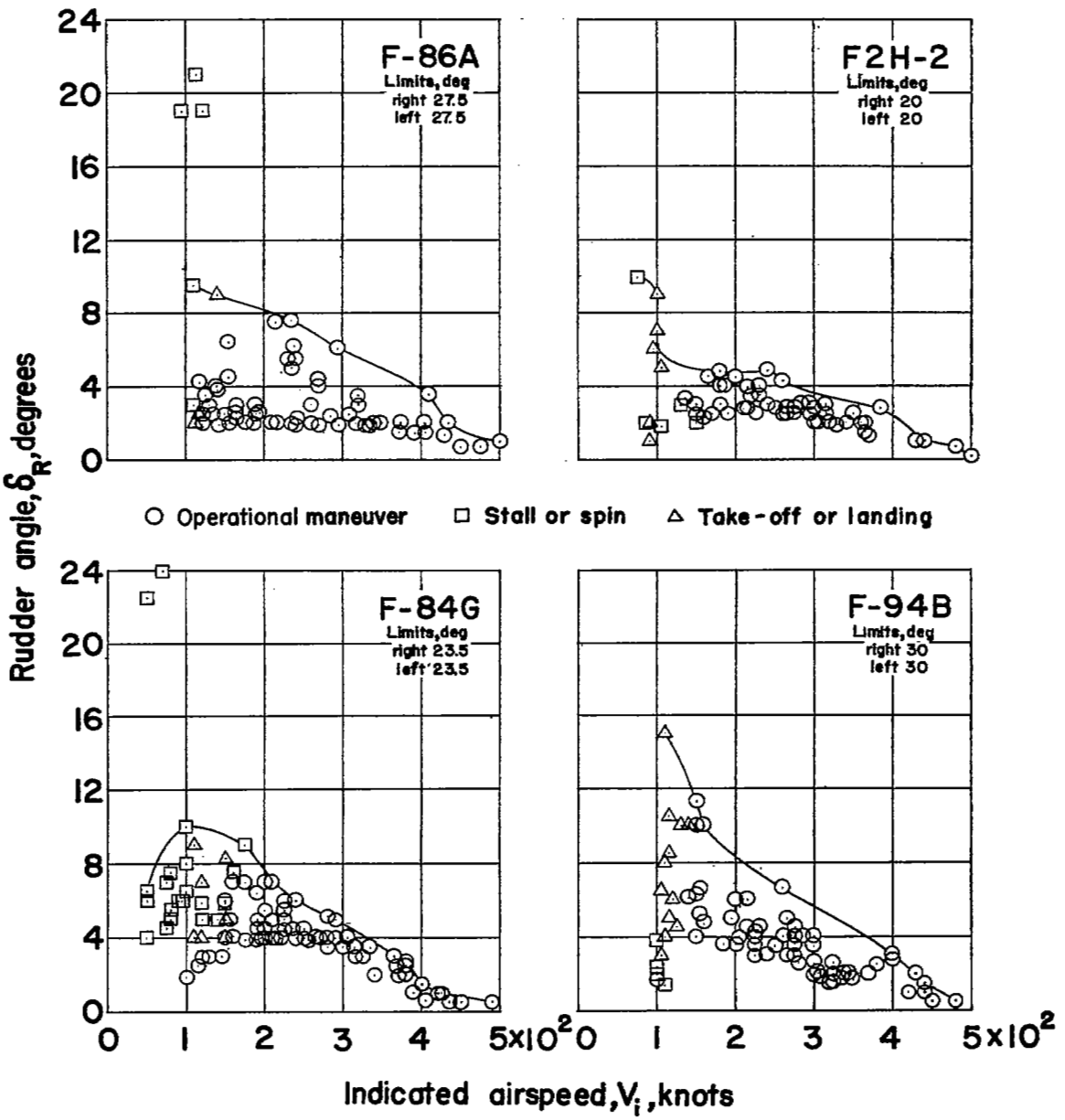

Figure 6.- Maximum rudder angles plotted against indicated airspeed.

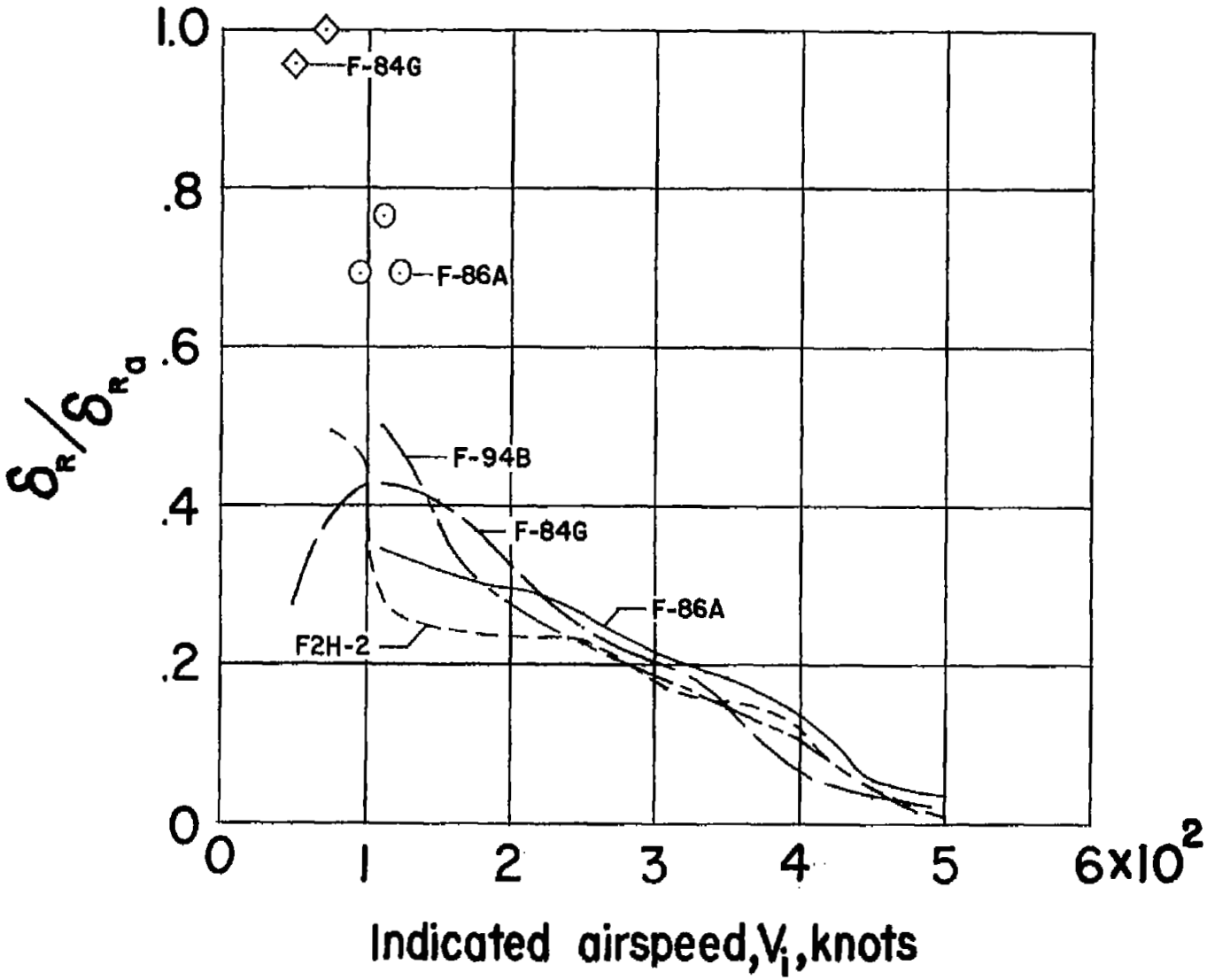

Figure 7.- Utilization of available rudder angles.

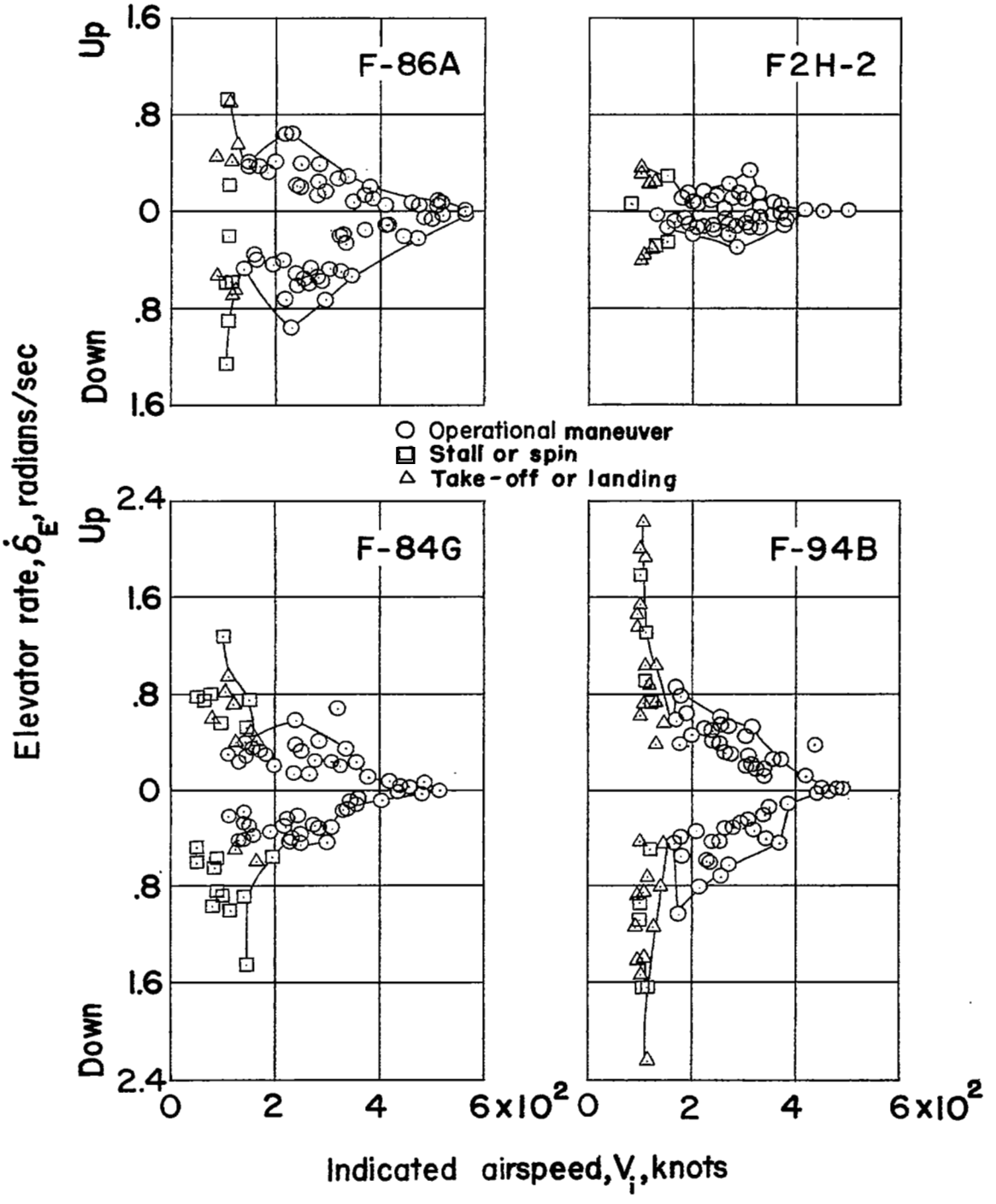

Figure 8.- Maximum elevator rates plotted against indicated airspeed.

[redacted]

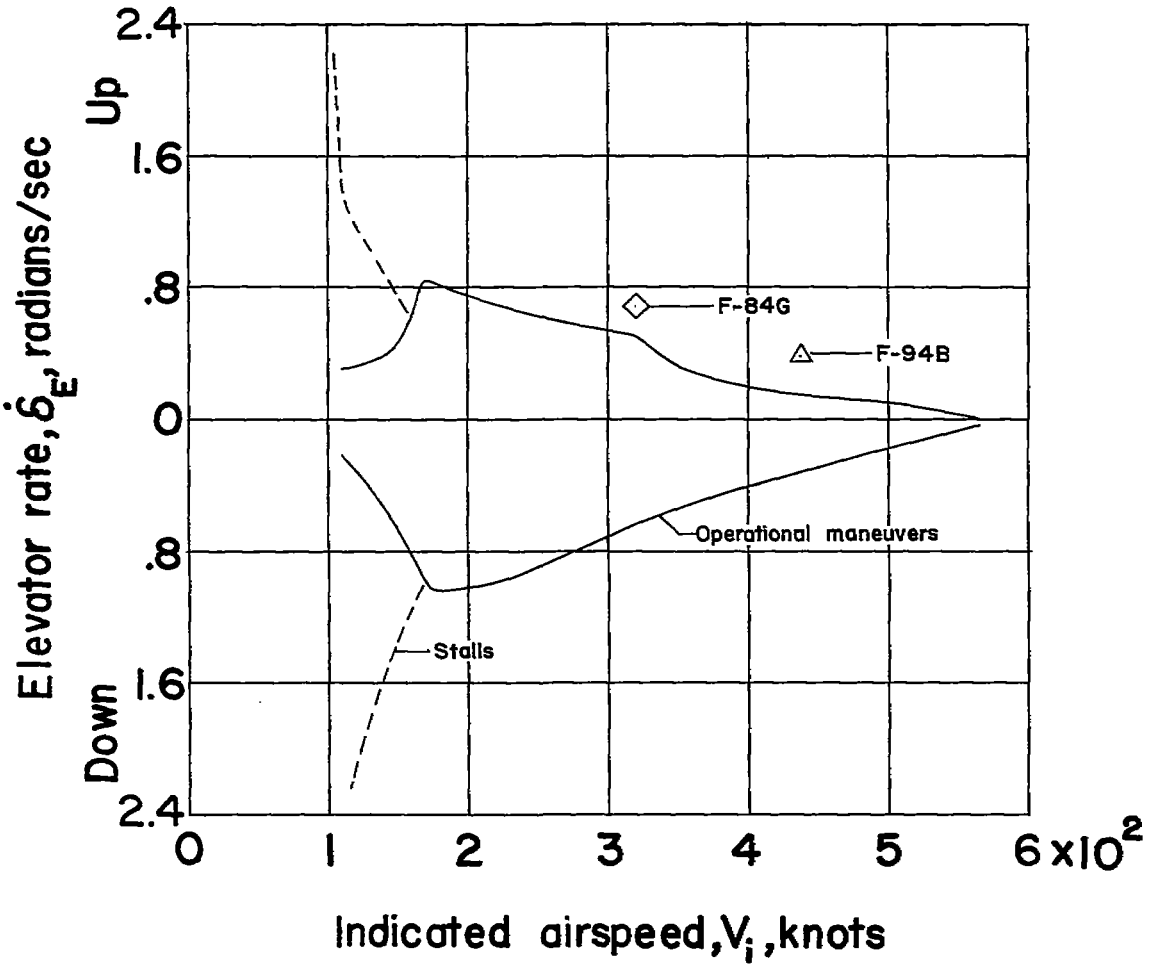

Figure 9.- Envelope of maximum elevator rate and indicated airspeed.

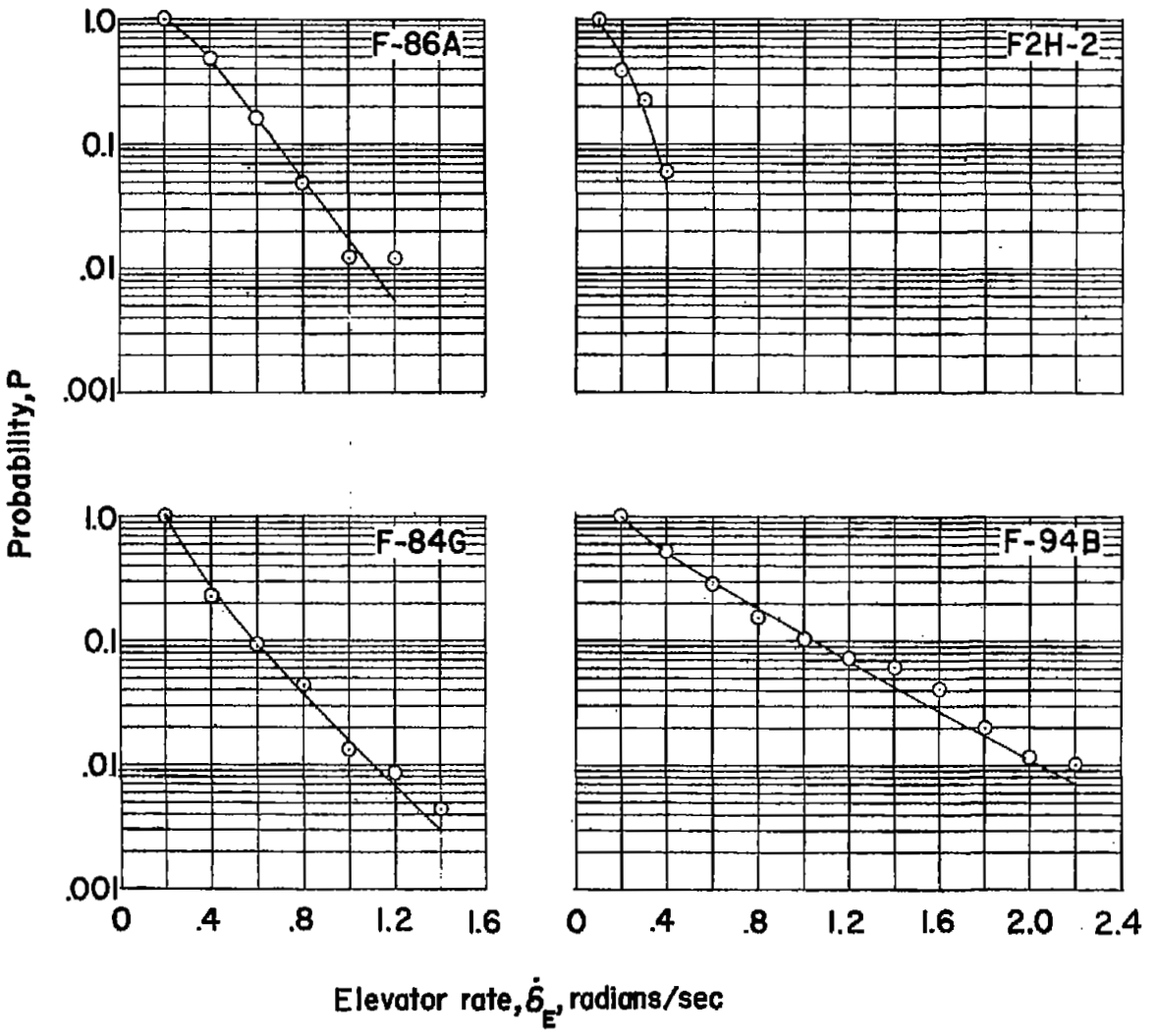

Figure 10.- Comparison of the test data with the fitted Pearson type III curve for probability of equaling or exceeding a given elevator rate.

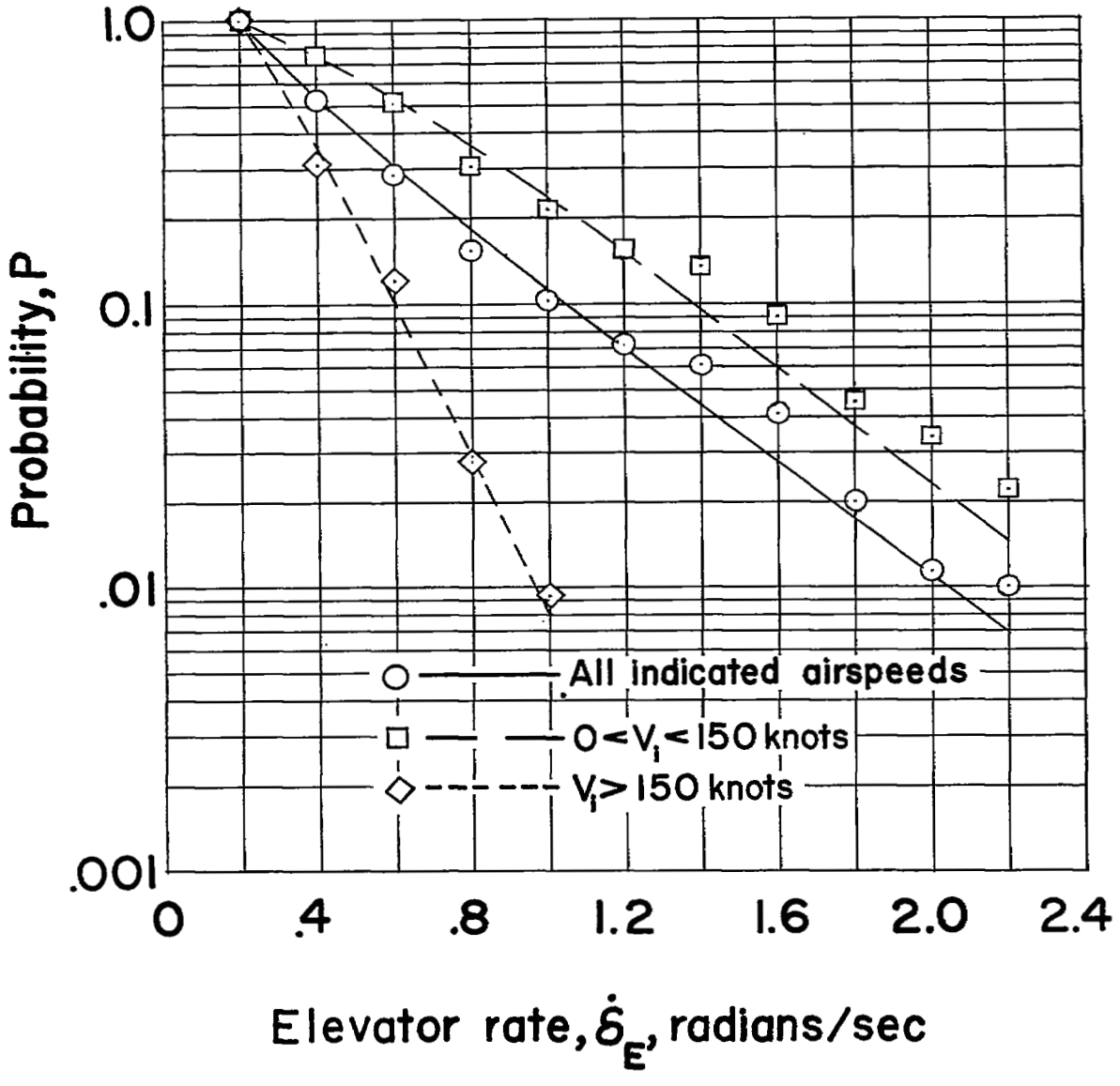

Figure 11.- Comparison of the data for the F-94B test airplane with the fitted Pearson type III curve for probability of equaling or exceeding a given elevator rate for three different speed ranges.

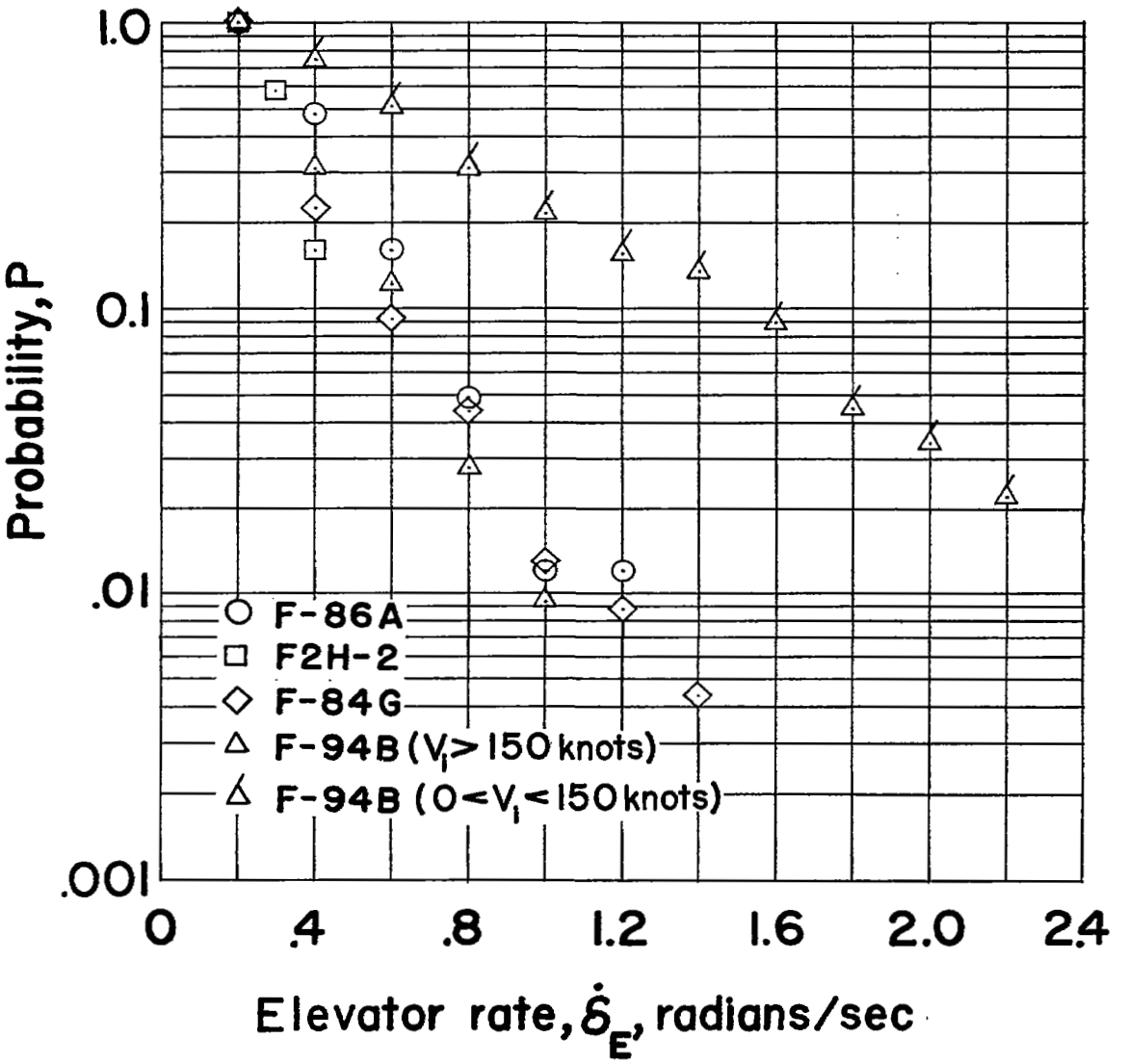

Figure 12.- Probability of equaling or exceeding a given elevator rate.

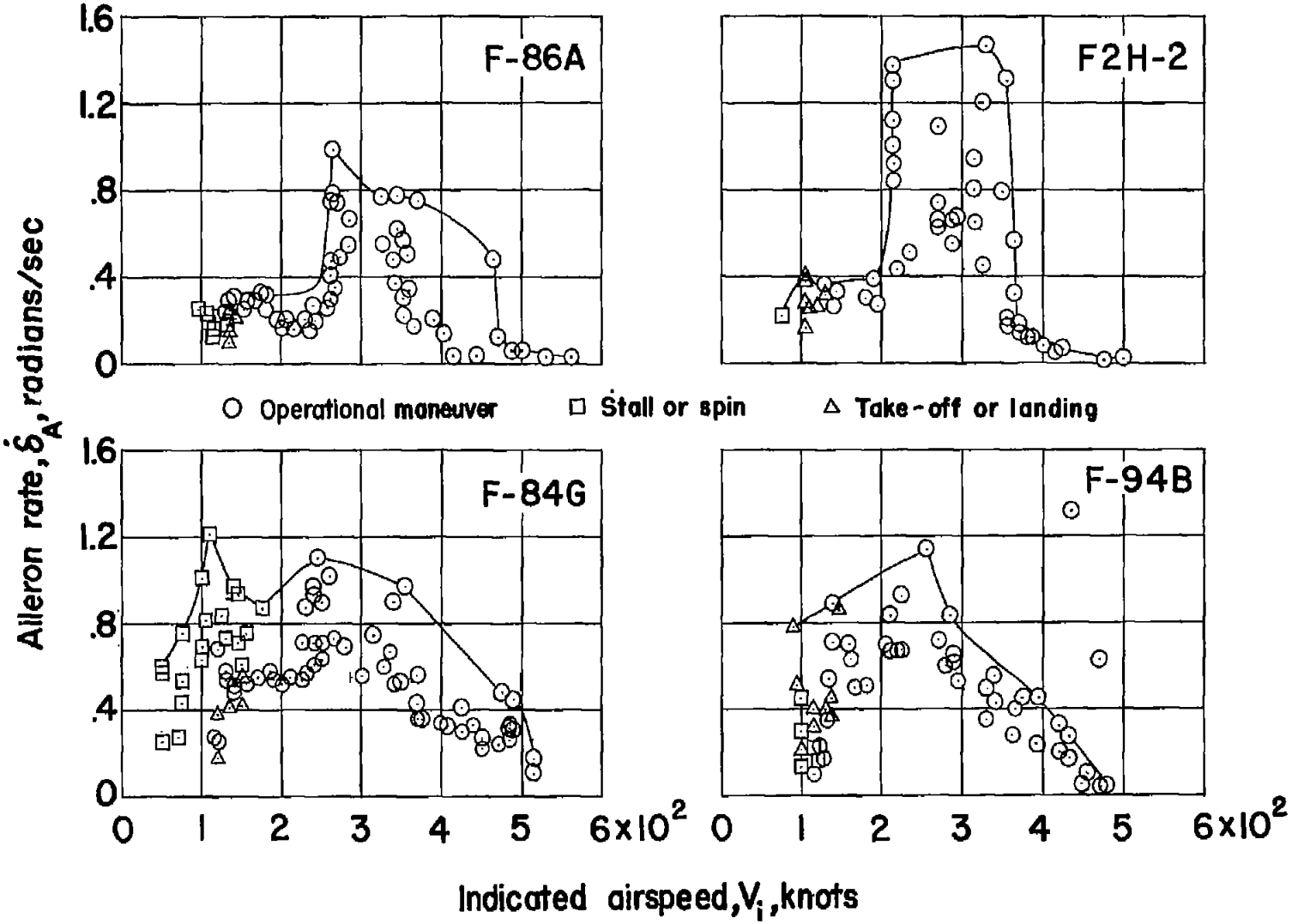

Figure 13.- Maximum right aileron rates plotted against indicated airspeed.

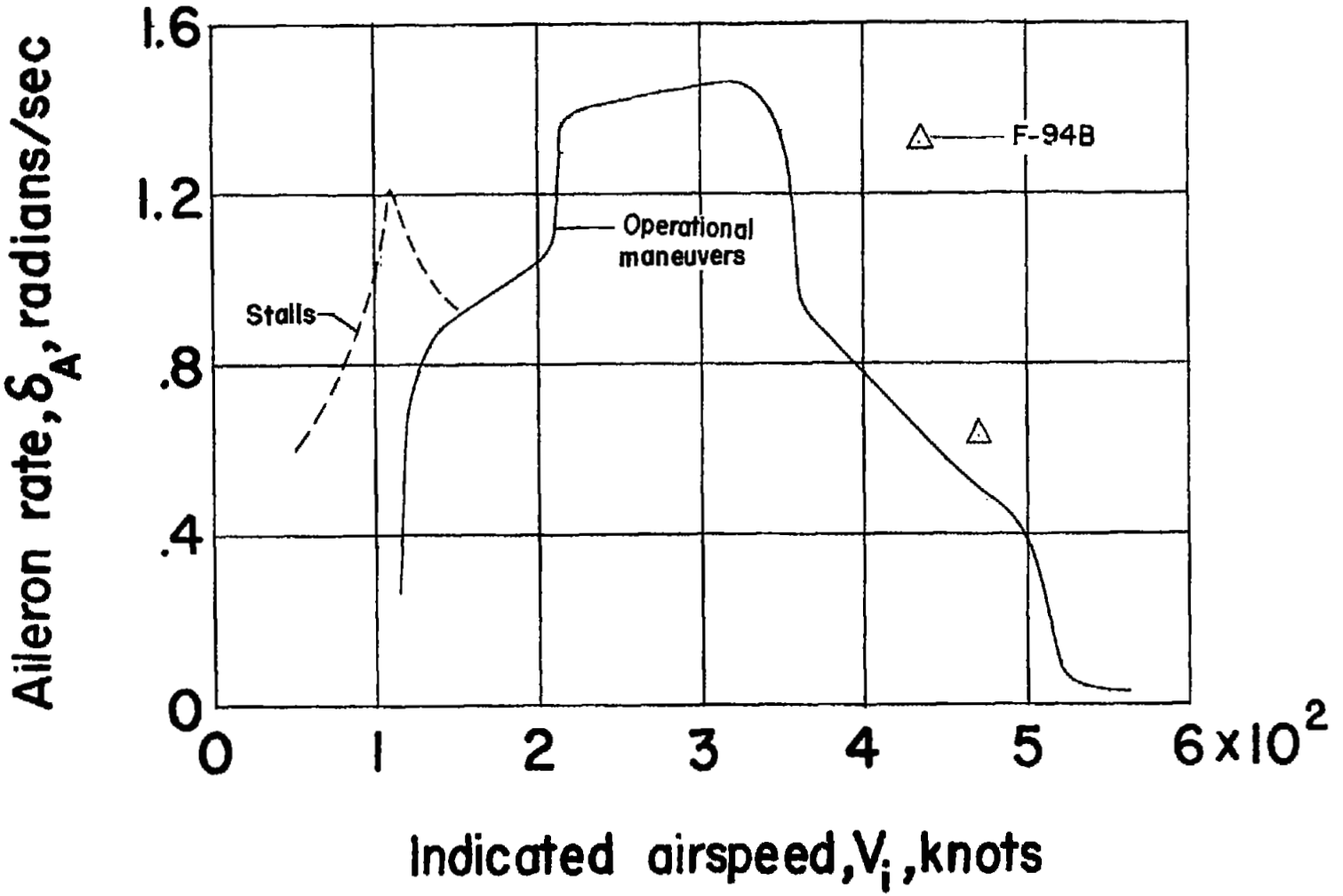

Figure 14.- Envelope of maximum right aileron rate and indicated airspeed.

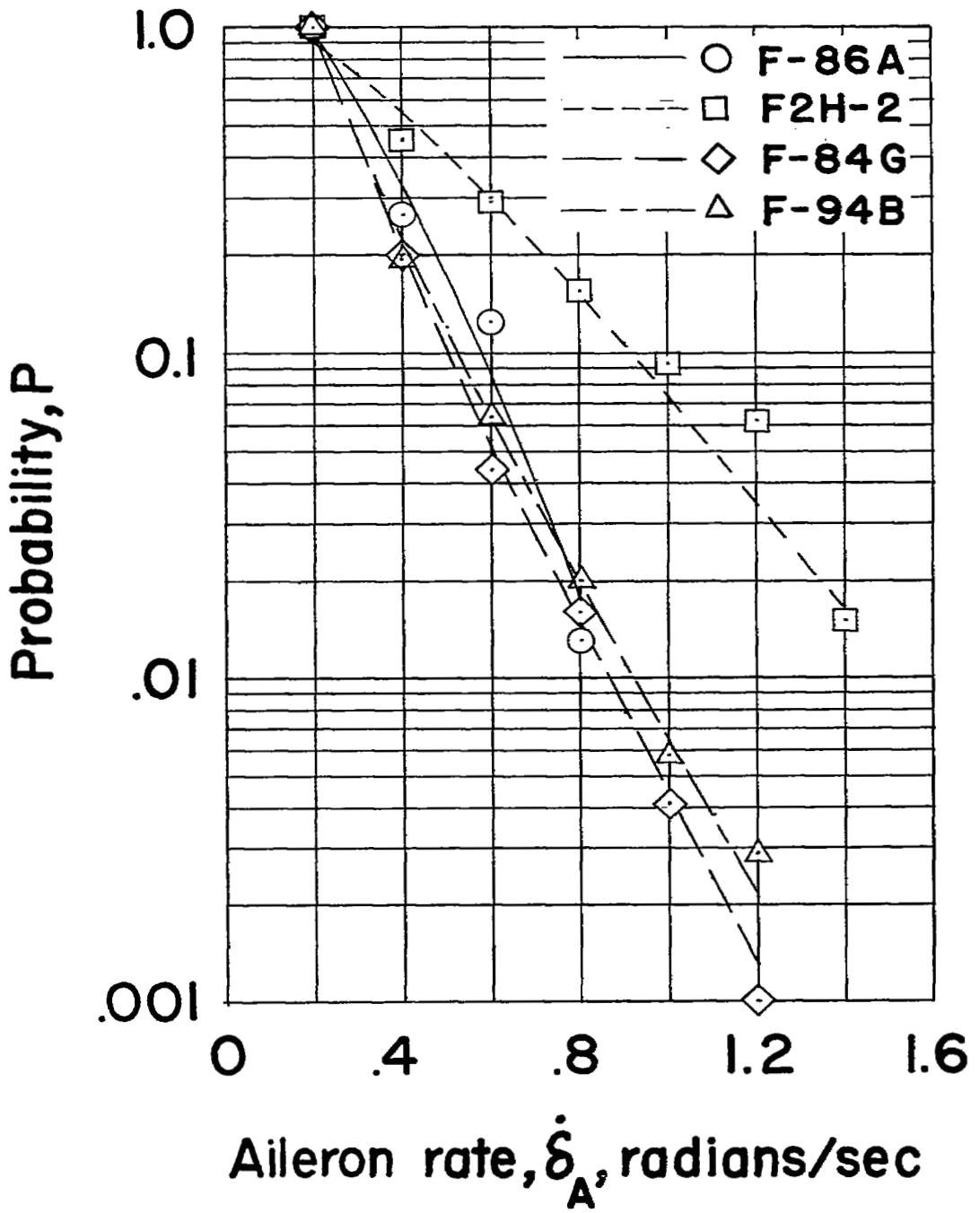

Figure 15.- Probability of equaling or exceeding a given aileron rate.

[redacted]

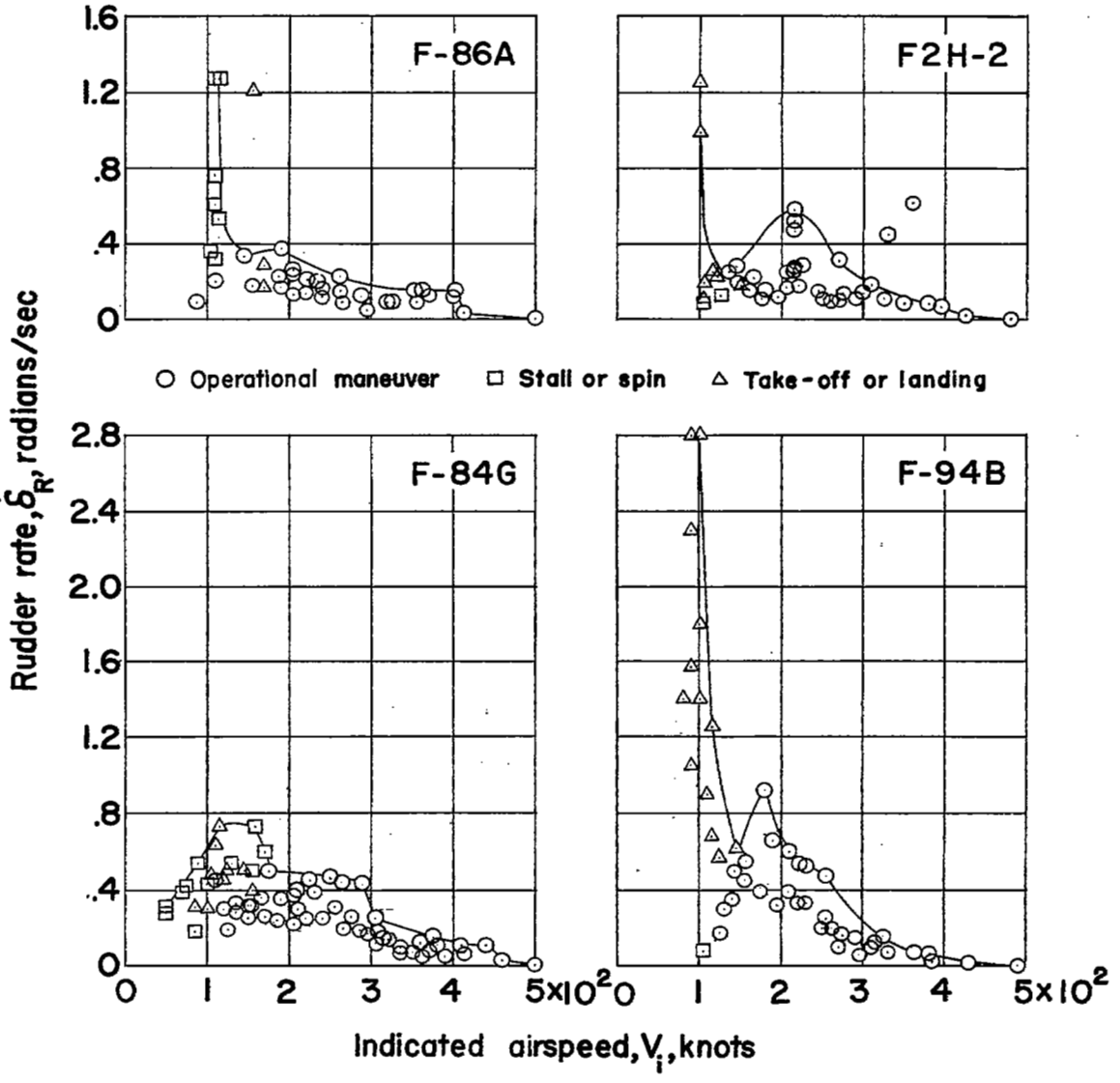

Figure 16.- Maximum rudder rates plotted against indicated airspeed.

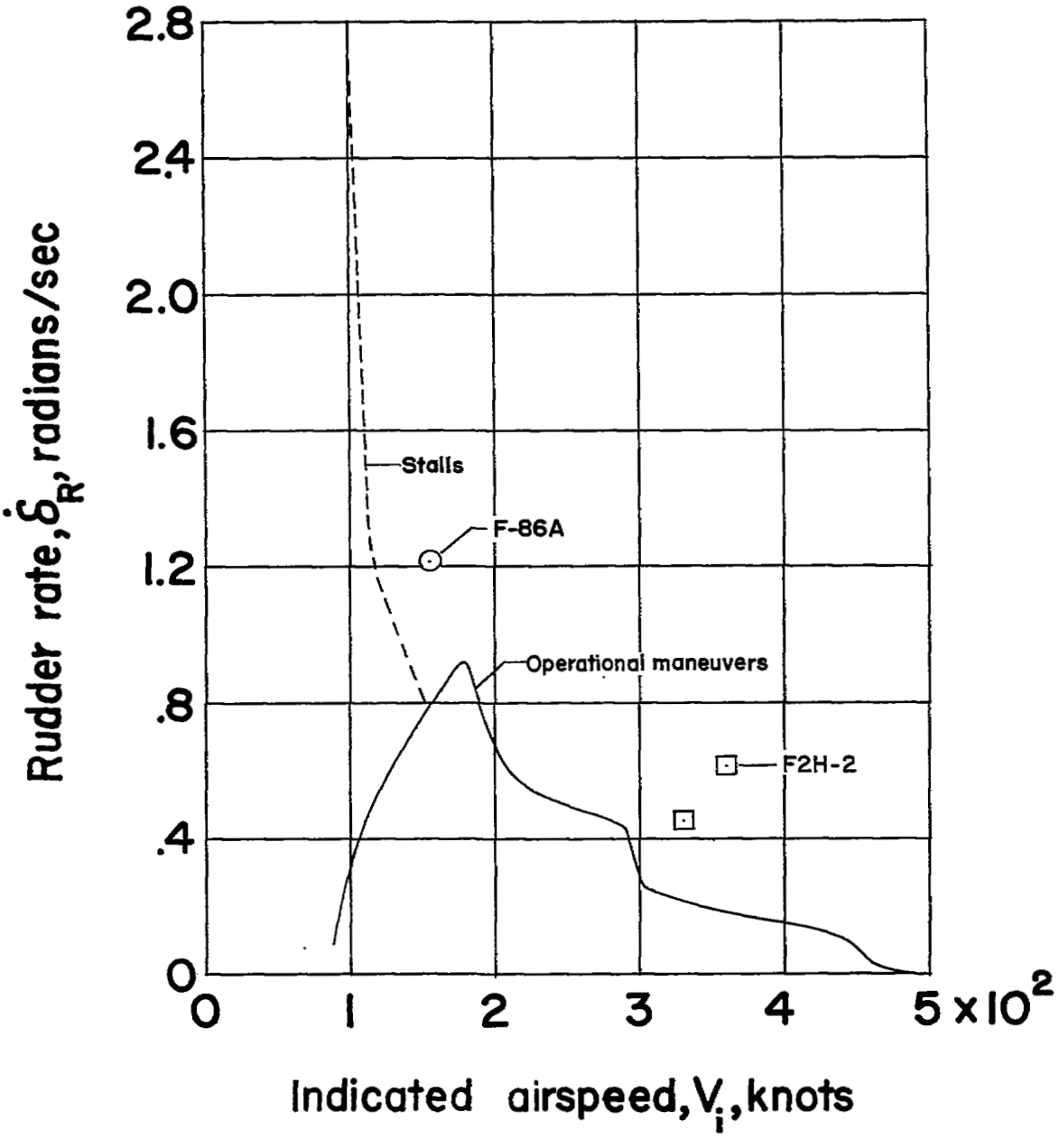

Figure 17.- Envelope of maximum rudder rate and indicated airspeed.

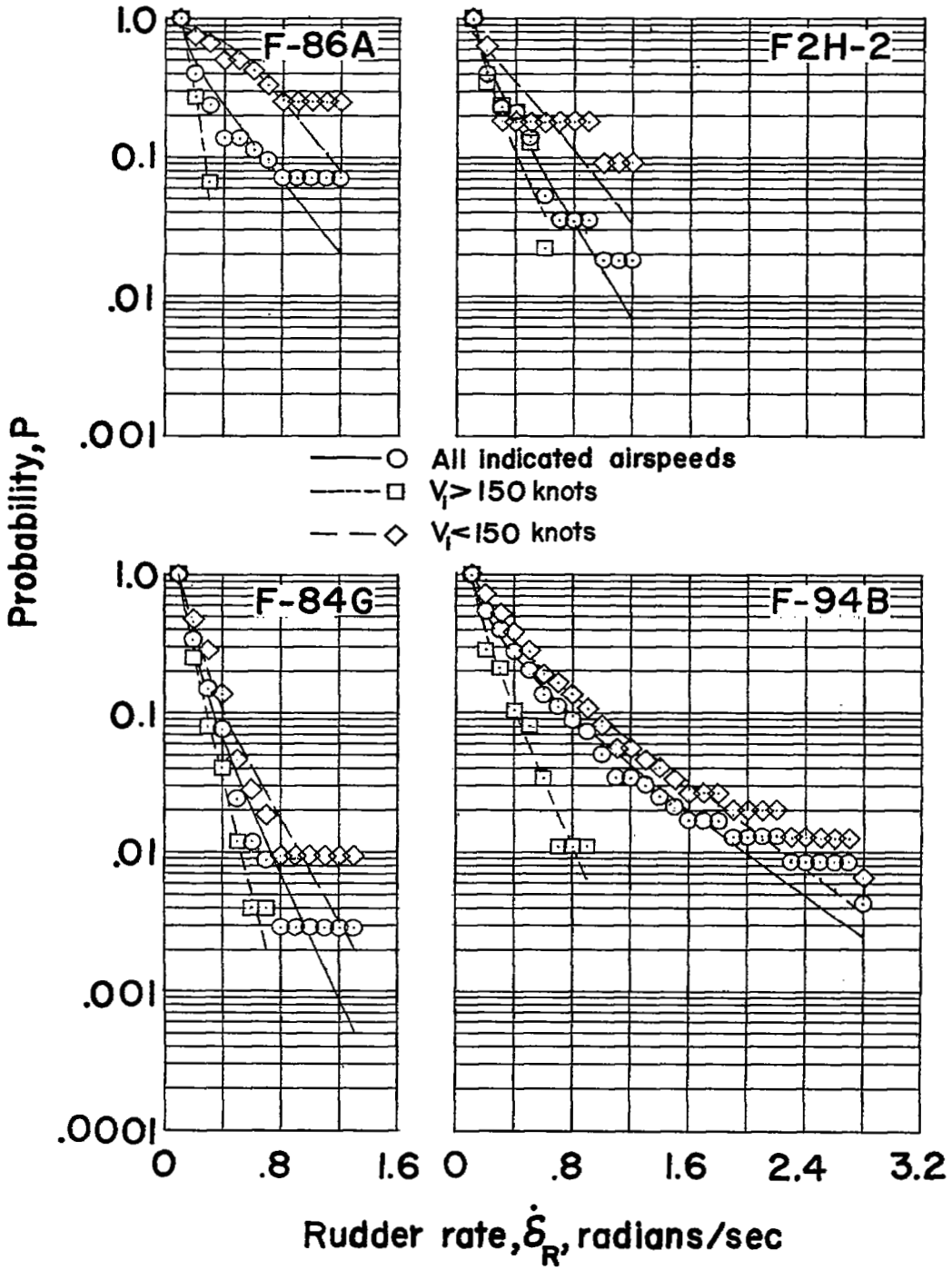

Figure 18.- Comparison of the test data with the fitted Pearson type III curve for probability of equaling or exceeding a given rudder rate for three different speed ranges.

[redacted]

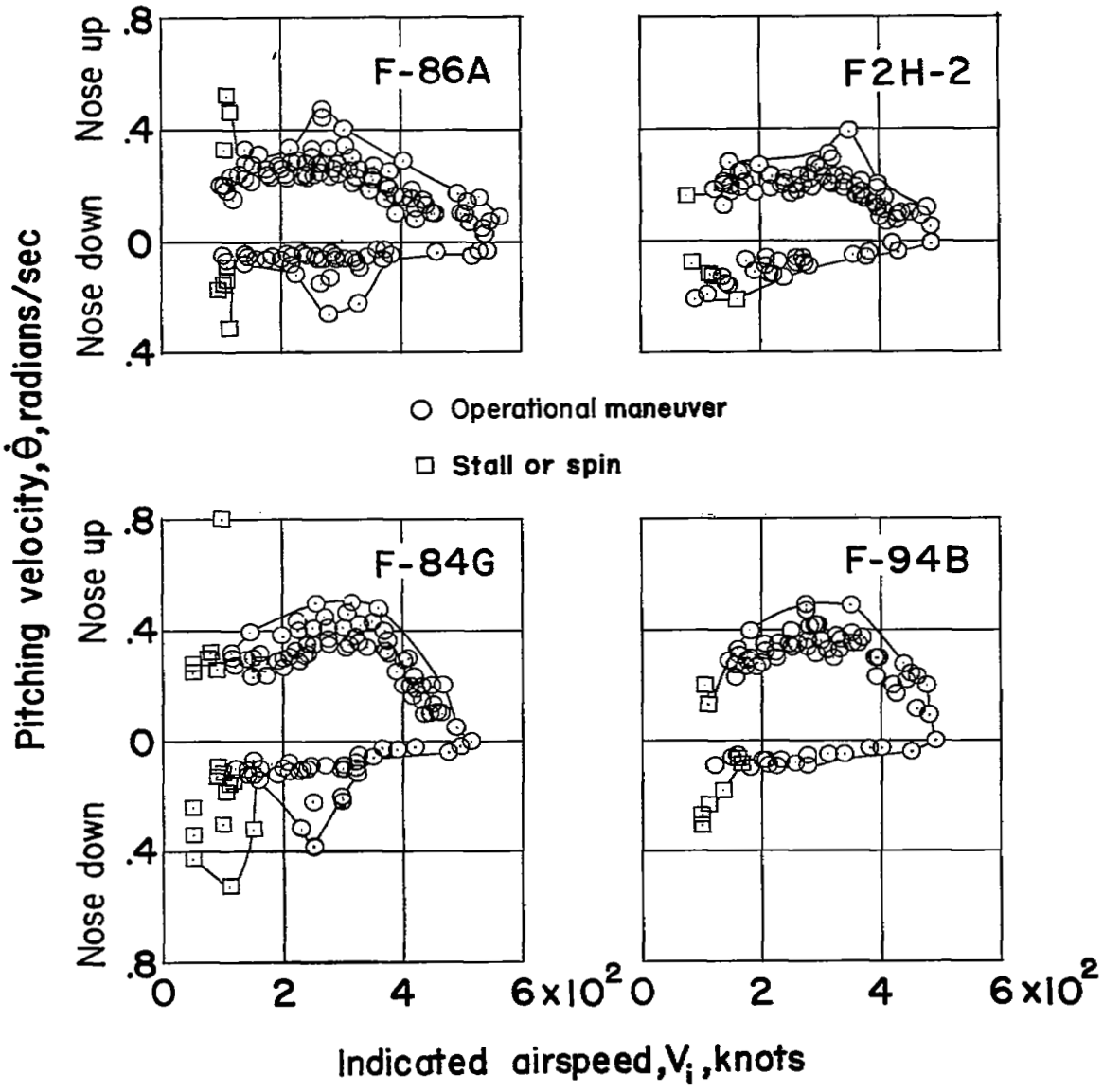

Figure 19.- Maximum pitching velocities plotted against indicated airspeed.

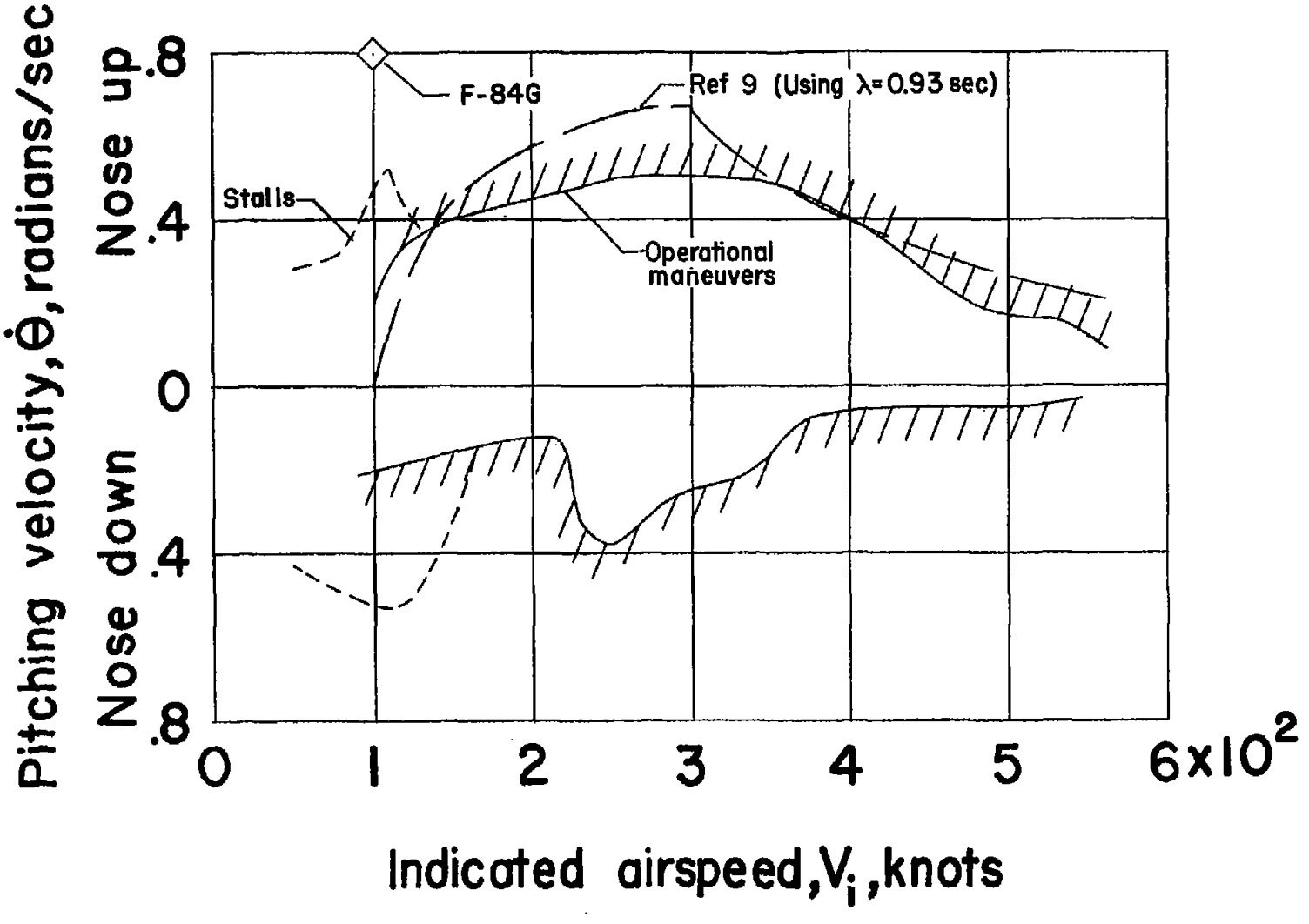

Figure 20.- Comparison of test envelope with a method of calculating pitching velocities.

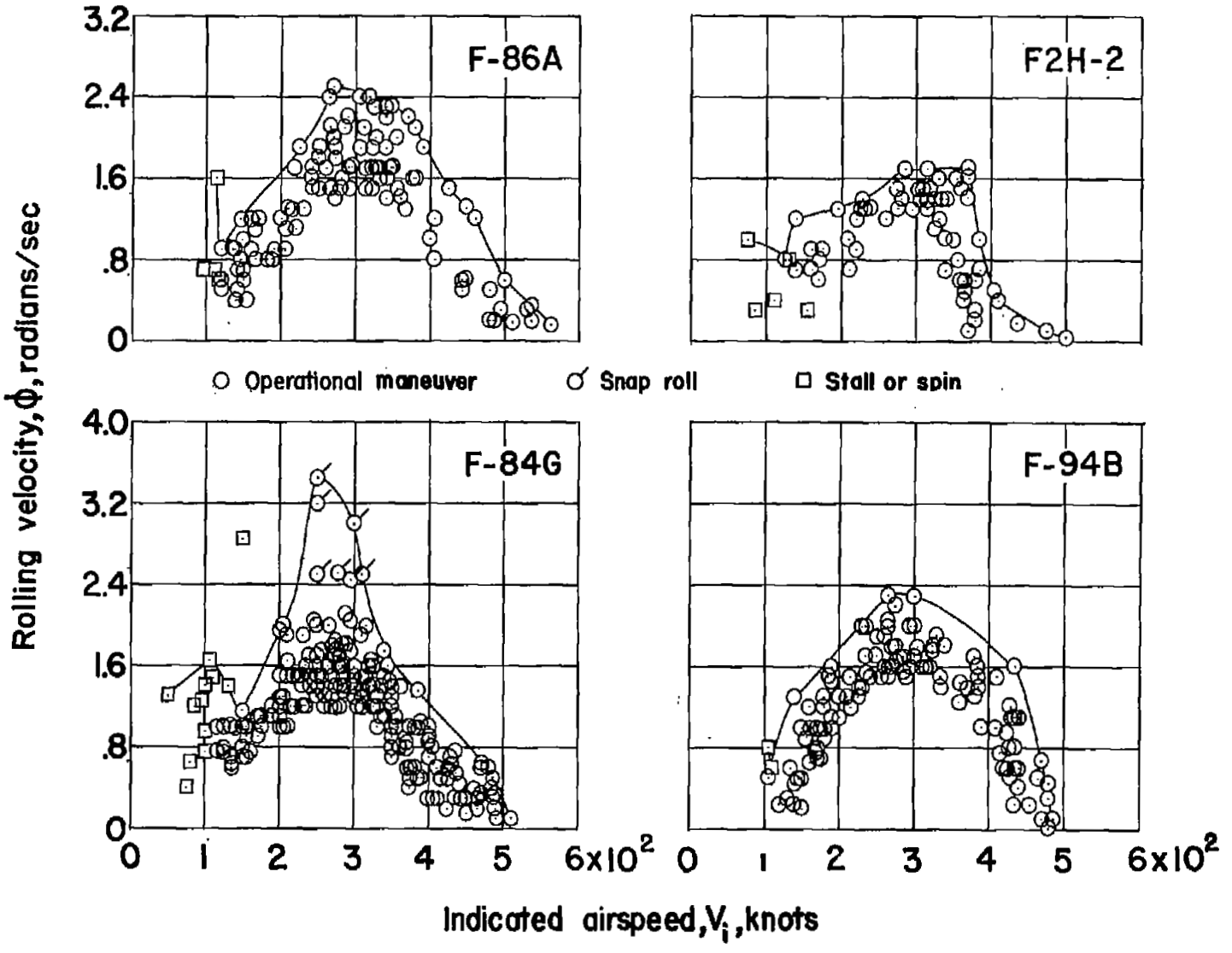

Figure 21.- Maximum rolling velocities plotted against indicated airspeed.

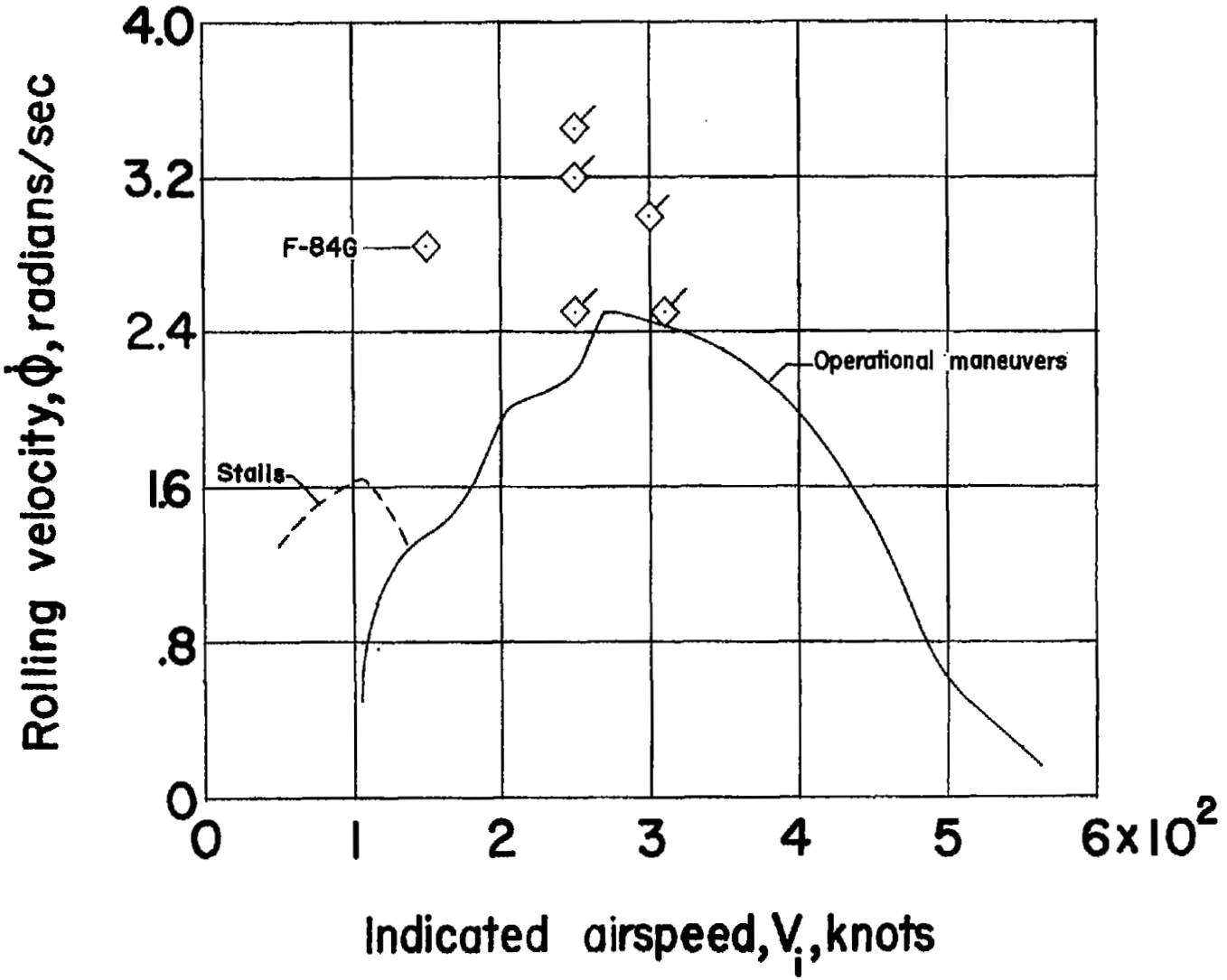

Figure 22.- Envelope of maximum rolling velocity and indicated airspeed.

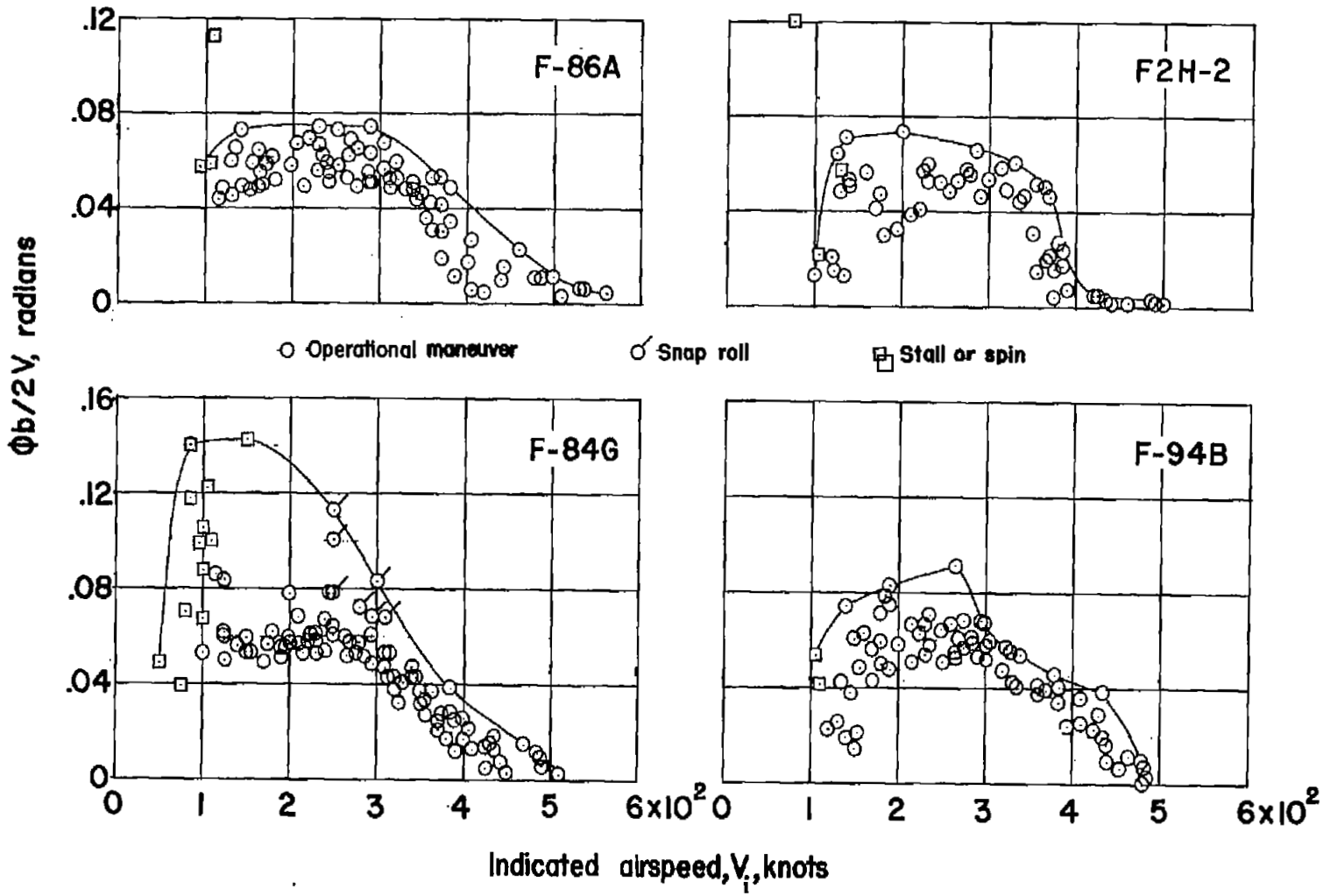

Figure 23.- Maximum wing-tip helix angles plotted against indicated airspeed.

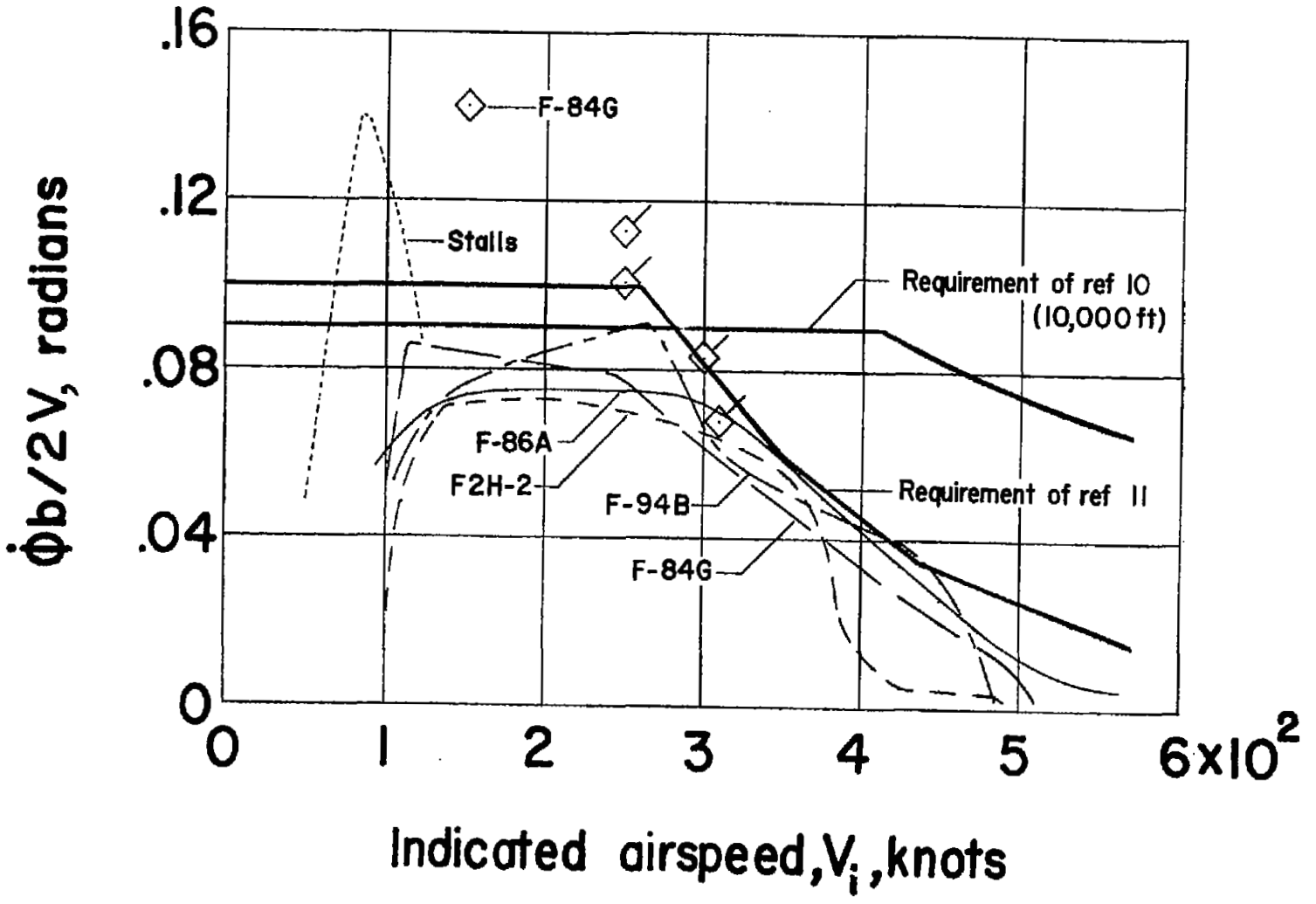

Figure 24.- Envelopes of maximum wing-tip helix angle and indicated airspeed.

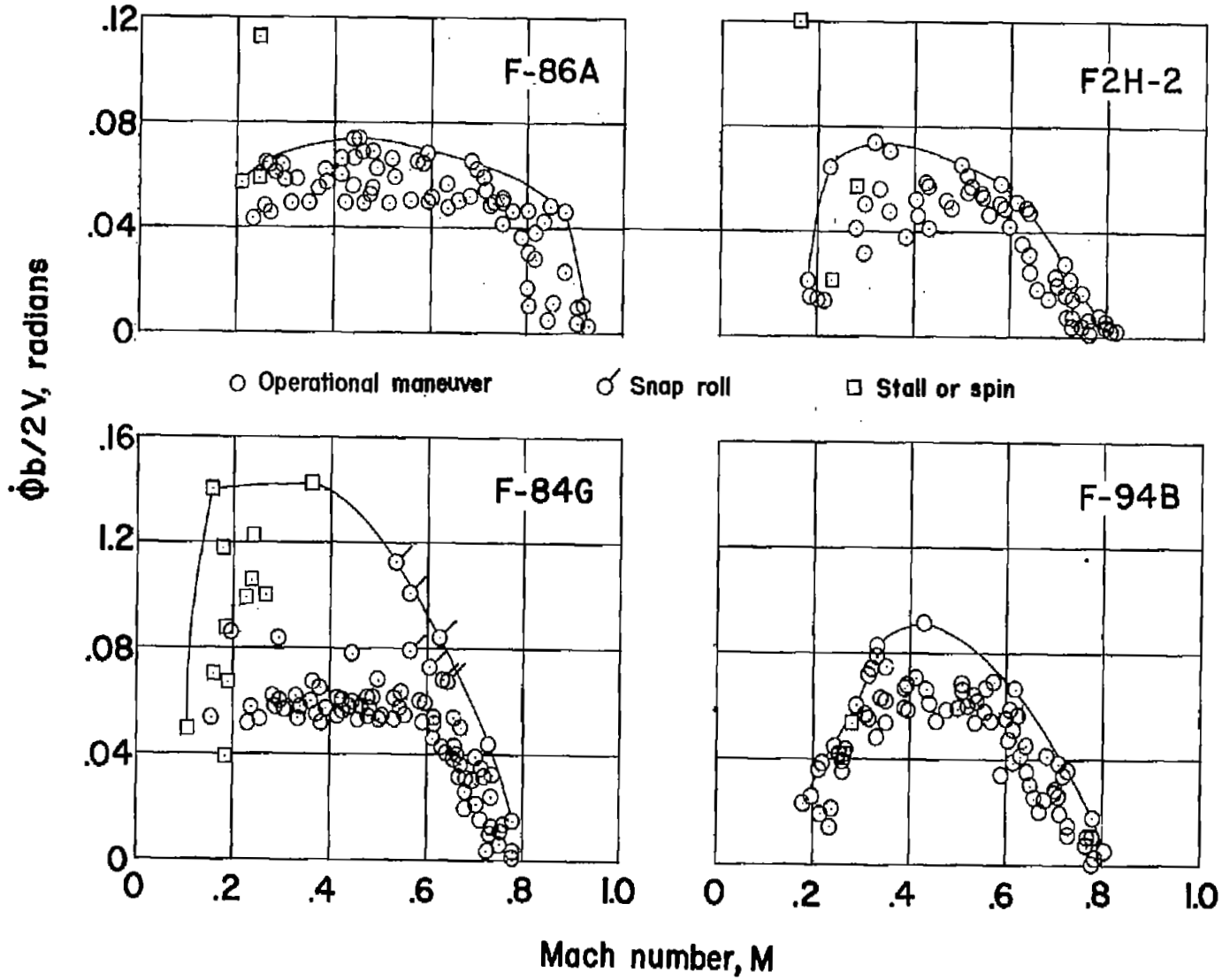

Figure 25.- Maximum wing-tip helix angles plotted against Mach number.

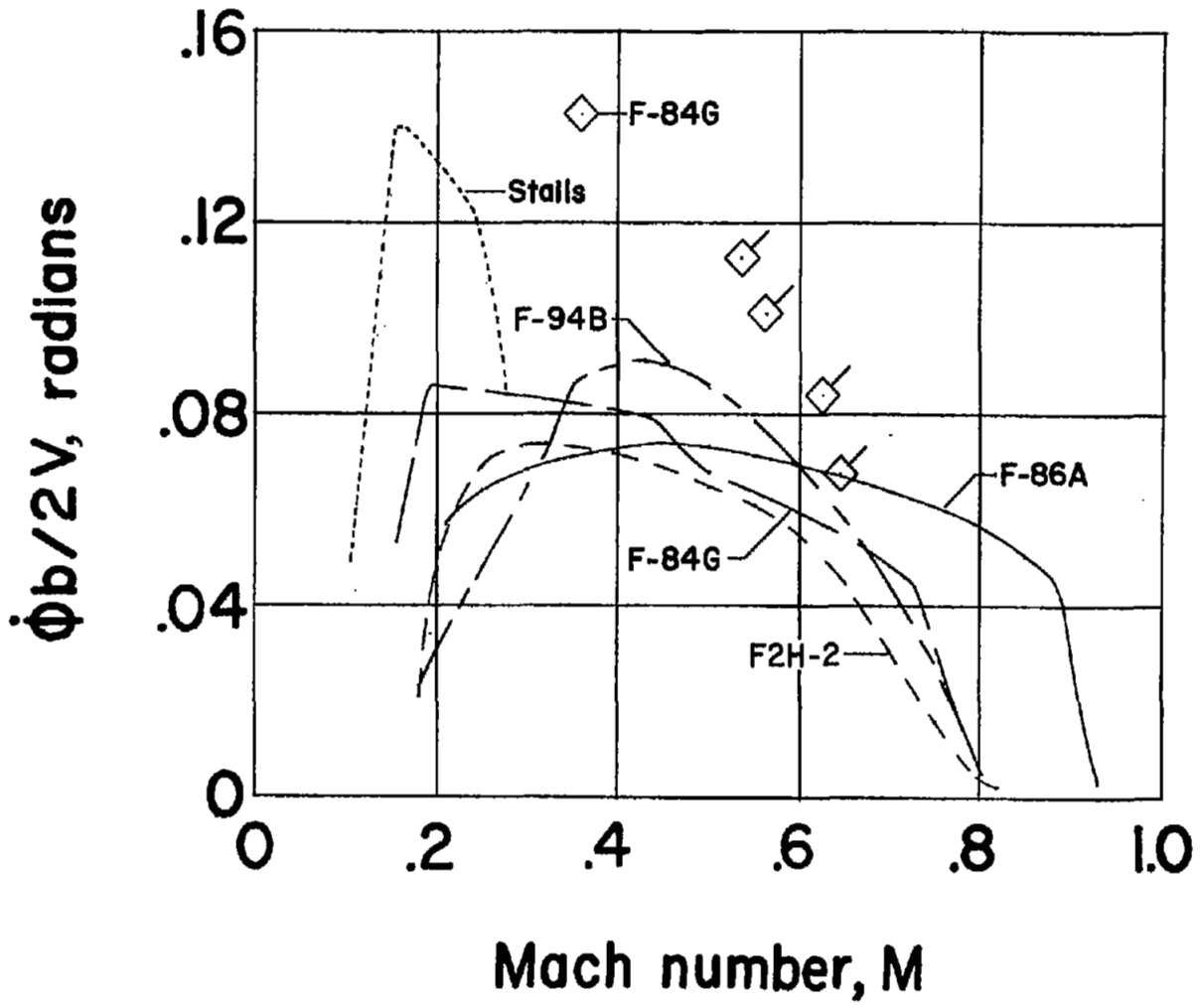

Figure 26.- Envelopes of maximum wing-tip helix angle and Mach number.

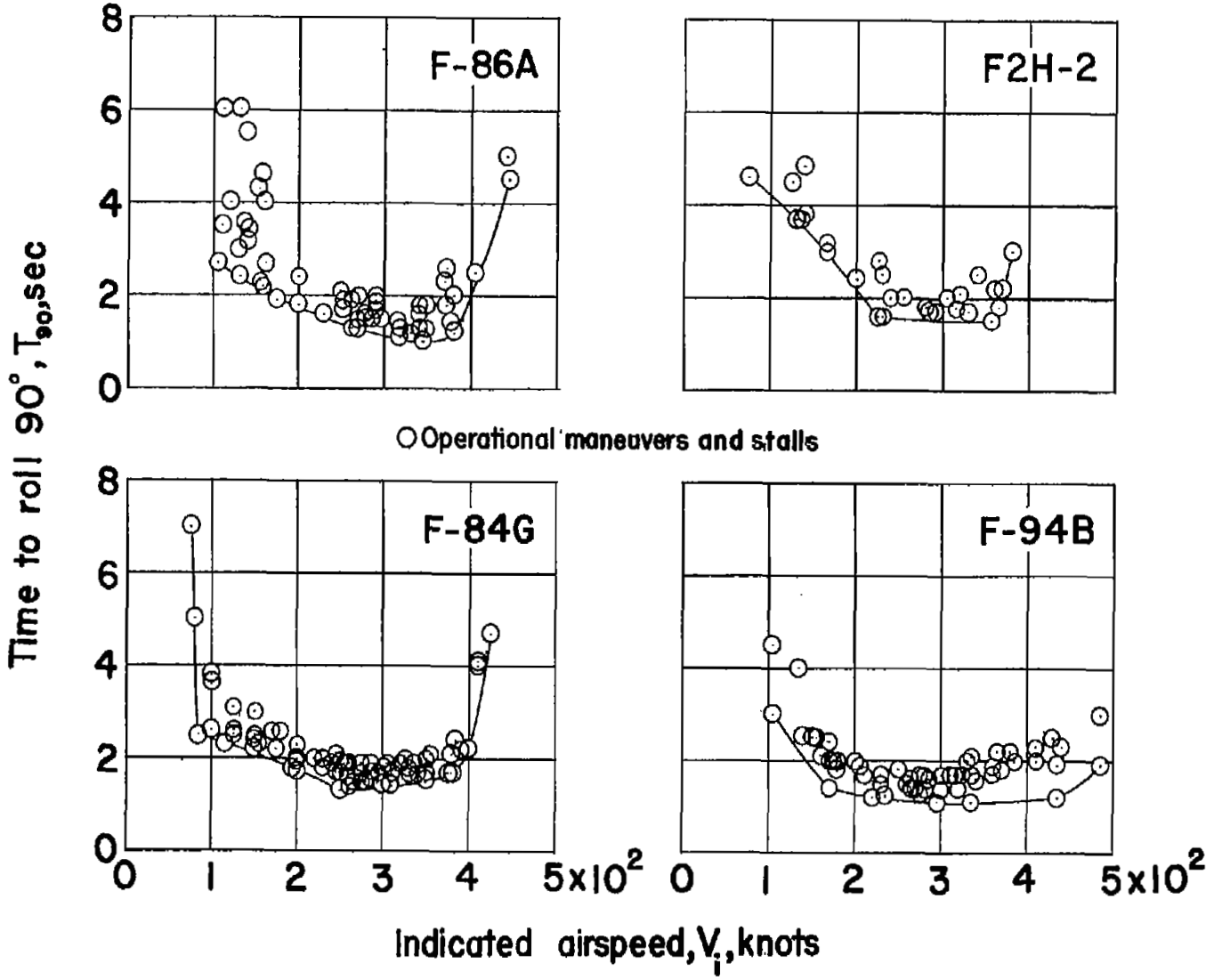

Figure 27.- Minimum times to roll 90° plotted against indicated airspeed.

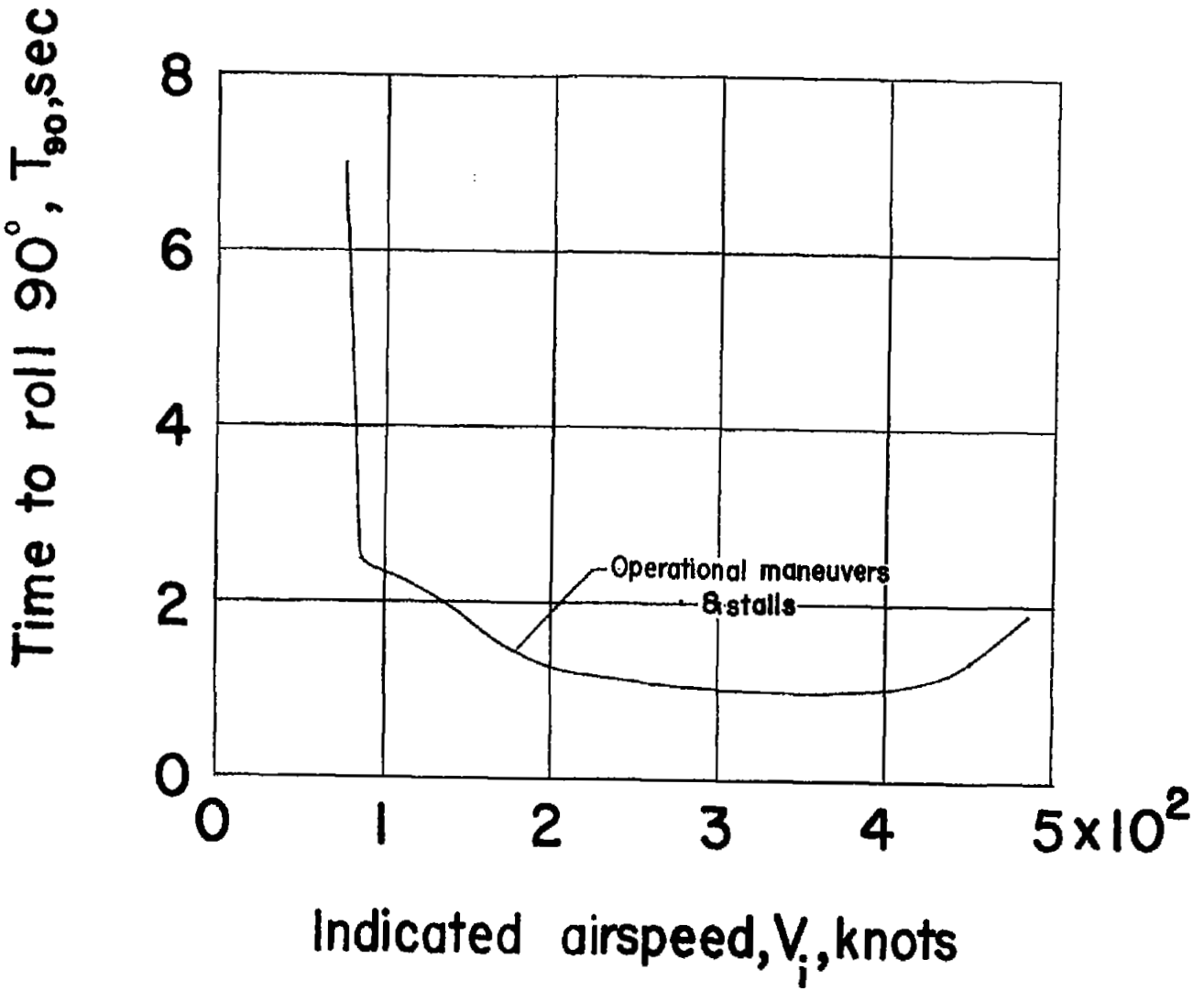

Figure 28.- Envelope of minimum time to roll 90° and indicated airspeed.

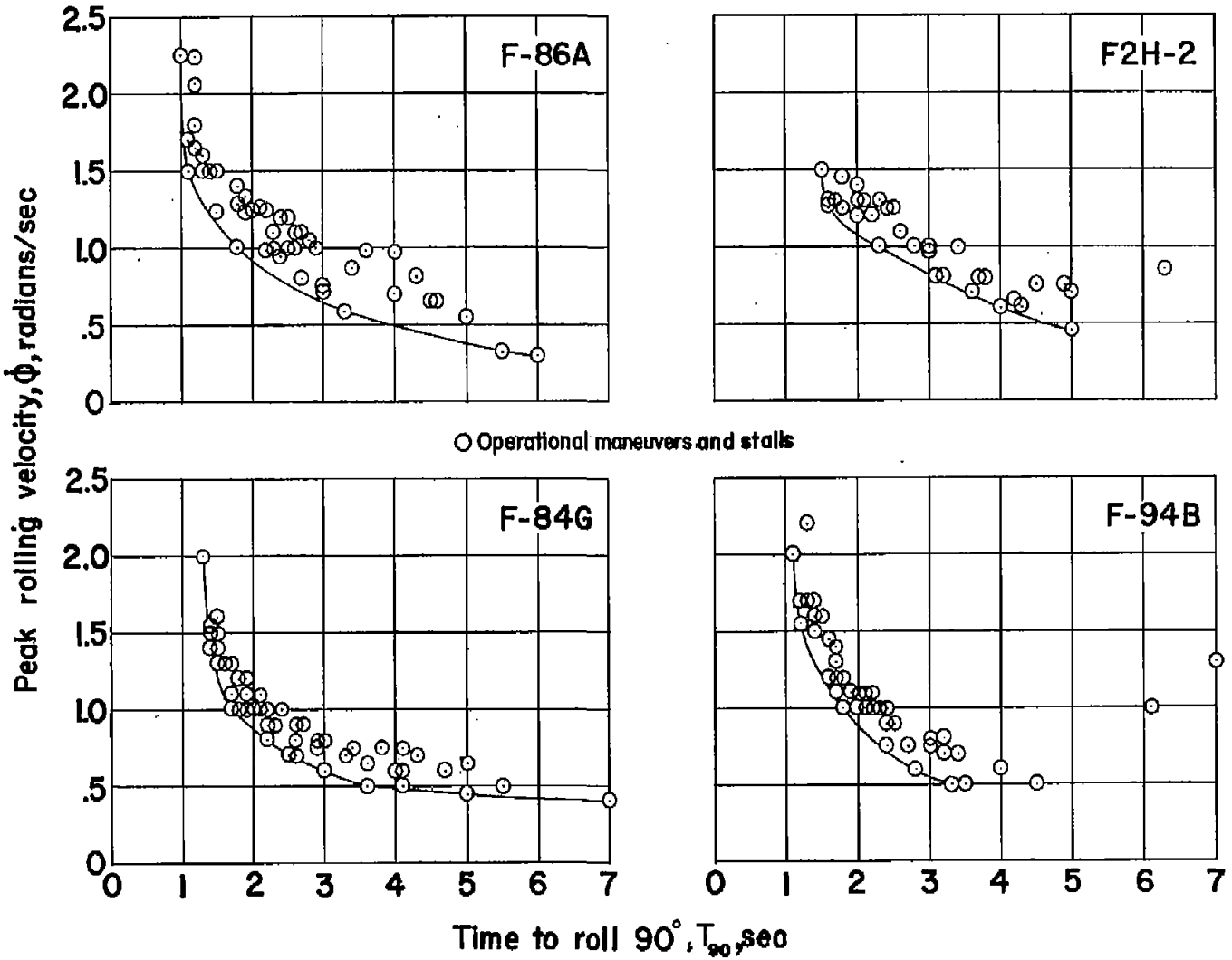

Figure 29.- Peak rolling velocities reached during roll to 90° plotted against time to roll 90°.

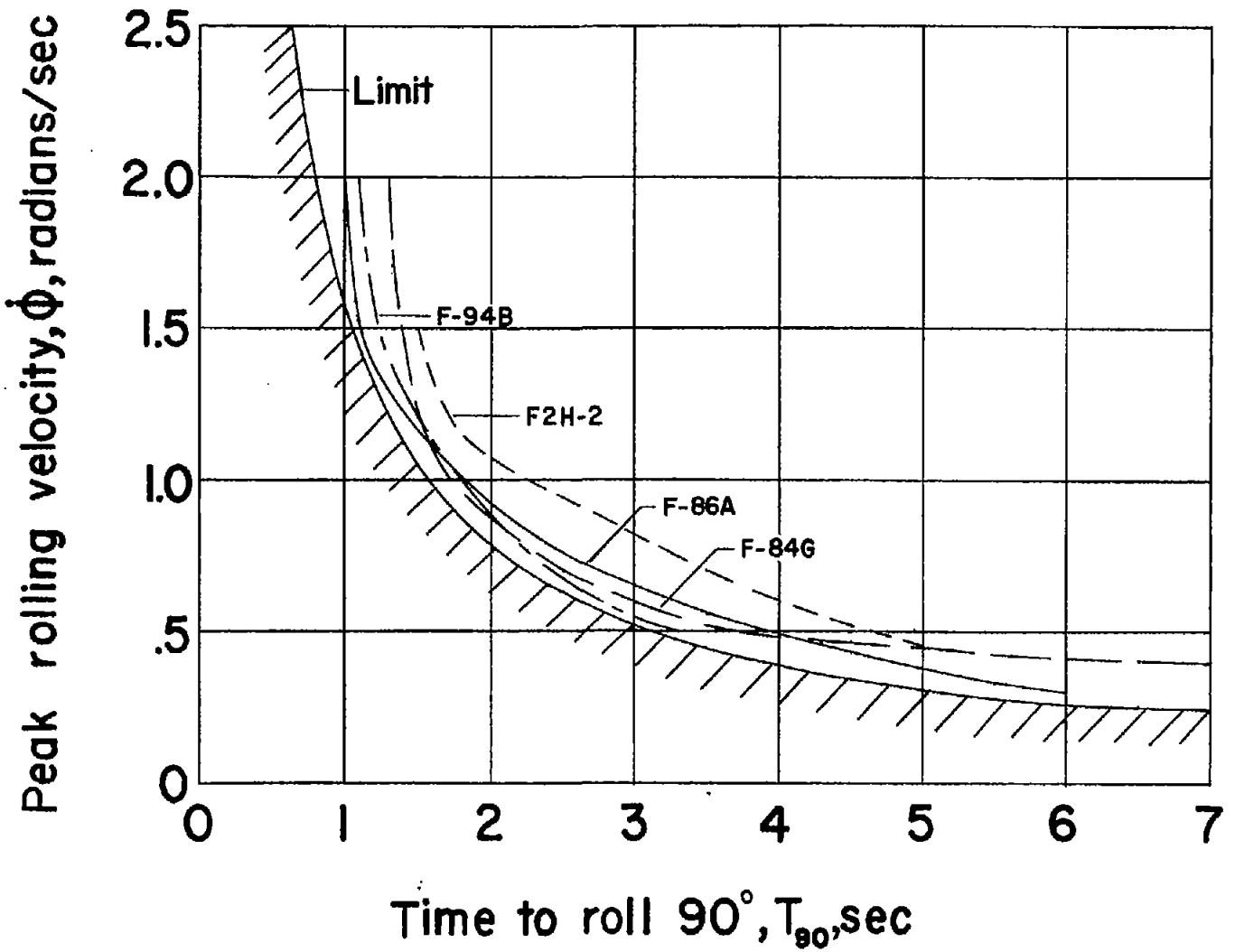

Figure 30.- Envelopes of peak rolling velocities reached during roll to 90° and time to roll 90°.

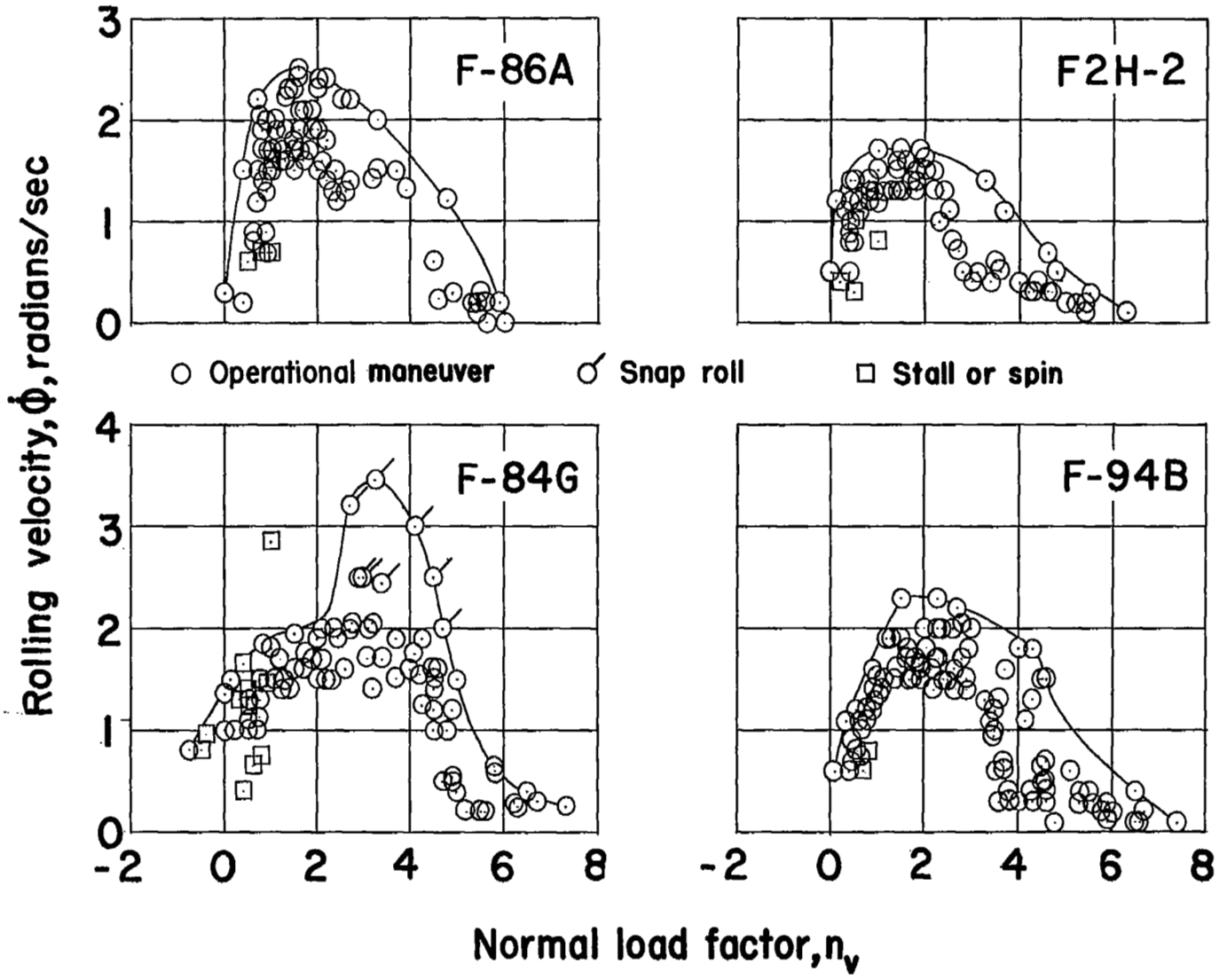

Figure 31.- Maximum rolling velocities plotted against normal load factor.

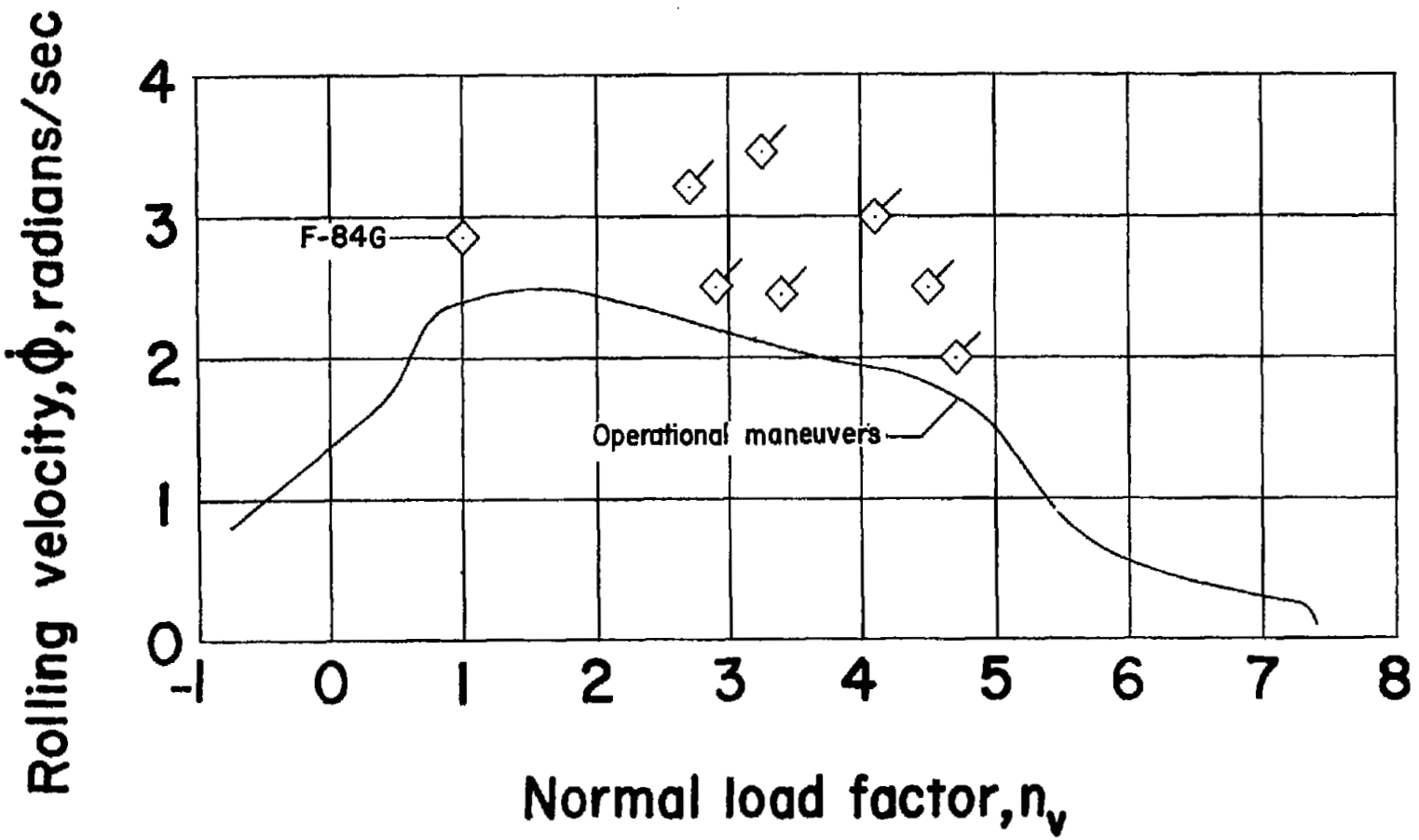

Figure 32.- Envelope of maximum rolling velocity and normal load factor.

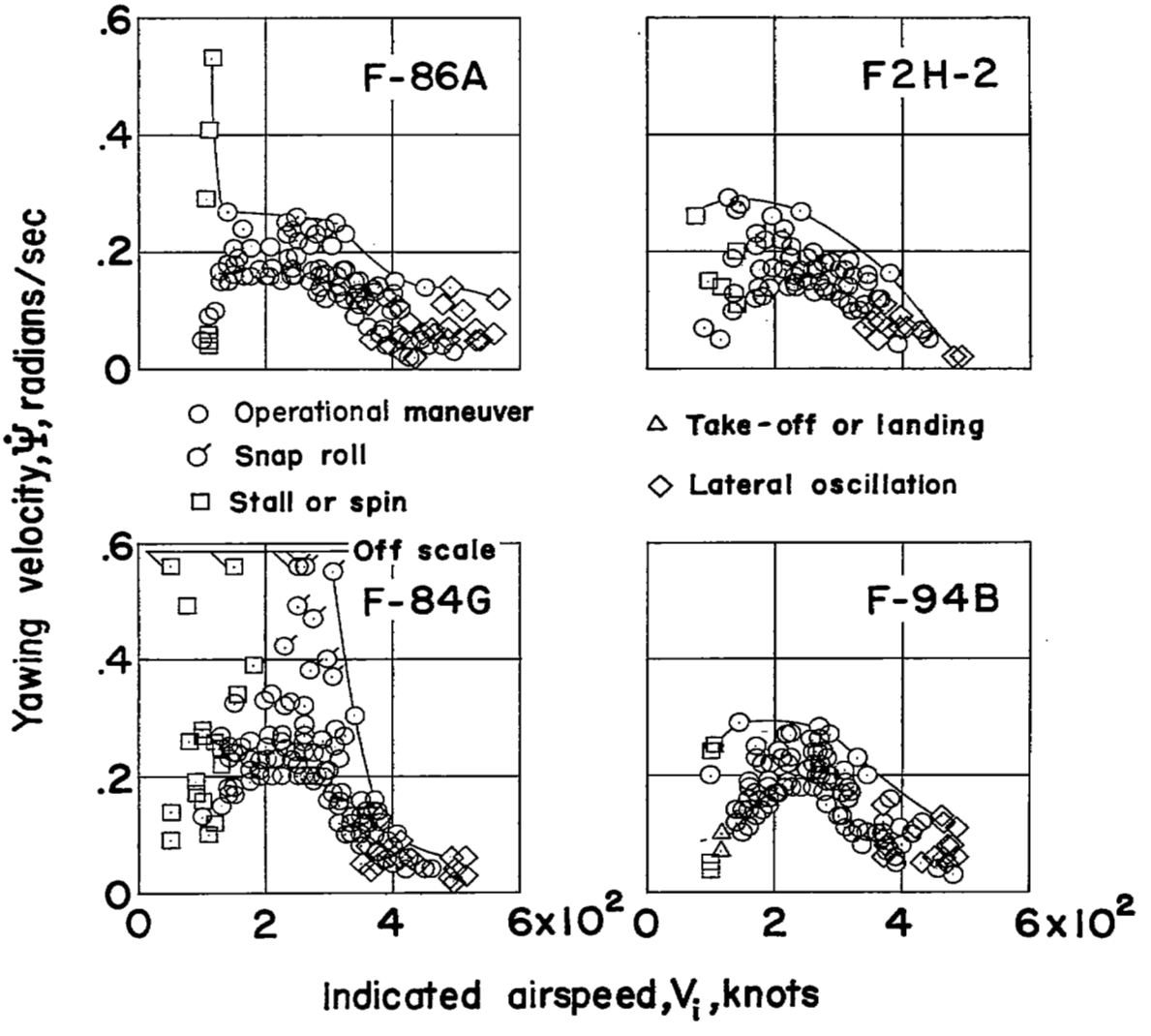

Figure 33.- Maximum yawing velocities plotted against indicated airspeed.

[redacted]

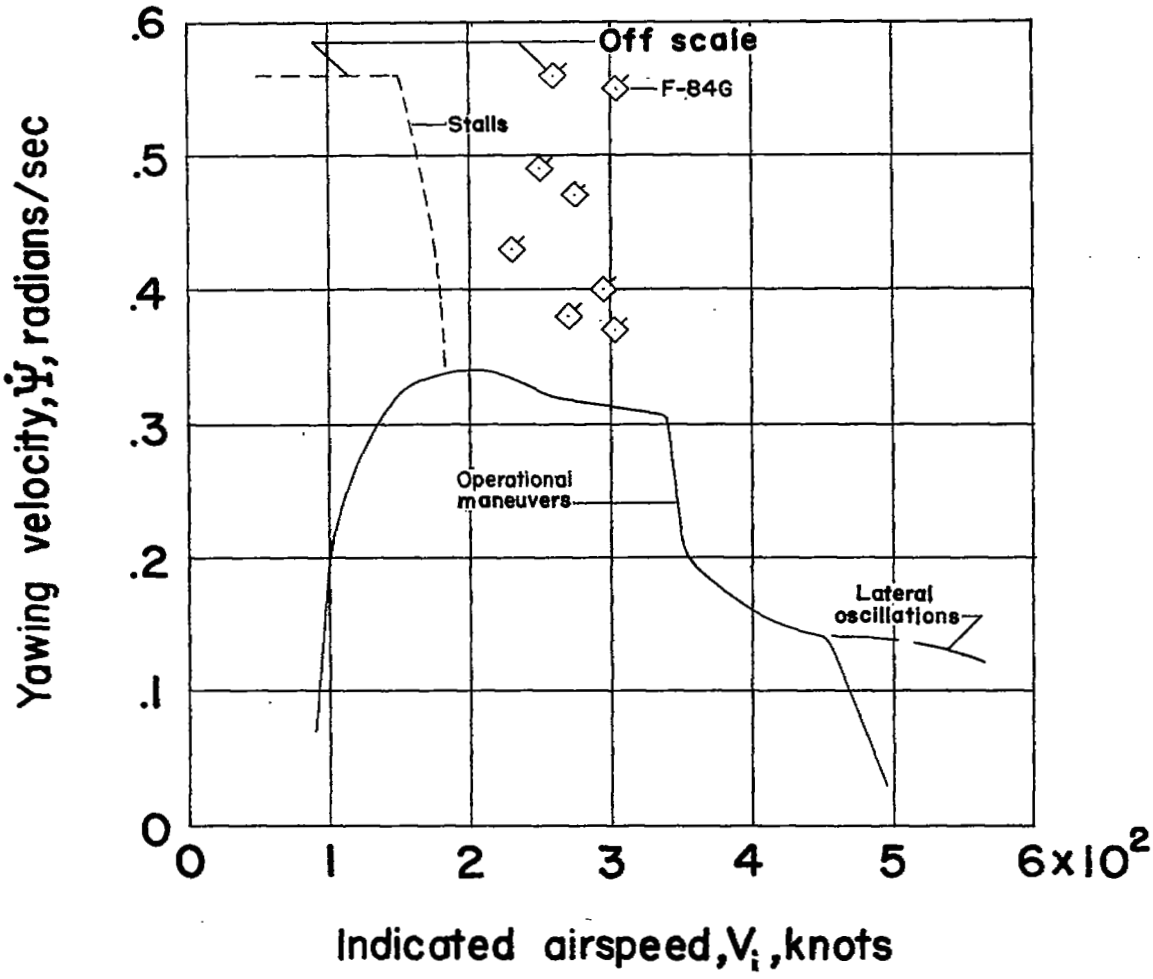

Figure 34.- Envelope of maximum yawing velocity and indicated airspeed.

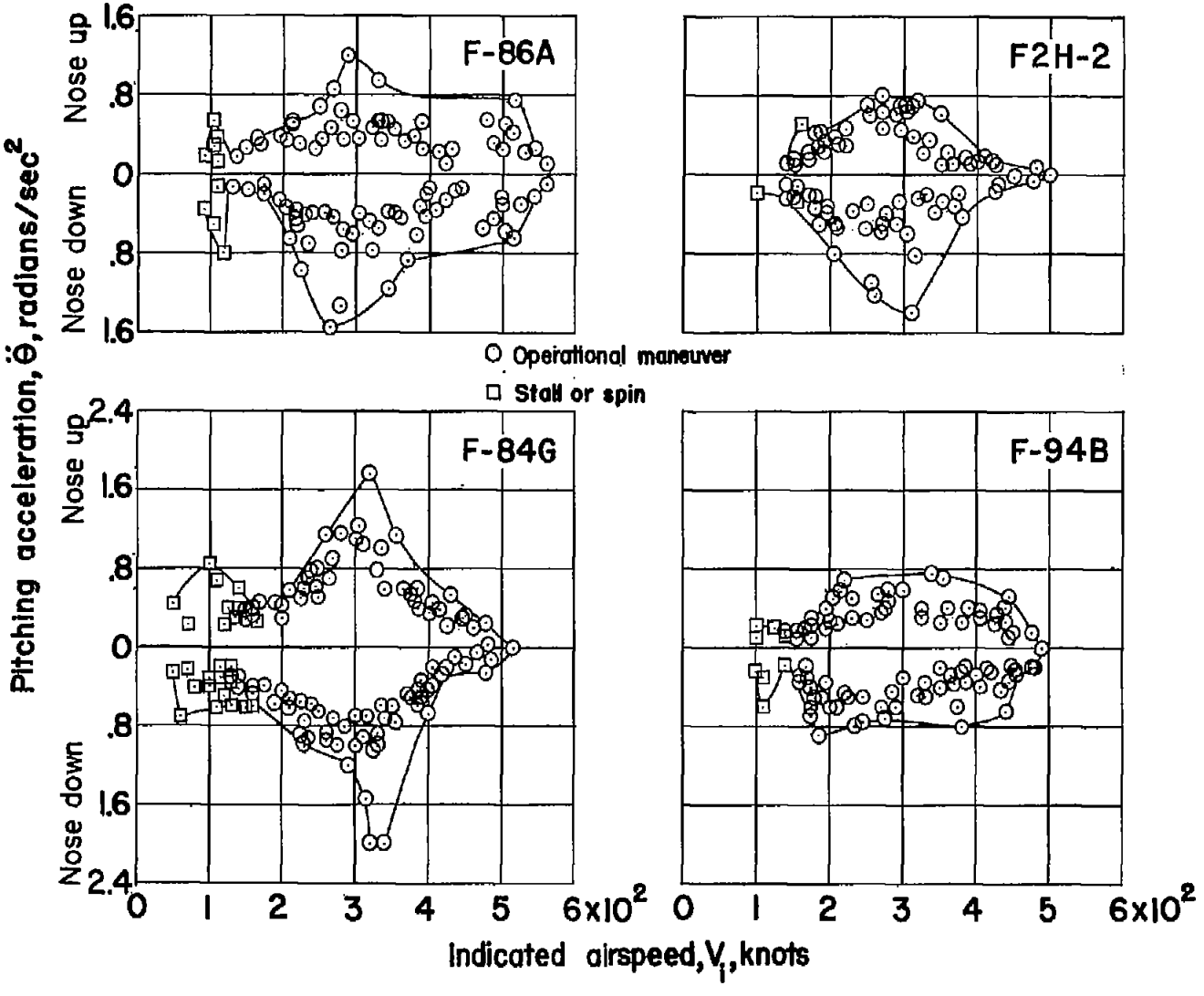

Figure 35.- Maximum pitching accelerations plotted against indicated airspeed.

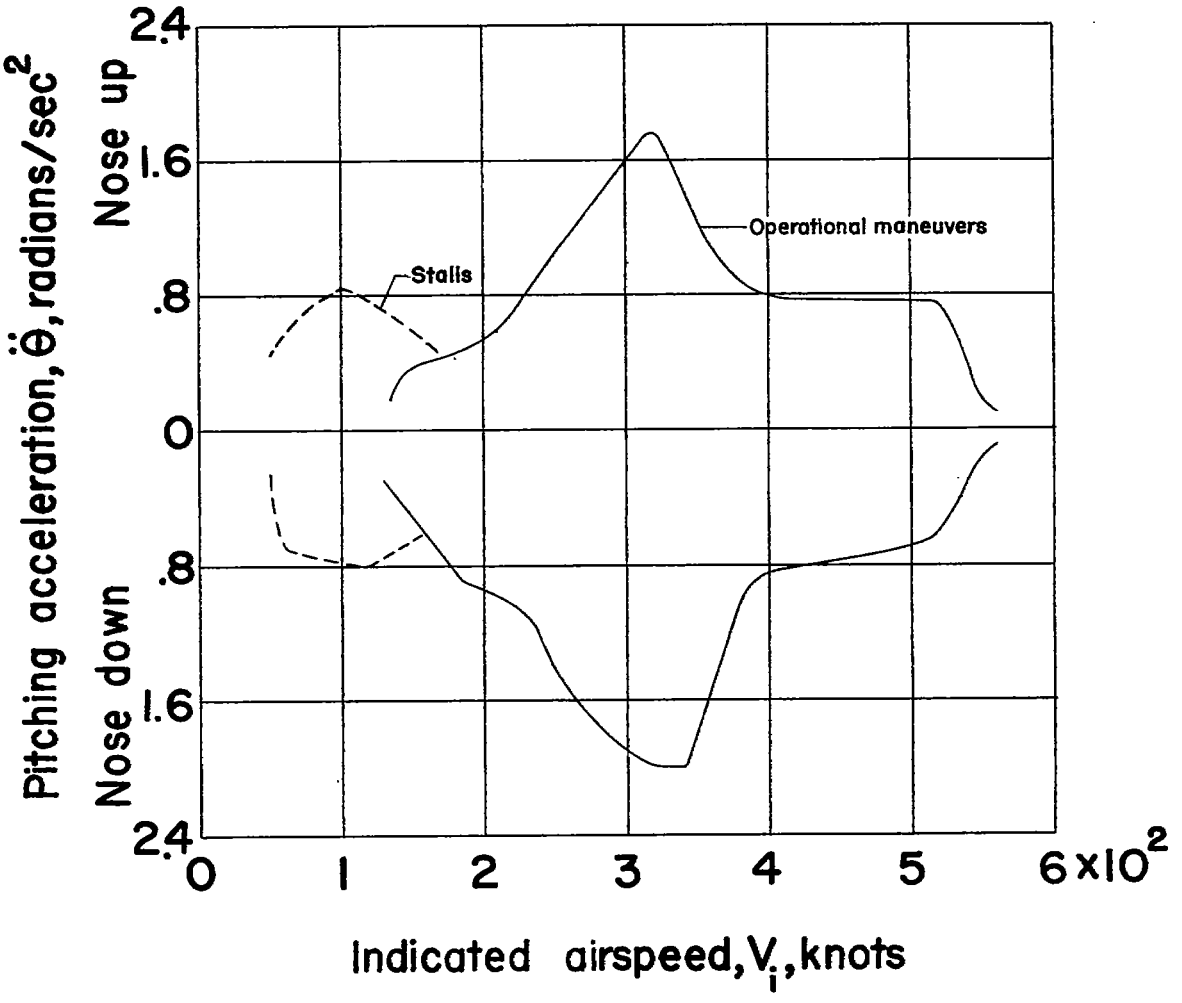

Figure 36.- Envelope of maximum pitching acceleration and indicated airspeed.

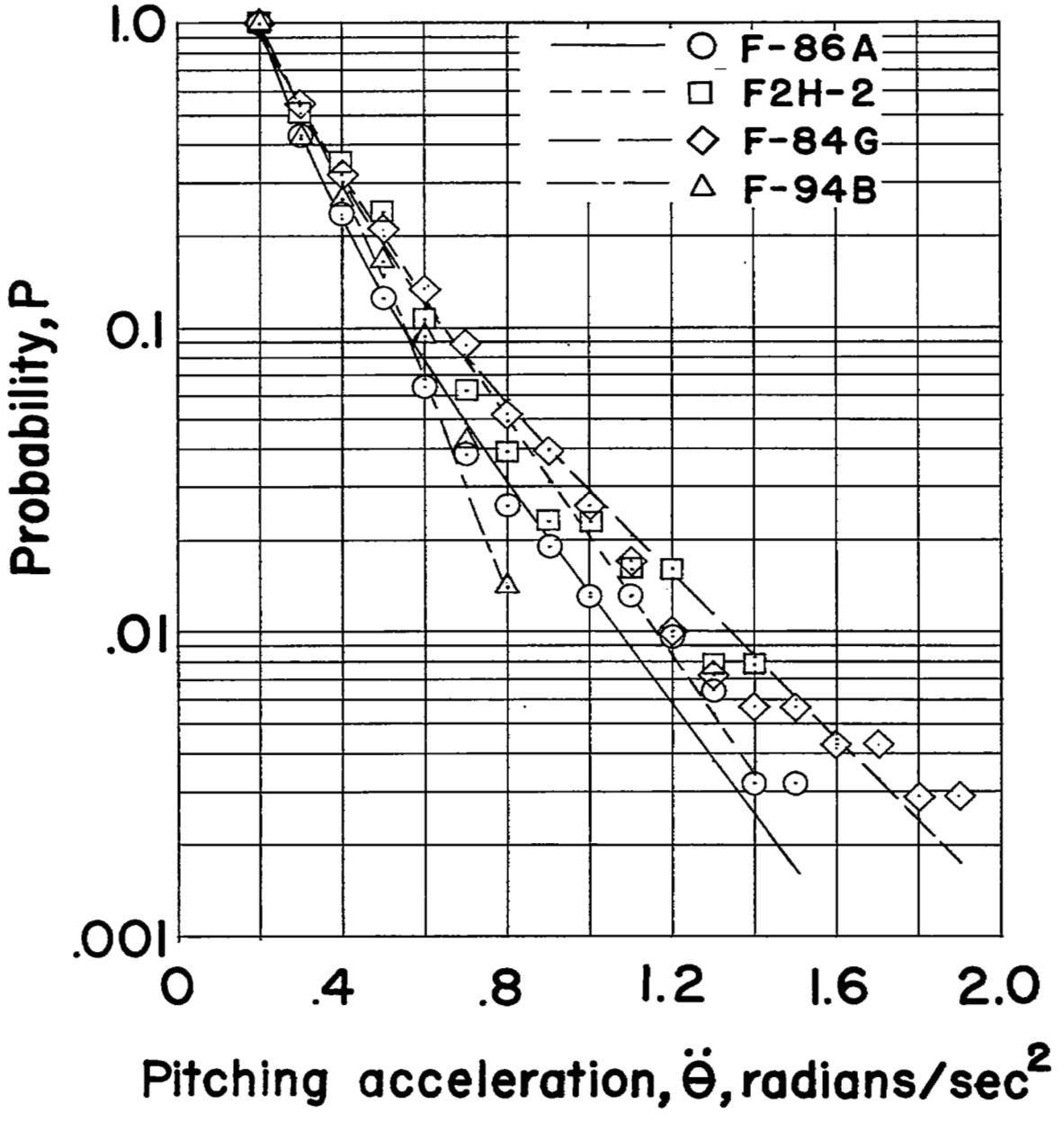

Figure 37.- Probability of equaling or exceeding a given pitching acceleration.

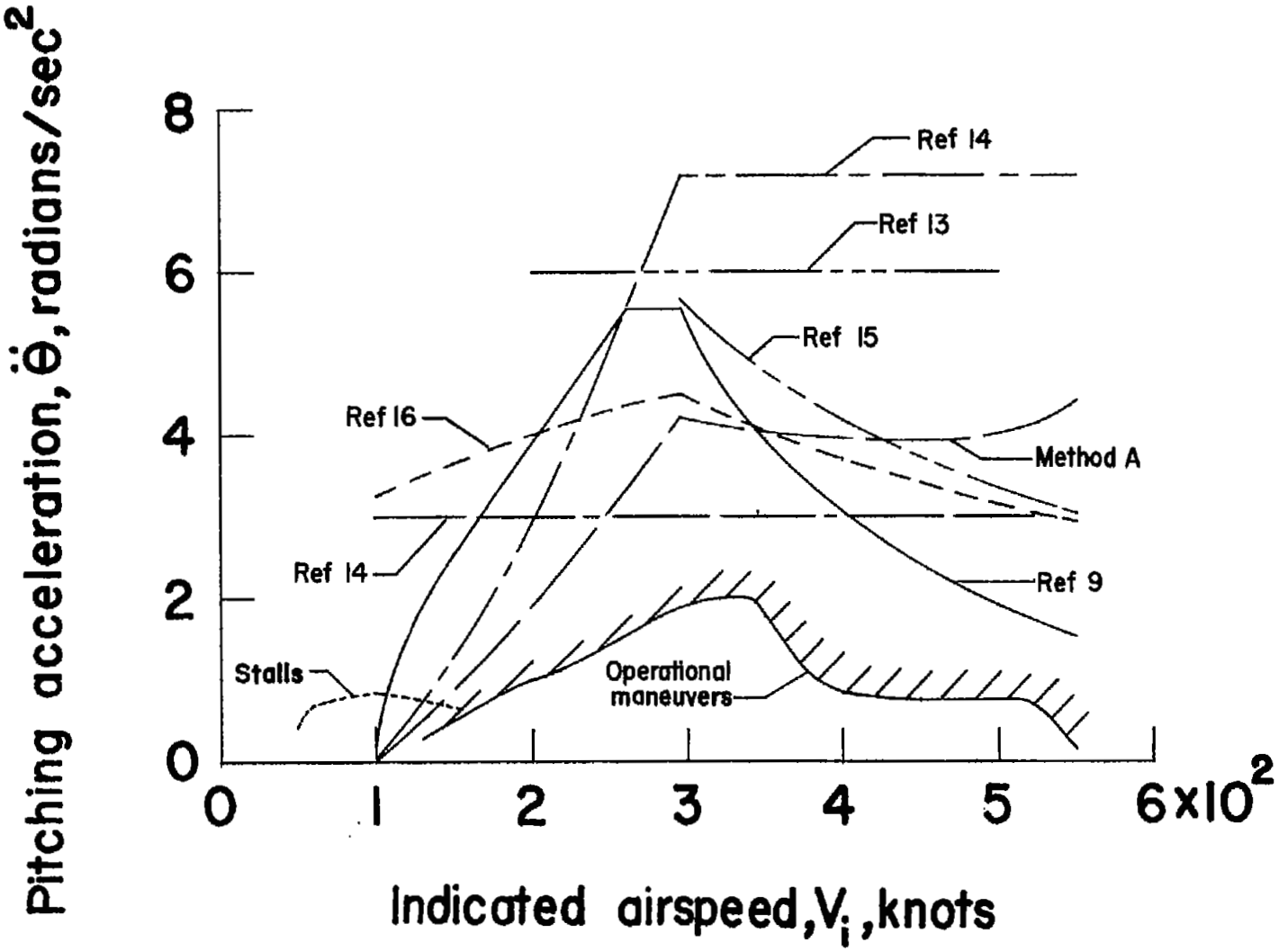

Figure 38.- Comparison of test results with various methods of calculating pitching accelerations.

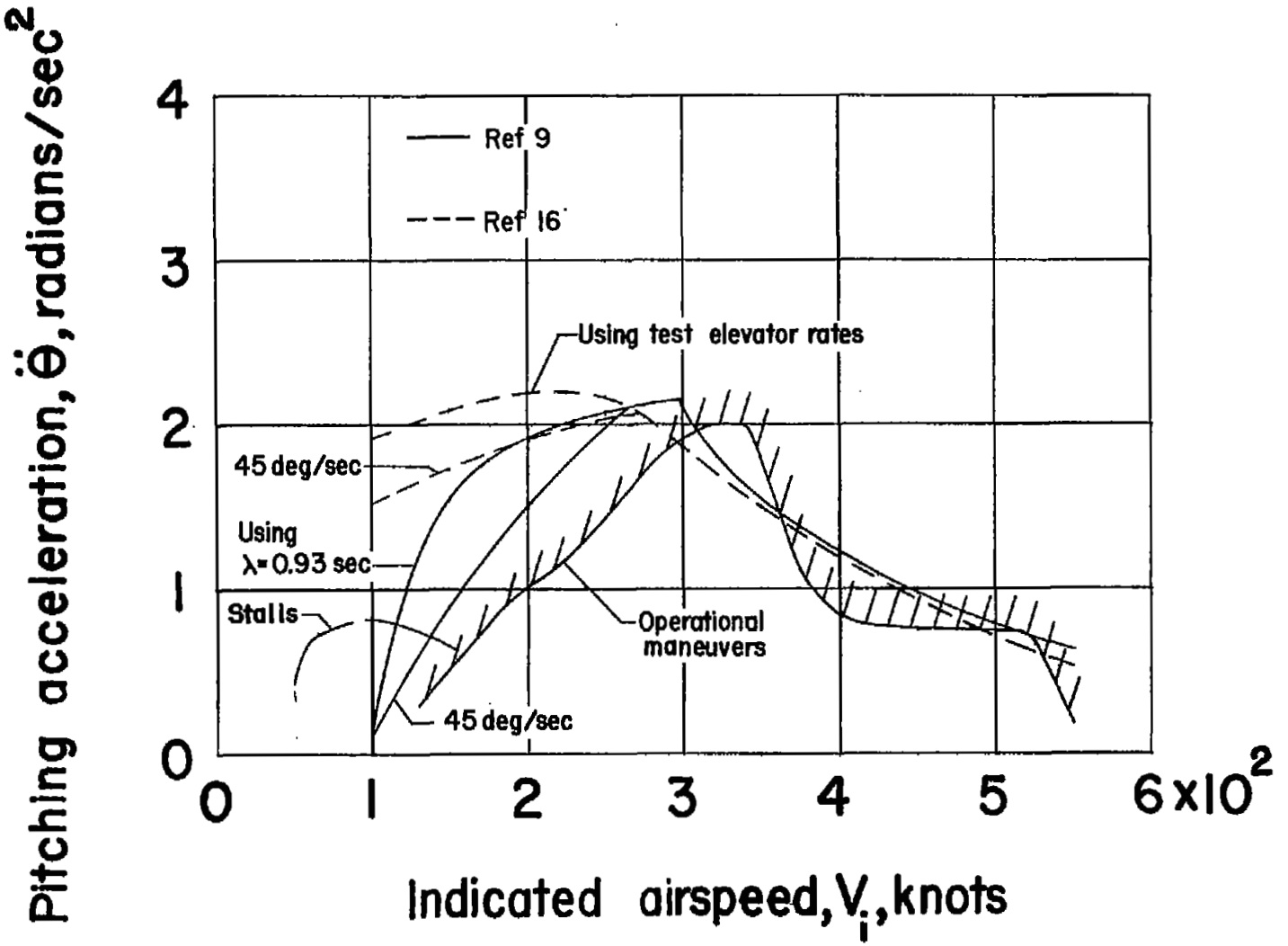

Figure 39.- Comparison of test results with two methods of calculating pitching accelerations based on test parameters.

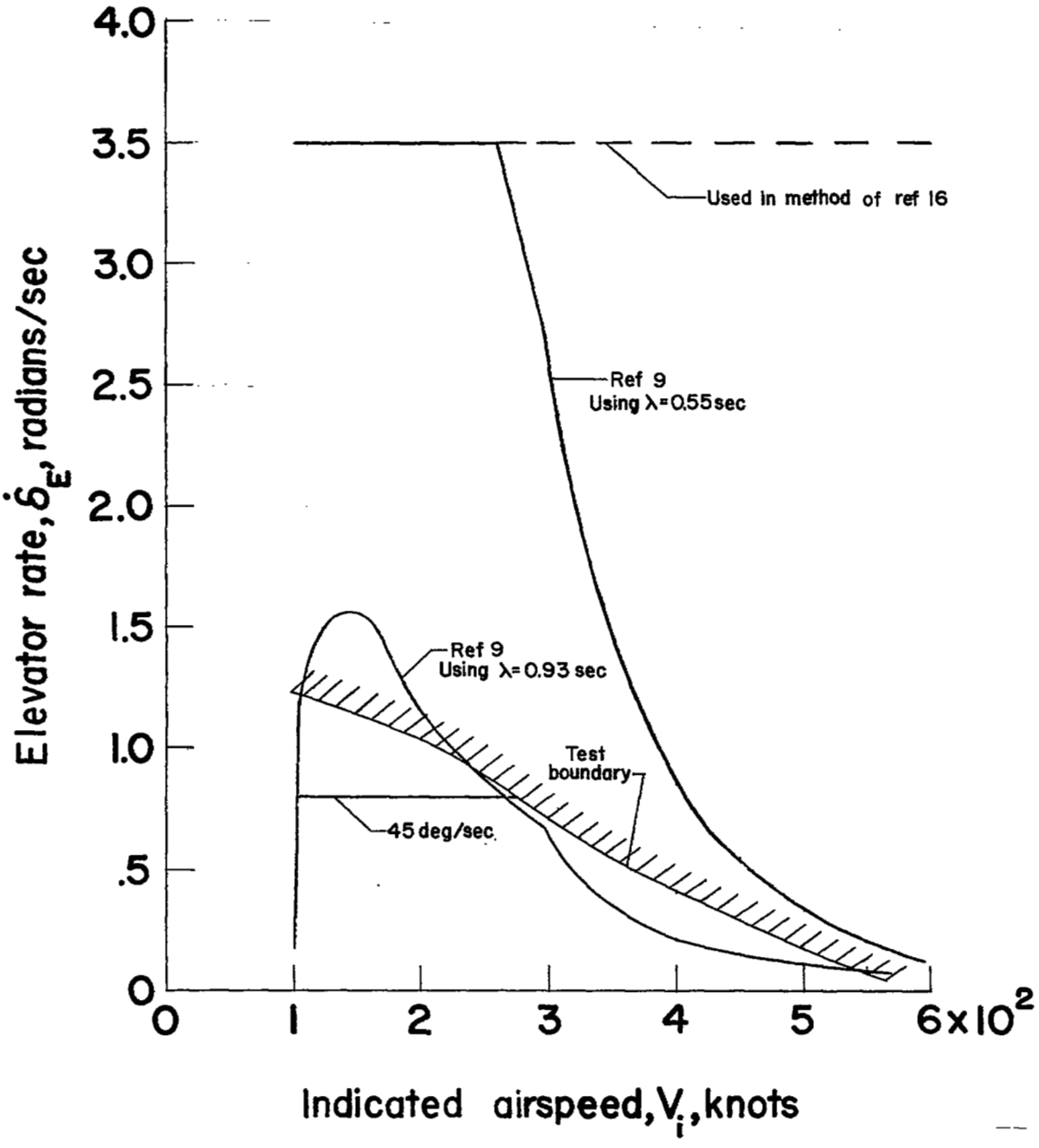

Figure 40.- Elevator rates associated with the methods of calculating pitching accelerations.

[redacted]

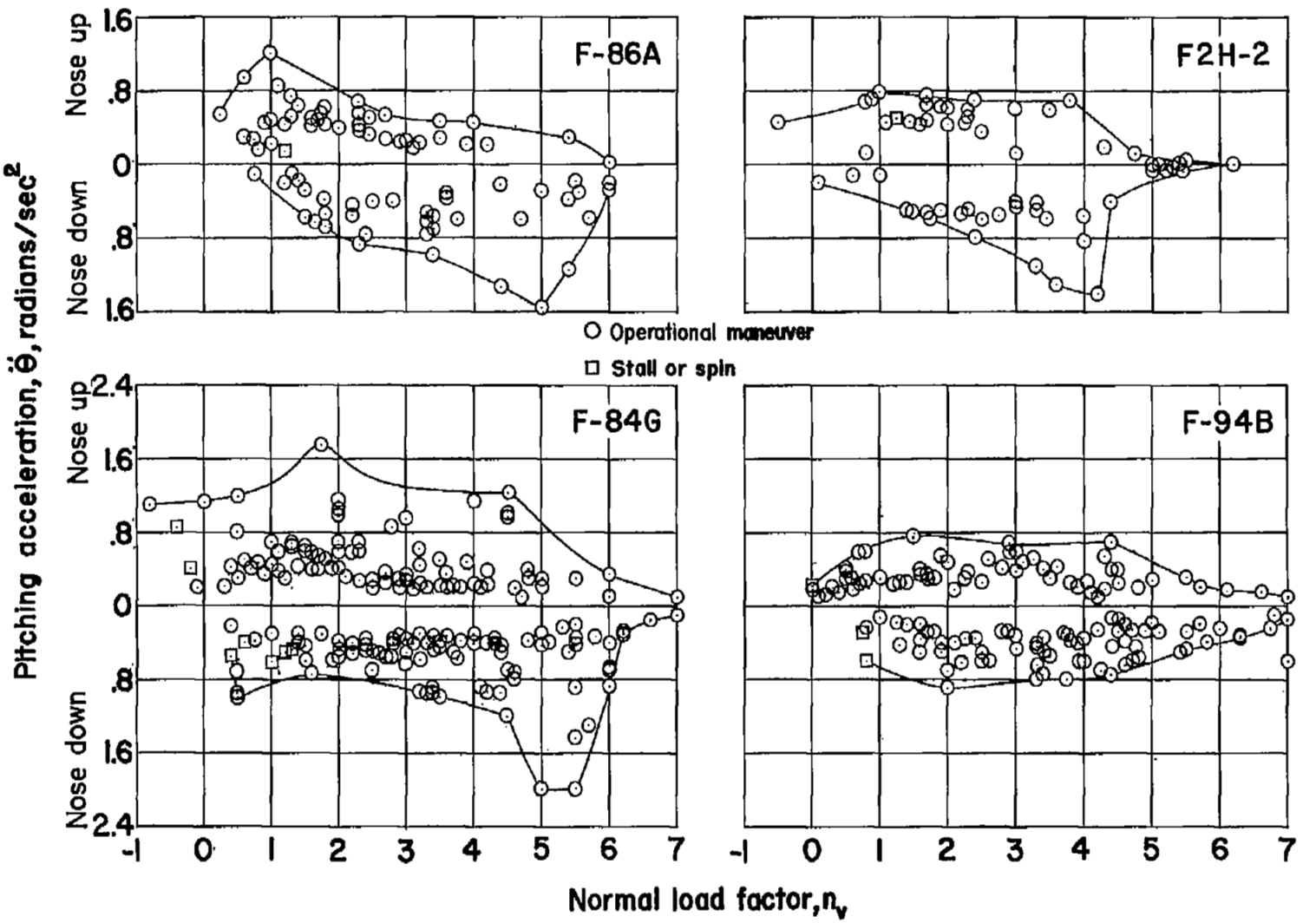

Figure 41.- Maximum pitching accelerations plotted against normal load factor.

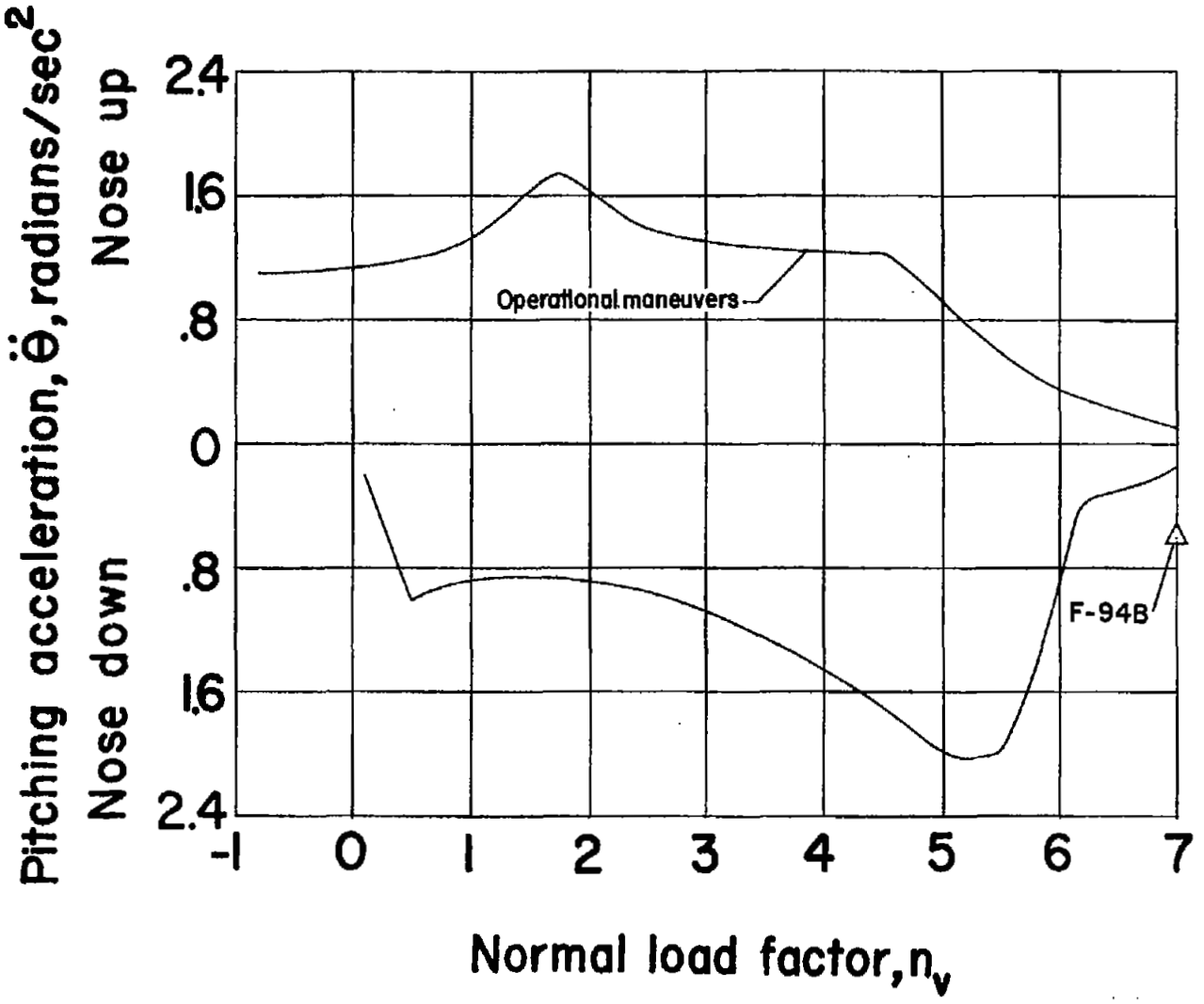

Figure 42.- Envelope of maximum pitching acceleration and normal load factor.

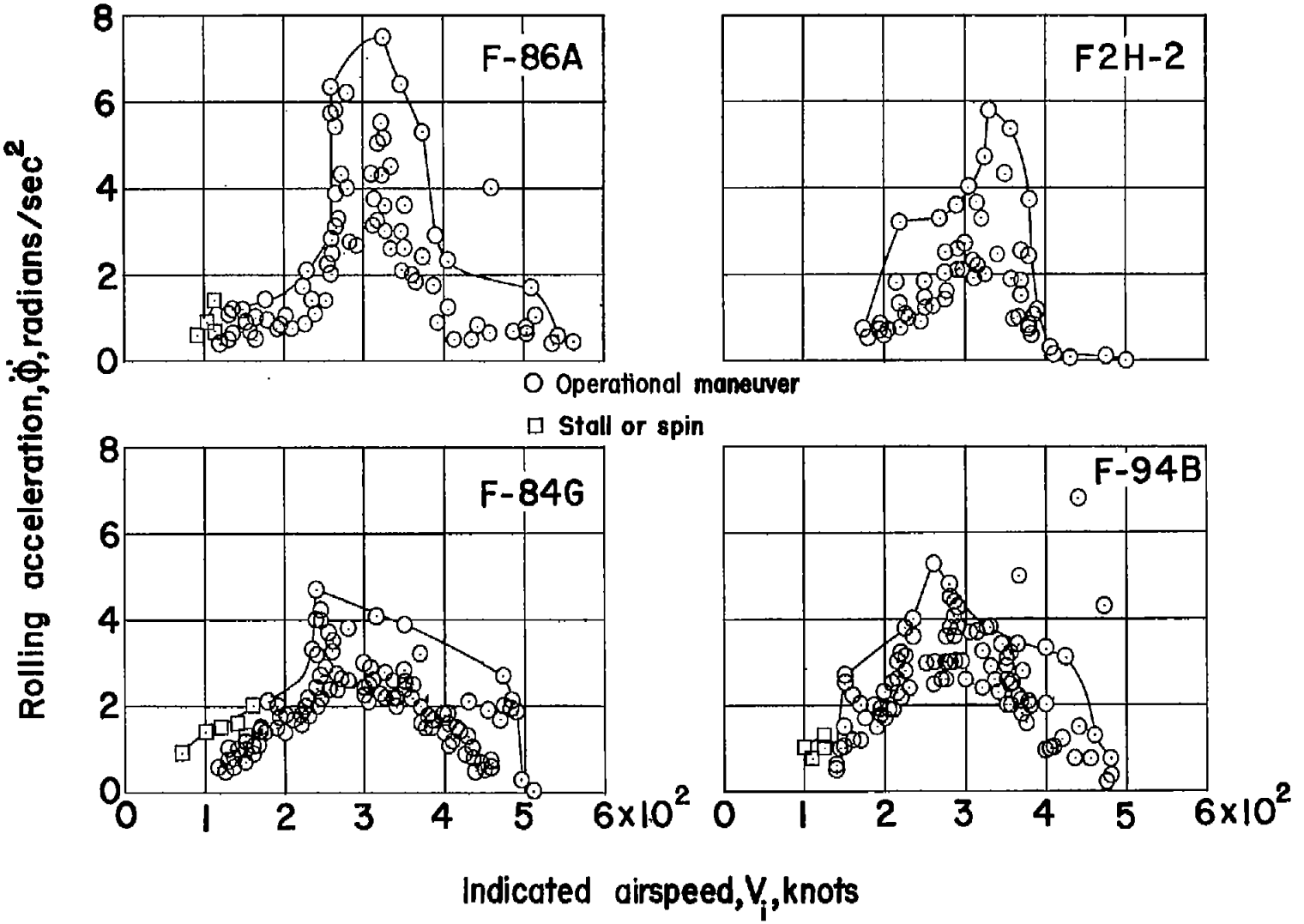

Figure 43.- Maximum rolling accelerations plotted against indicated airspeed.

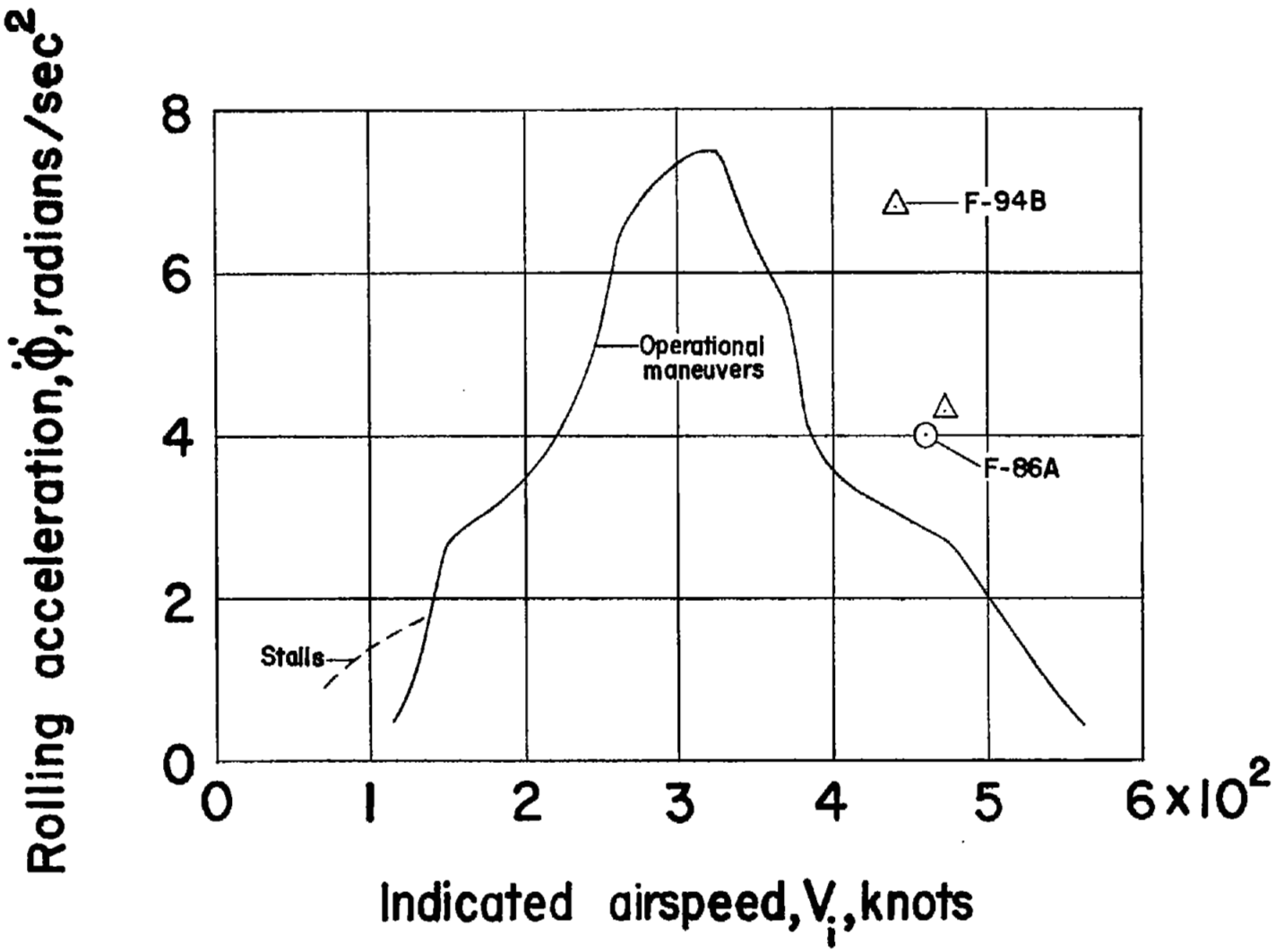

Figure 44.- Envelope of maximum rolling acceleration and indicated airspeed.

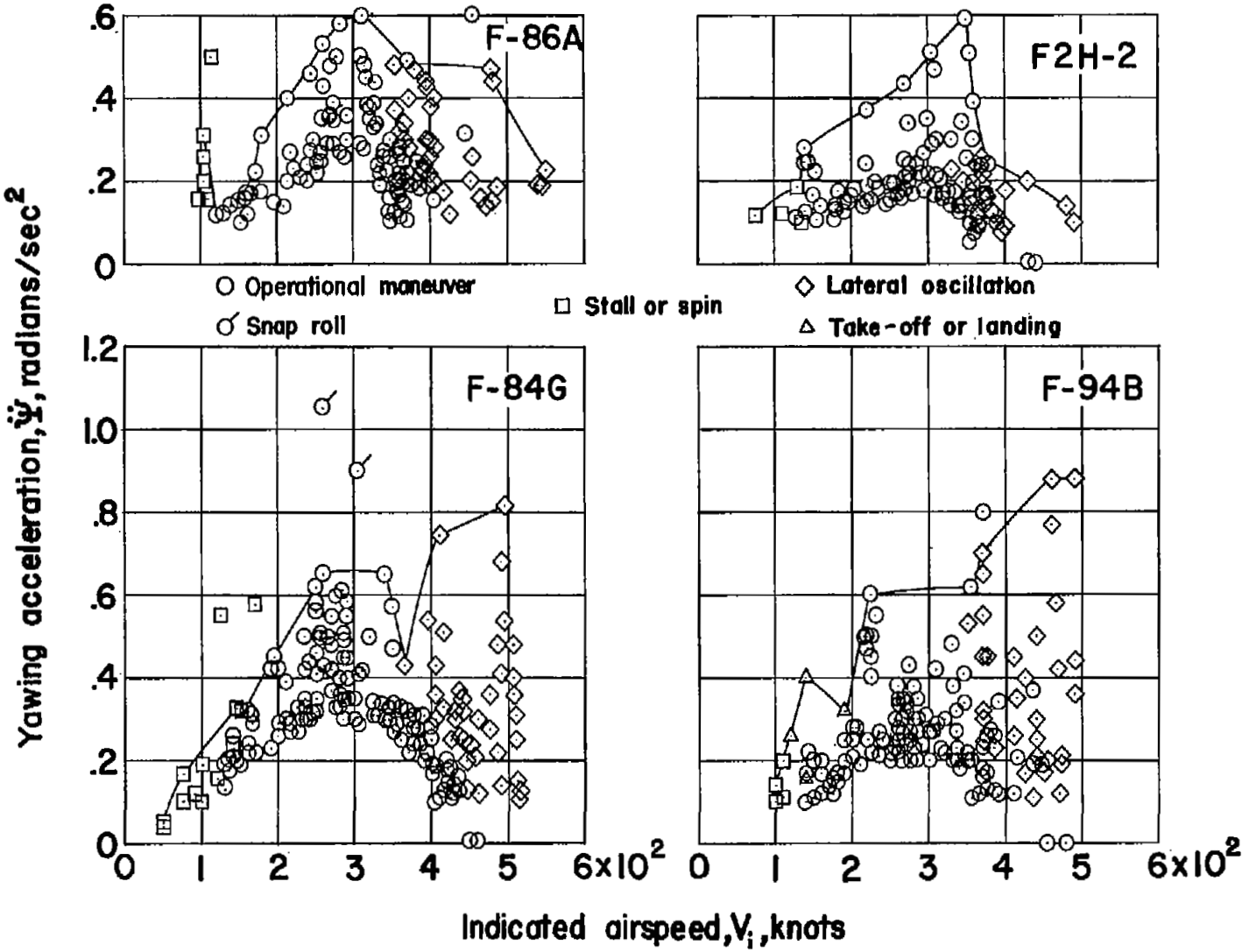

Figure 45.- Maximum yawing accelerations plotted against indicated airspeed.

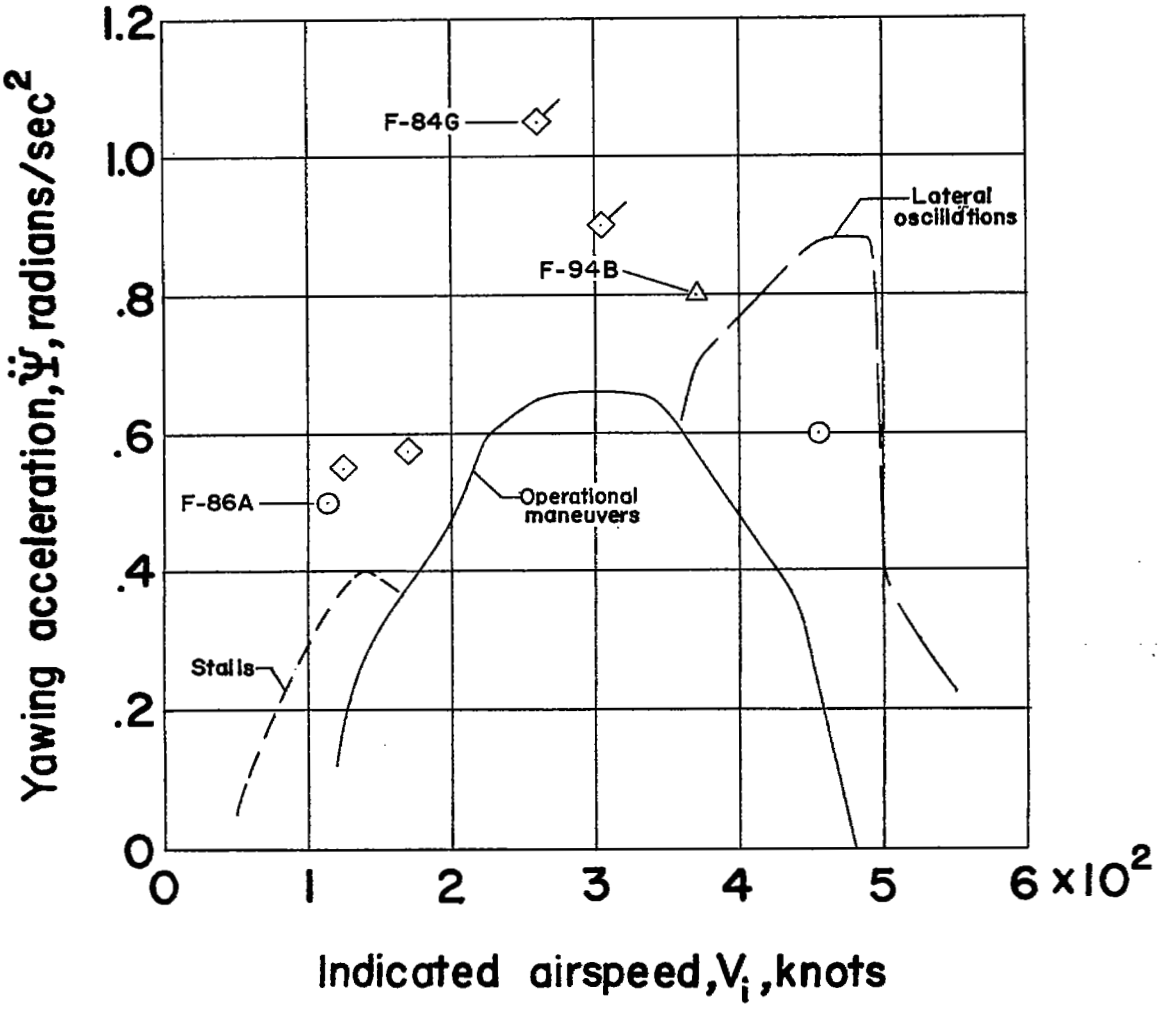

Figure 46.- Envelope of maximum yawing acceleration and indicated airspeed.

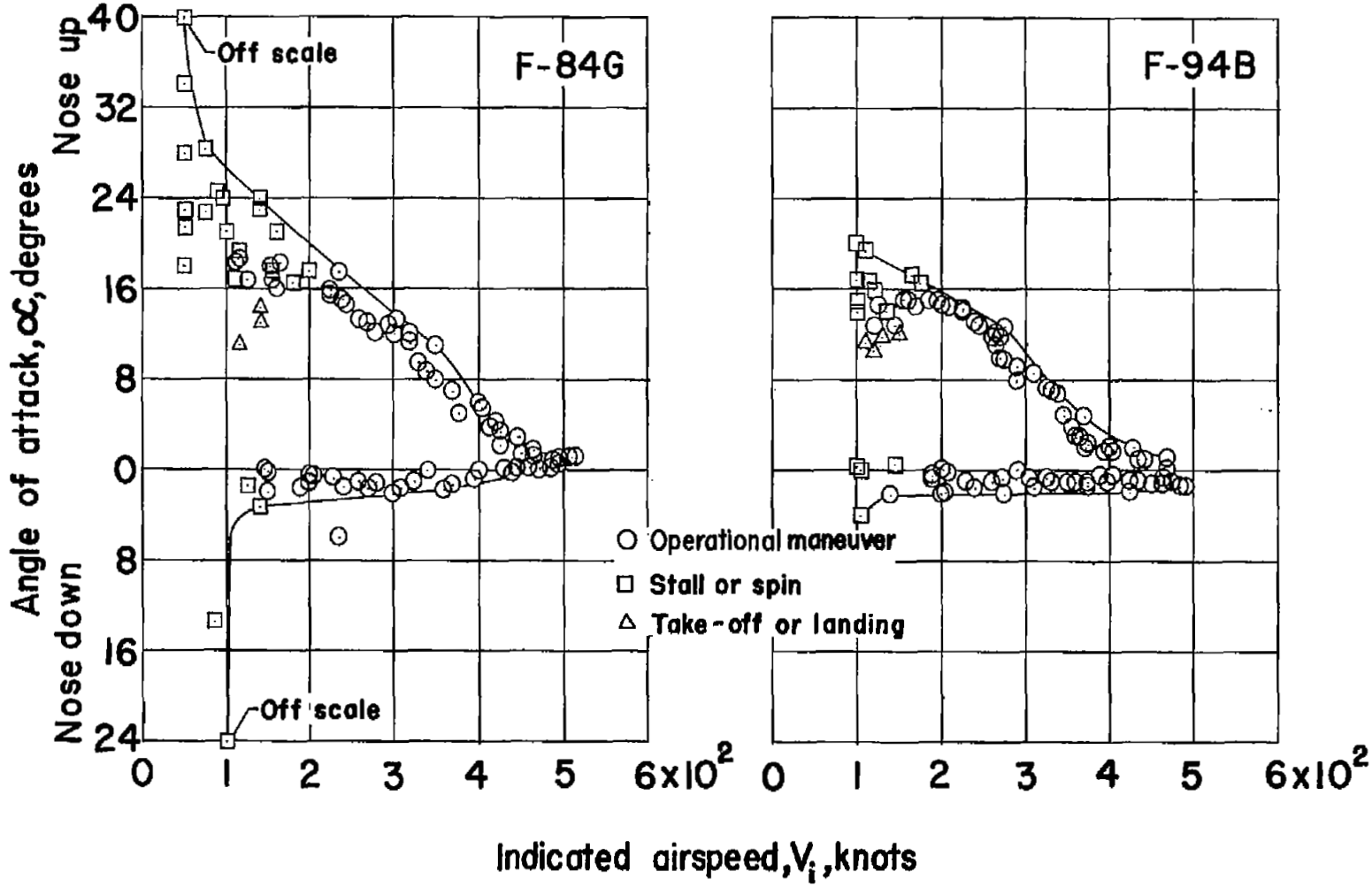

Figure 47.- Maximum angles of attack plotted against indicated airspeed.

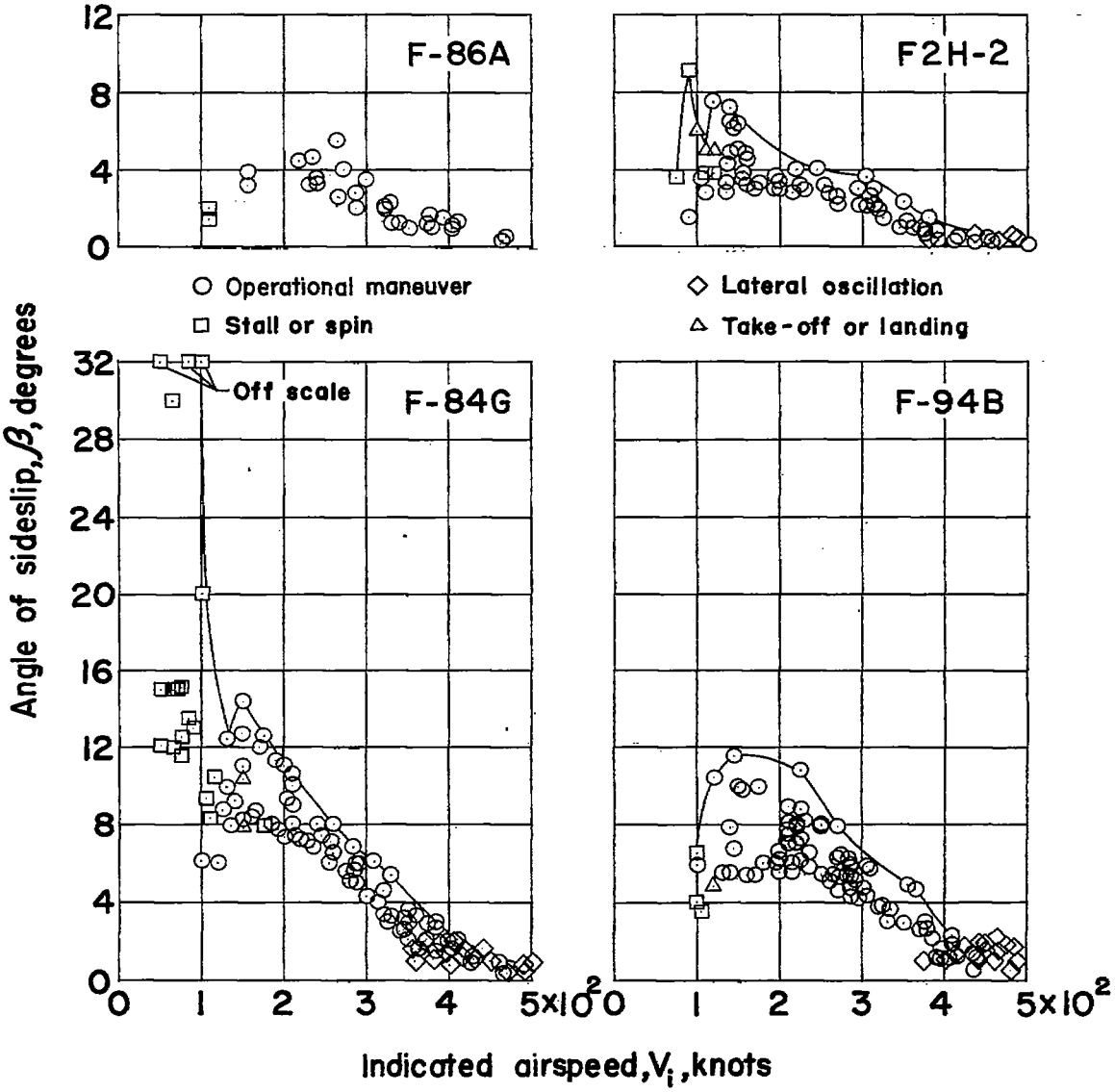

Figure 48.- Maximum angles of sideslip plotted against indicated airspeed.

[redacted]

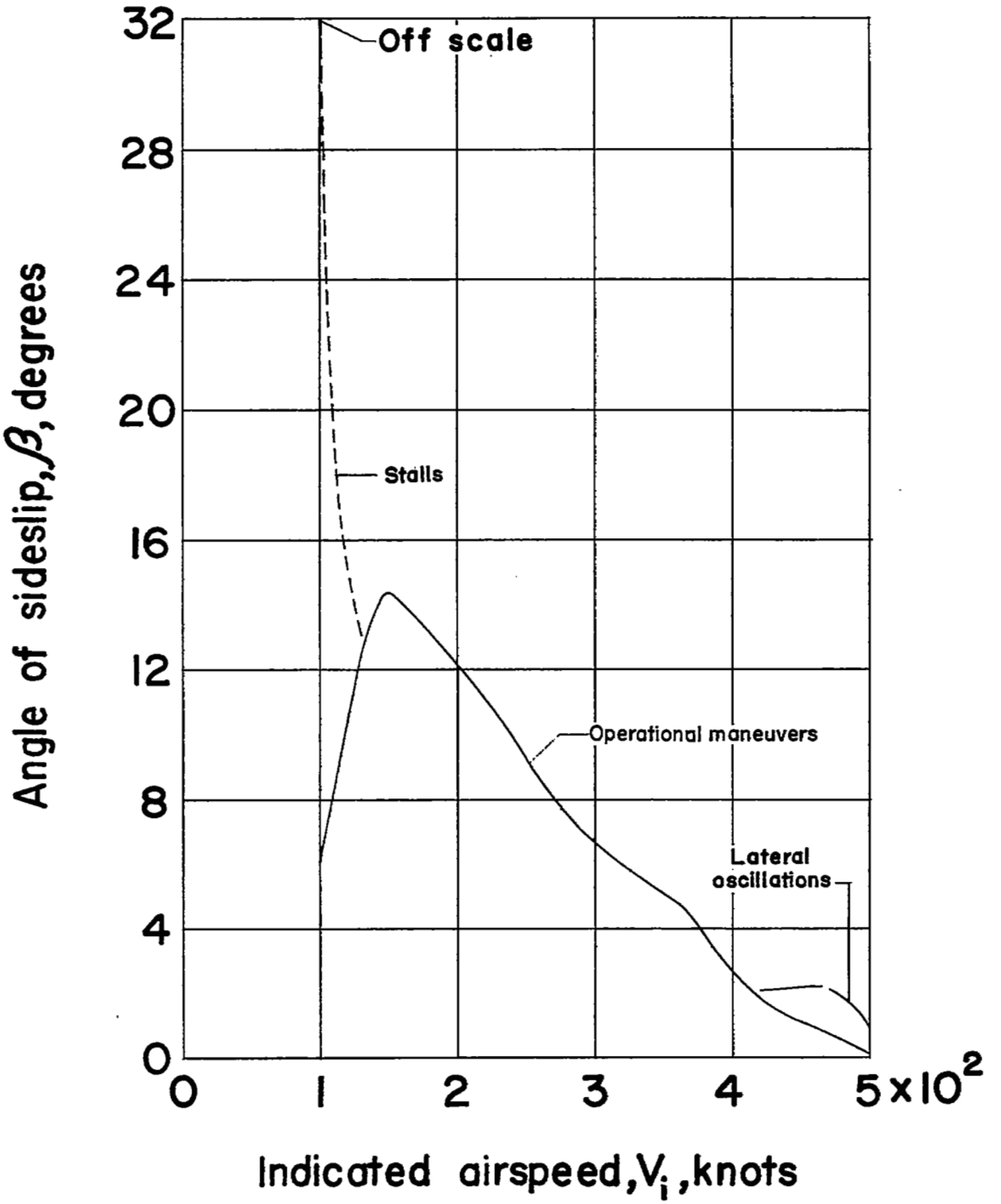

Figure 49.- Envelope of maximum angle of sideslip and indicated airspeed.

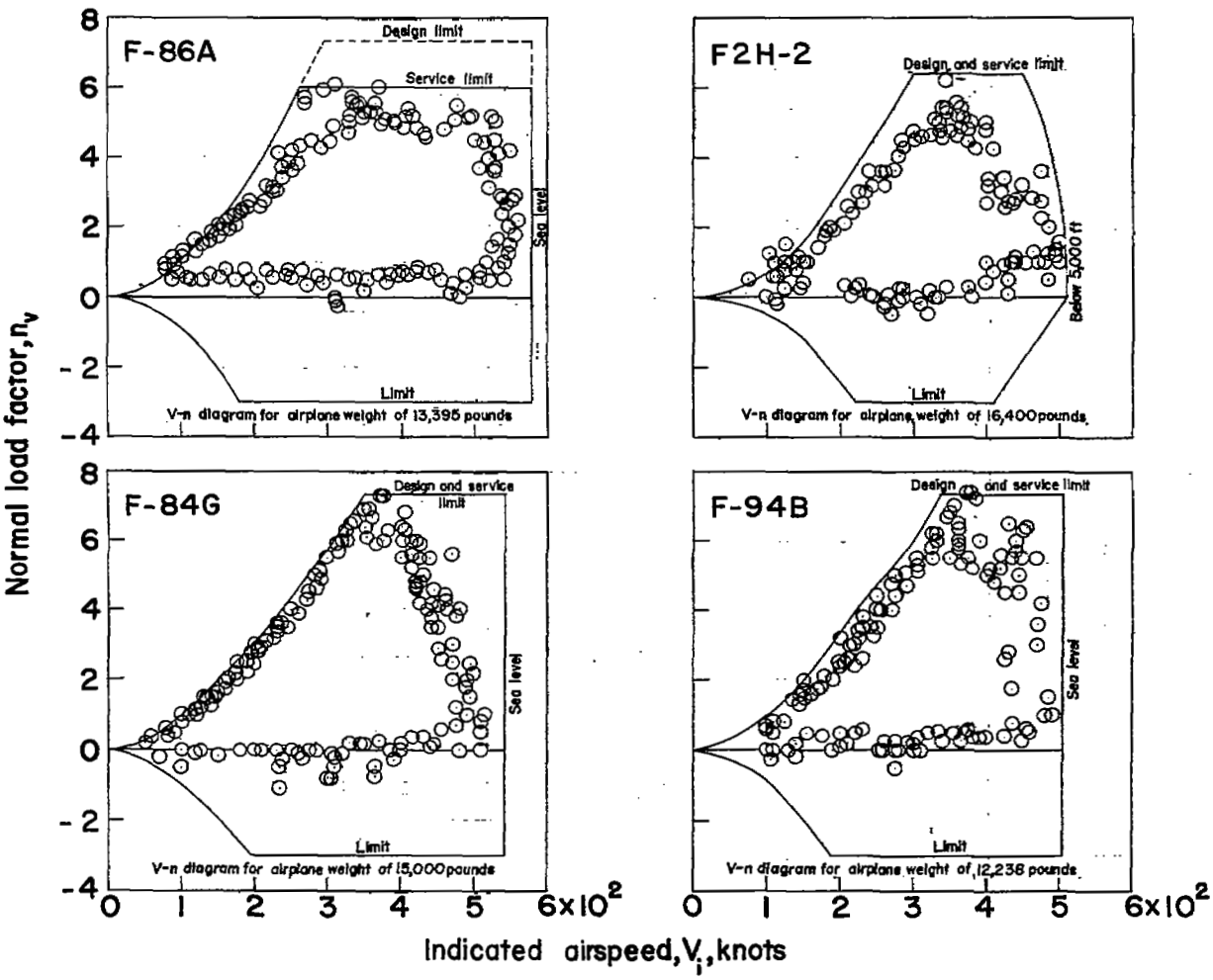

Figure 50.- Comparison of measured normal load factors with the airplane operational V-n diagram.

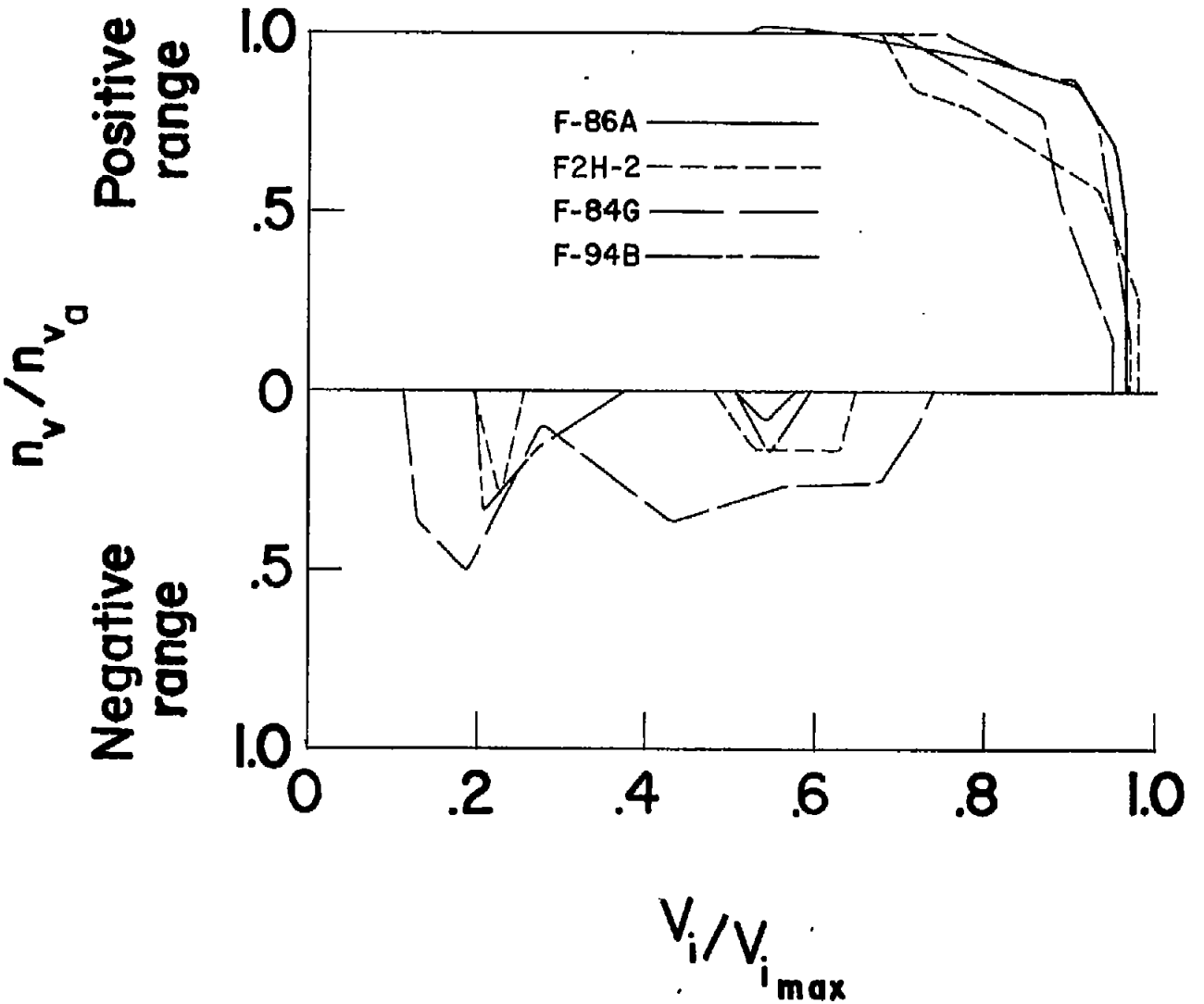

Figure 51.- Utilization of normal-load-factor service limits.

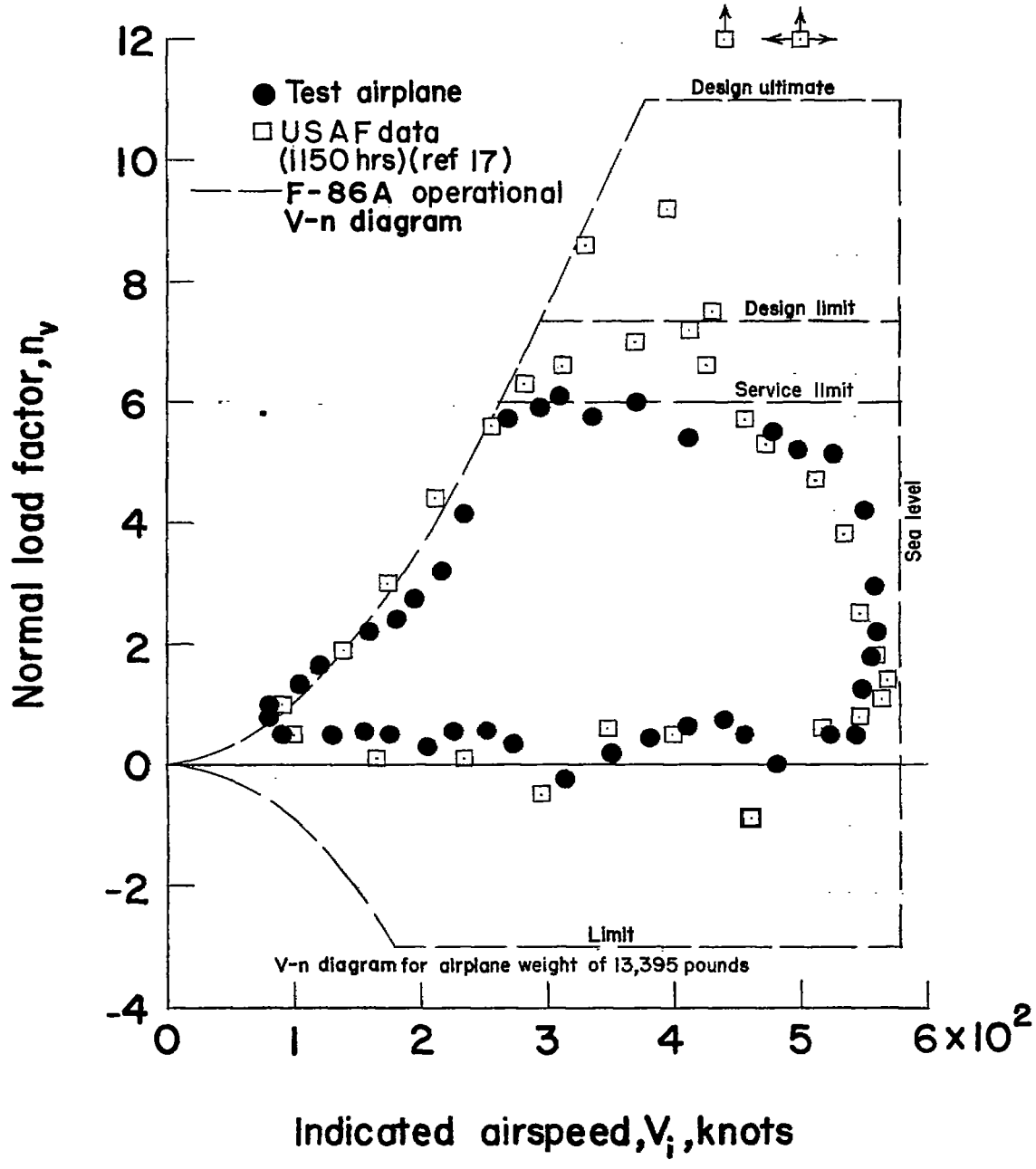

Figure 52.- Comparison of normal load factors obtained for the F-86A test airplane with those obtained from 1,150 hours of USAF training operations.

[redacted]

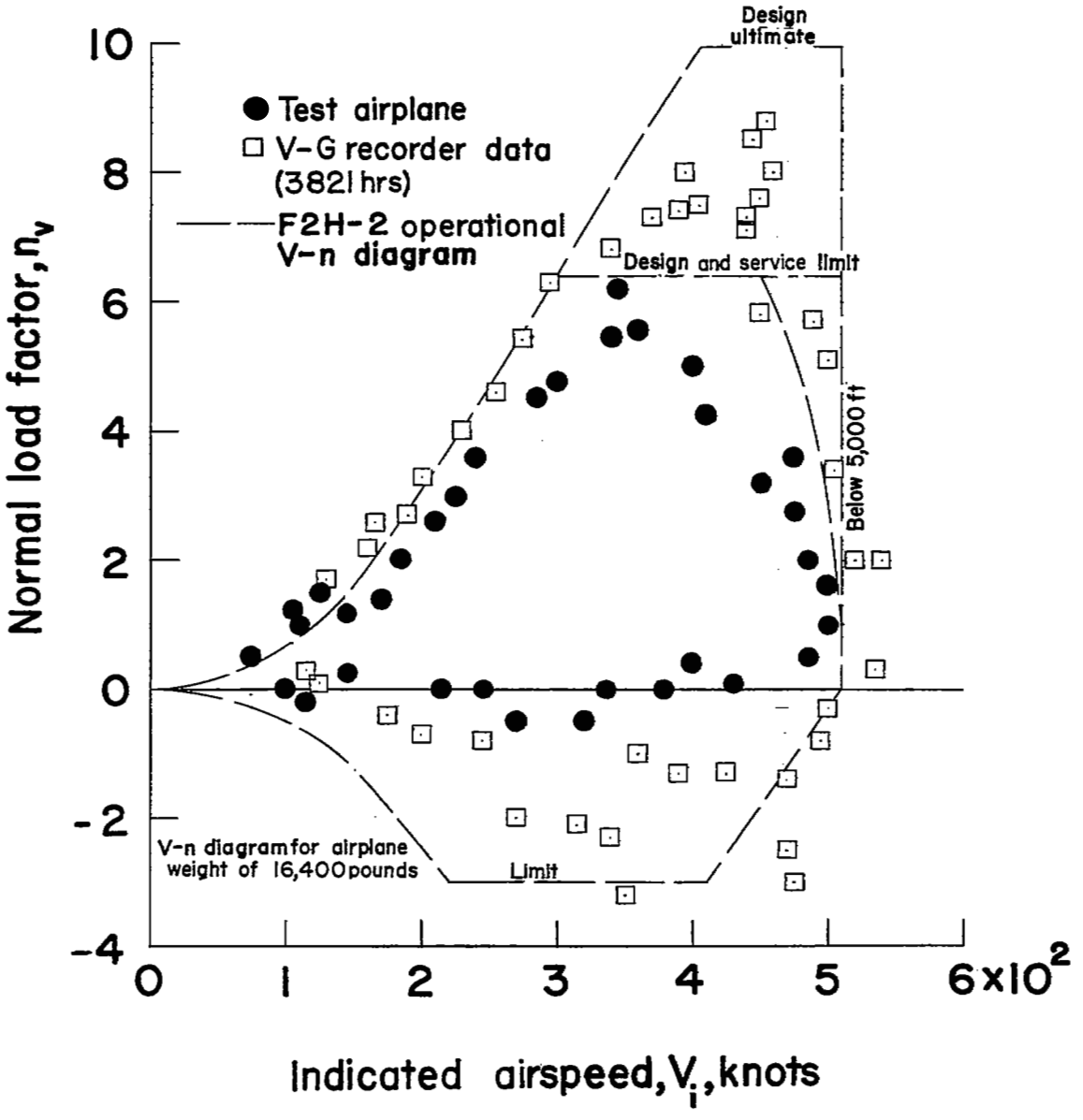

Figure 53.- Comparison of normal load factors obtained for the F2H-2 test airplane with those obtained from 3,821 hours of USMC training operations.

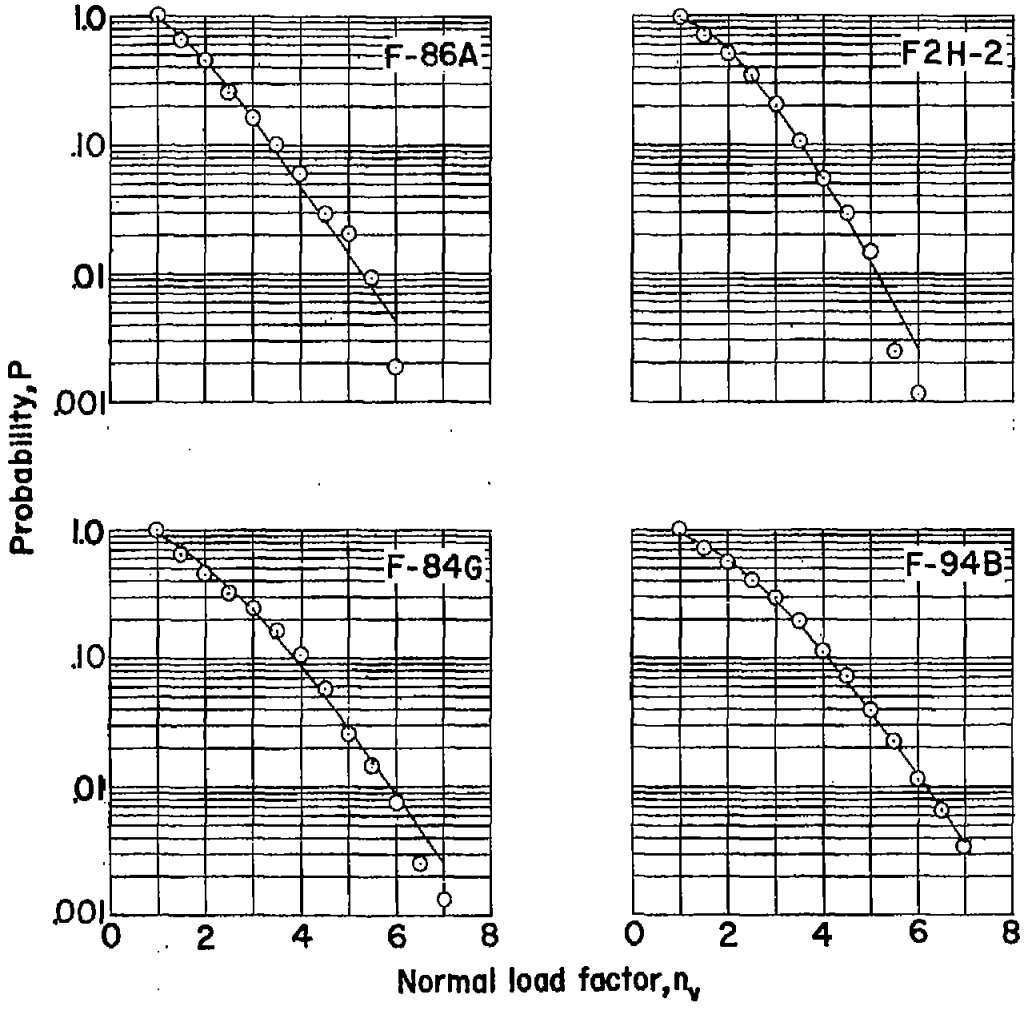

Figure 54.- Comparison of the test data with the fitted Pearson type III curve for probability of equaling or exceeding a given normal load factor.

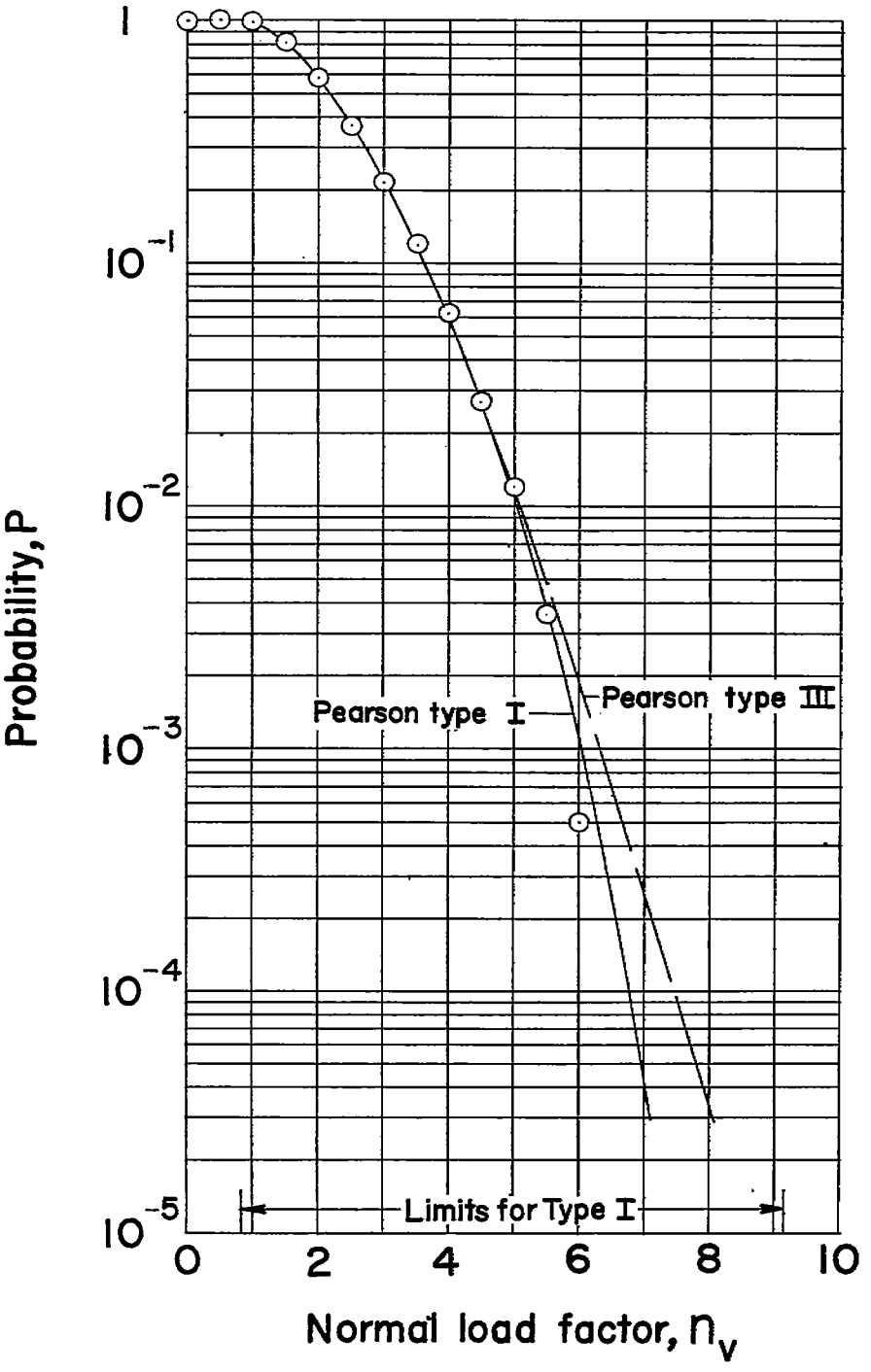

Figure 55.- Comparison of the Pearson type III and type I curves, as fitted to the test data of the F-86A airplane, for probability of equaling or exceeding a given normal load factor.

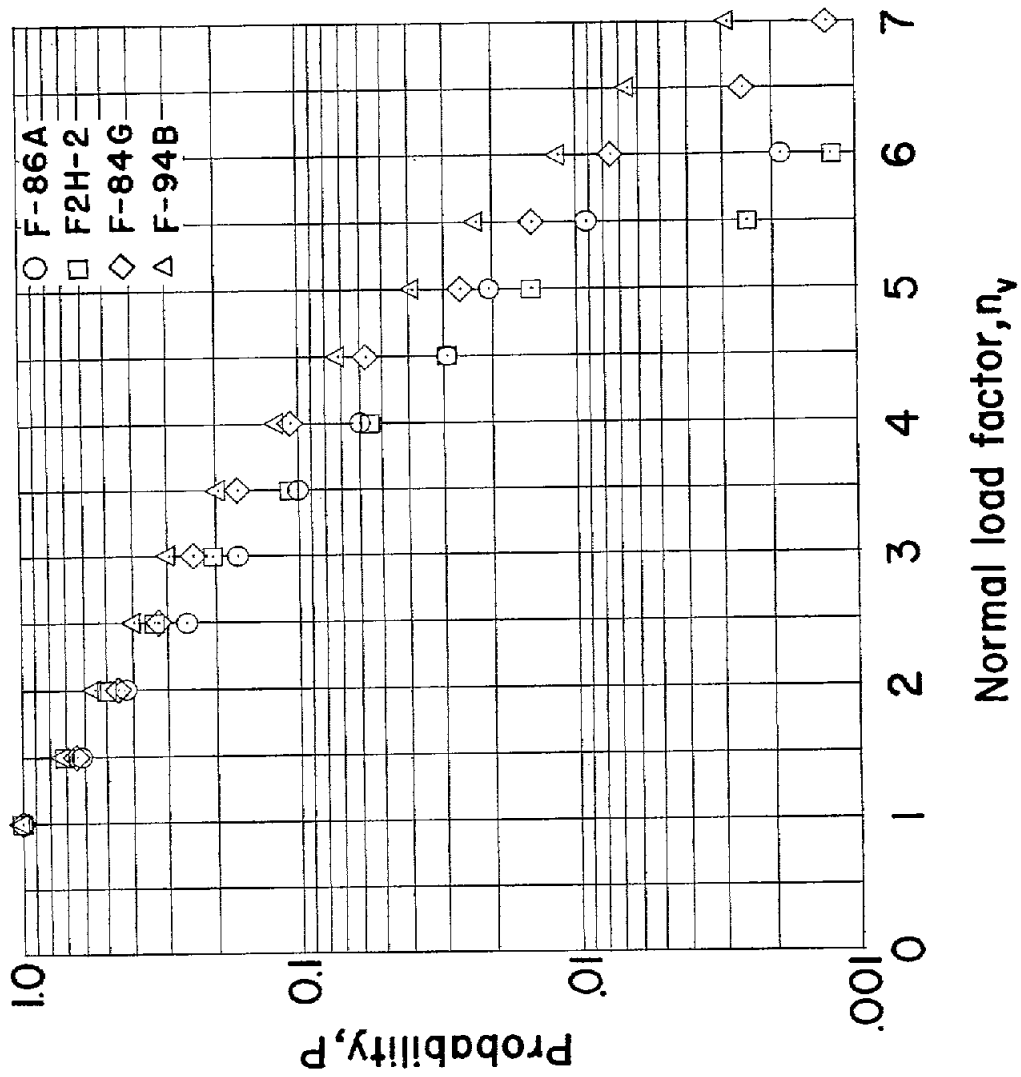

Figure 56.- Probability of equaling or exceeding a given normal load factor.

[redacted]

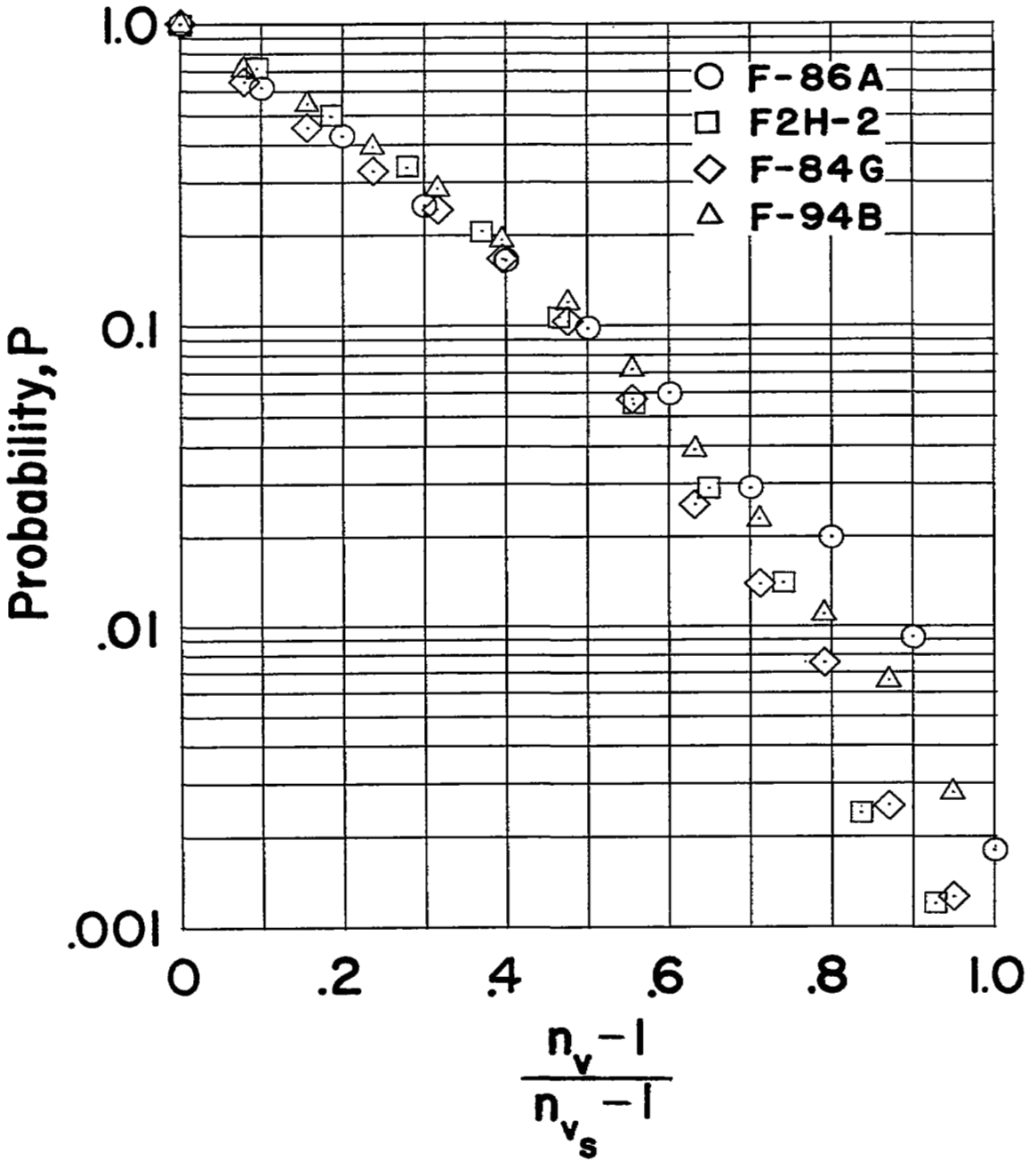

Figure 57.- Probability of equaling or exceeding a given fraction of the service limit positive normal load factor.

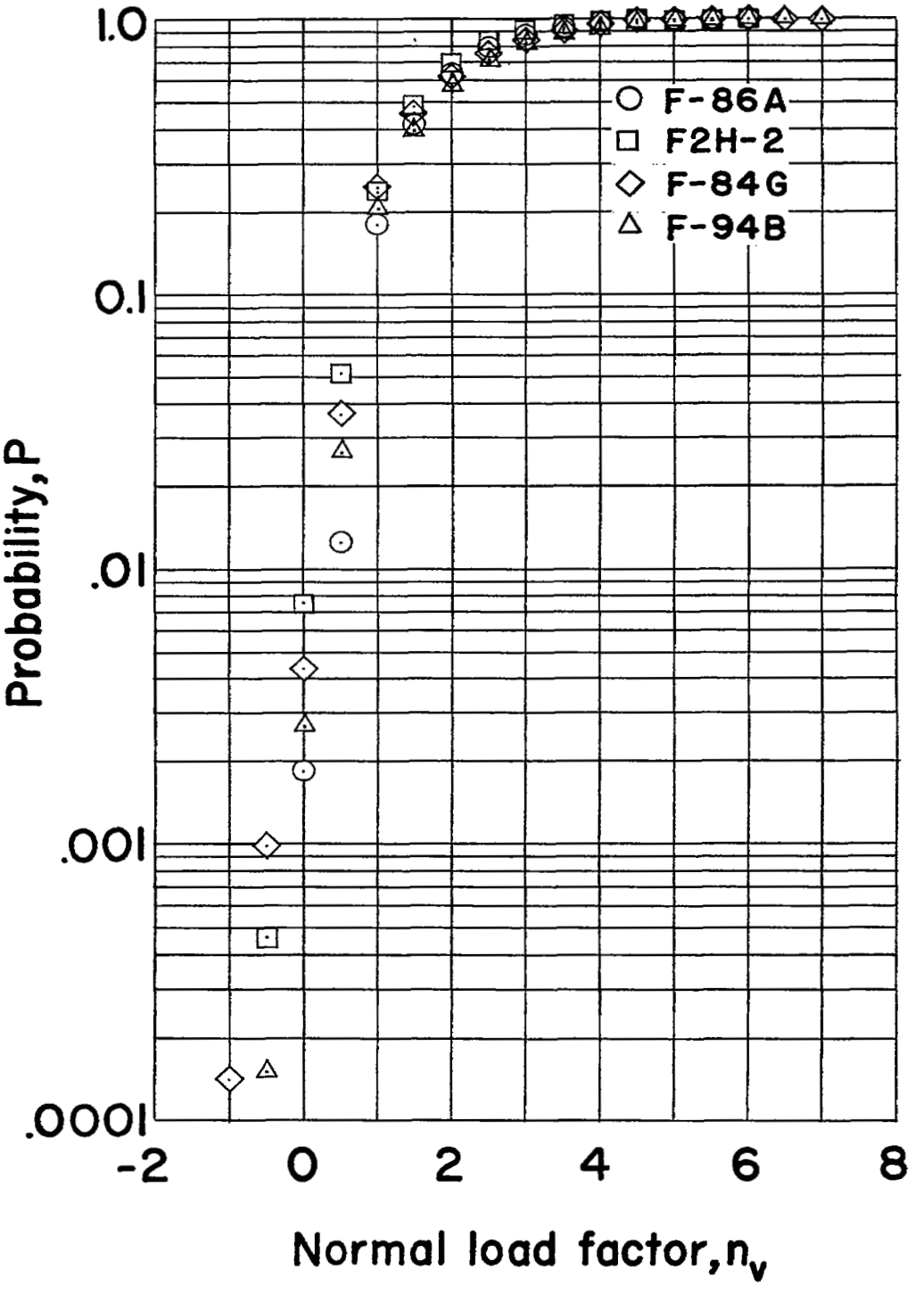

Figure 58.- Probability of normal load factor being equal to or less than a given value.

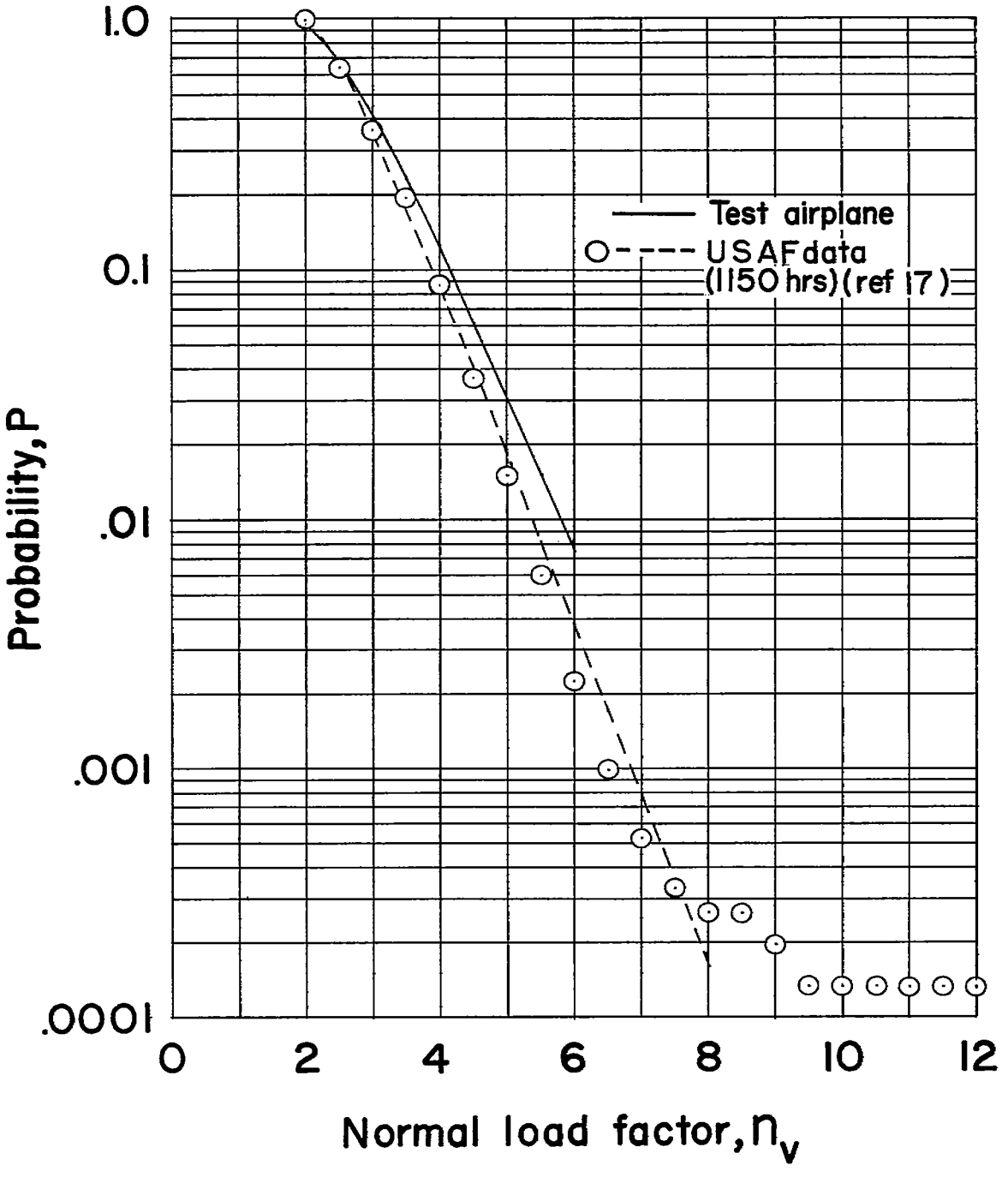

Figure 59.- Comparison of the probability of equaling or exceeding a given normal load factor obtained for the F-86A test airplane with that obtained from 1,150 hours of USAF training operations.

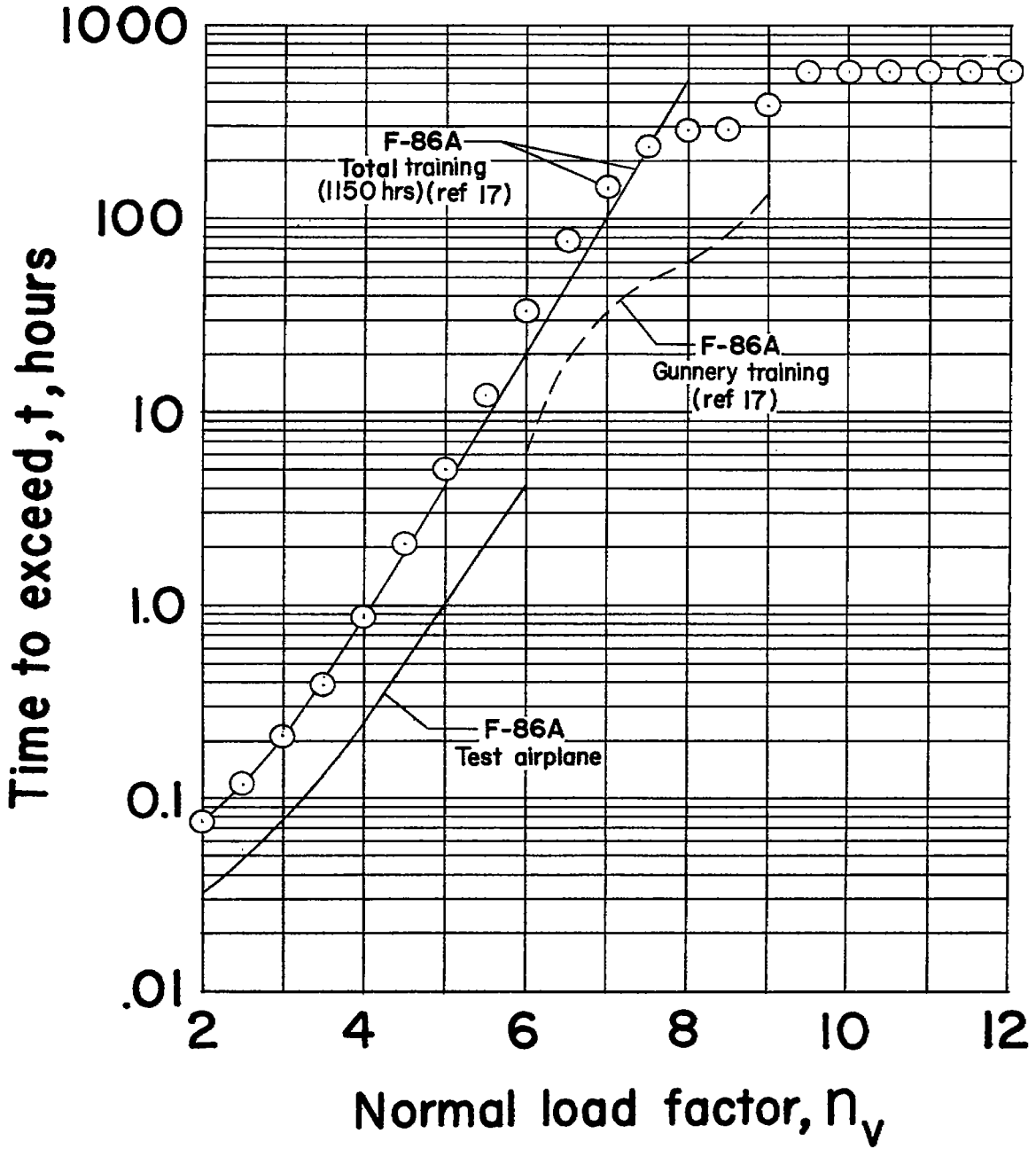

Figure 60.- Comparison of the average flight time required to equal or exceed a given normal load factor obtained for the F-86A test airplane with that obtained from 1,150 hours of USAF training operations.

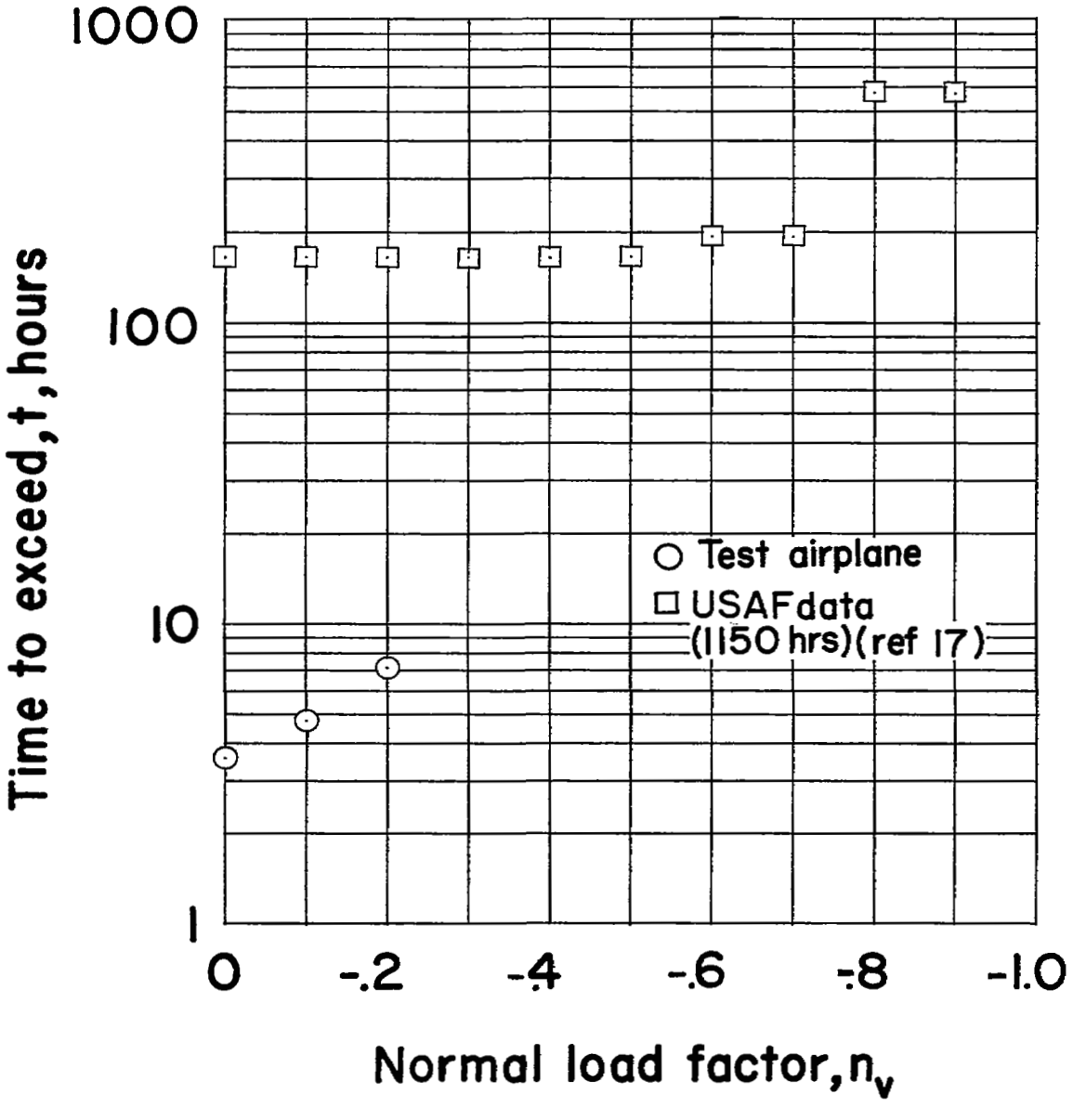

Figure 61.- Comparison of the average flight time required to equal or exceed a given negative normal load factor obtained for the F-86A test airplane with that obtained from 1,150 hours of USAF training operations.

[redacted]

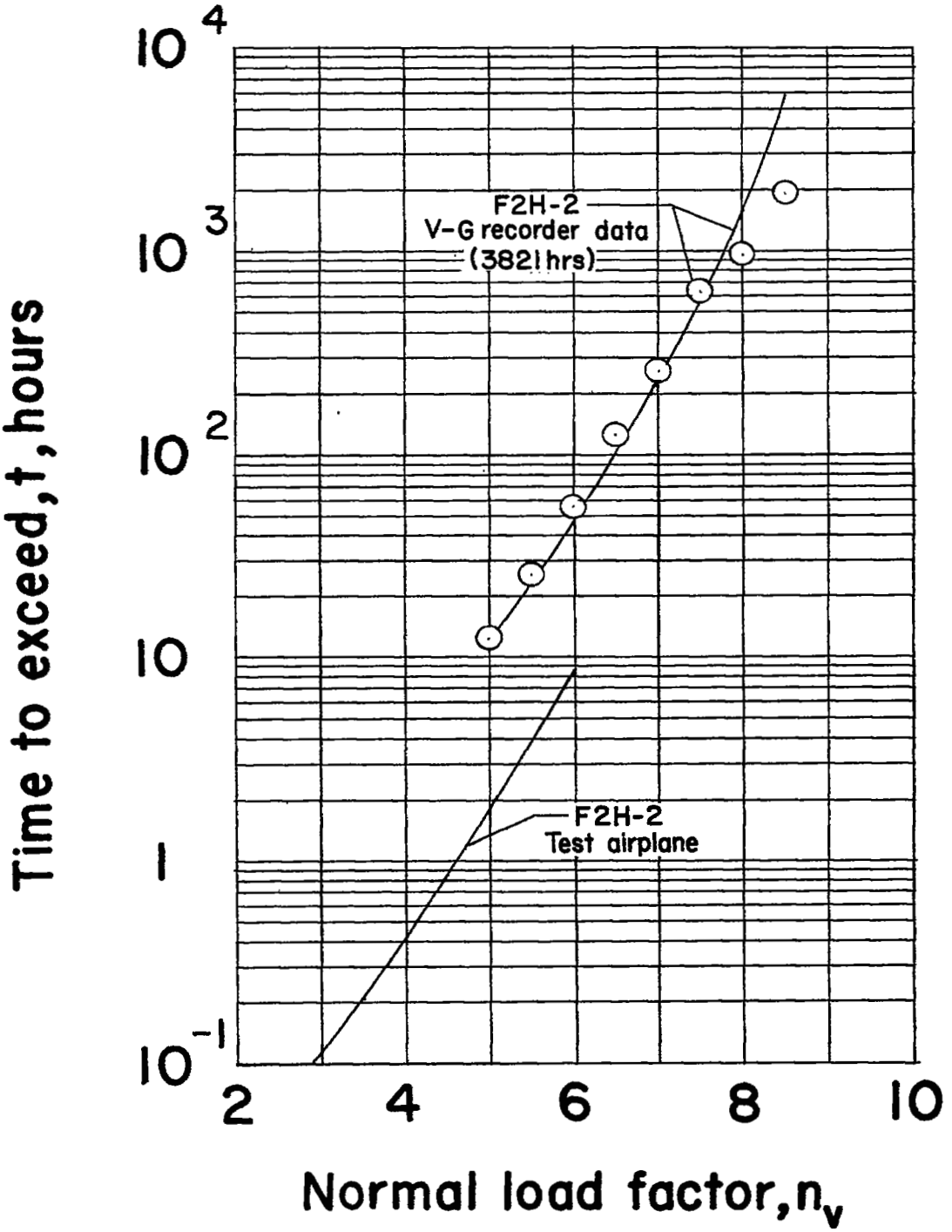

Figure 62.- Comparison of the average flight time required to equal or exceed a given normal load factor obtained for the F2H-2 test airplane with that obtained from 3,821 hours of USMC training operations.

CONFIDENTIAL

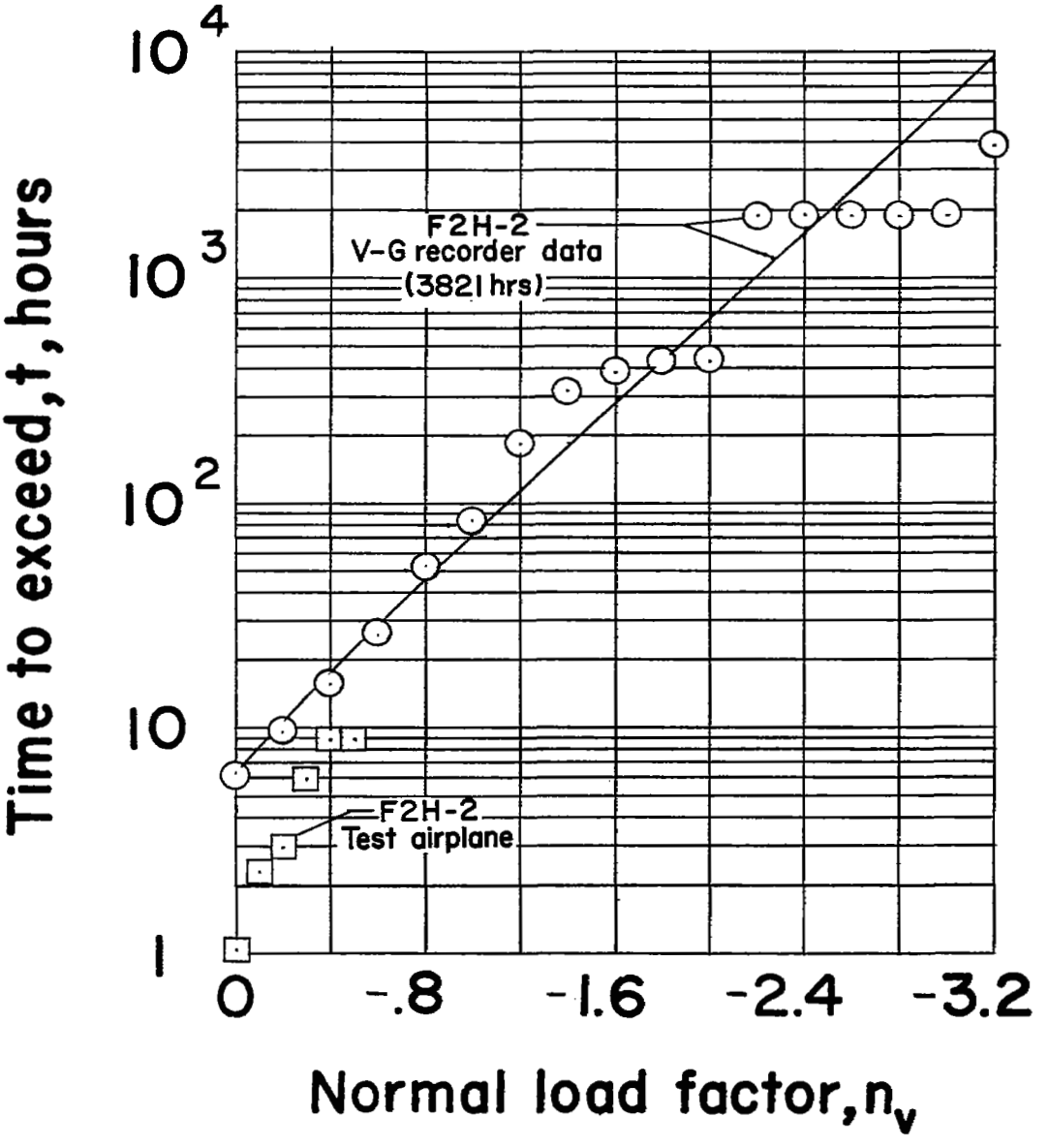

Figure 63.- Comparison of the average flight time required to equal or exceed a given negative normal load factor obtained for the F2H-2 test airplane with that obtained from 3,821 hours of USMC training operations.

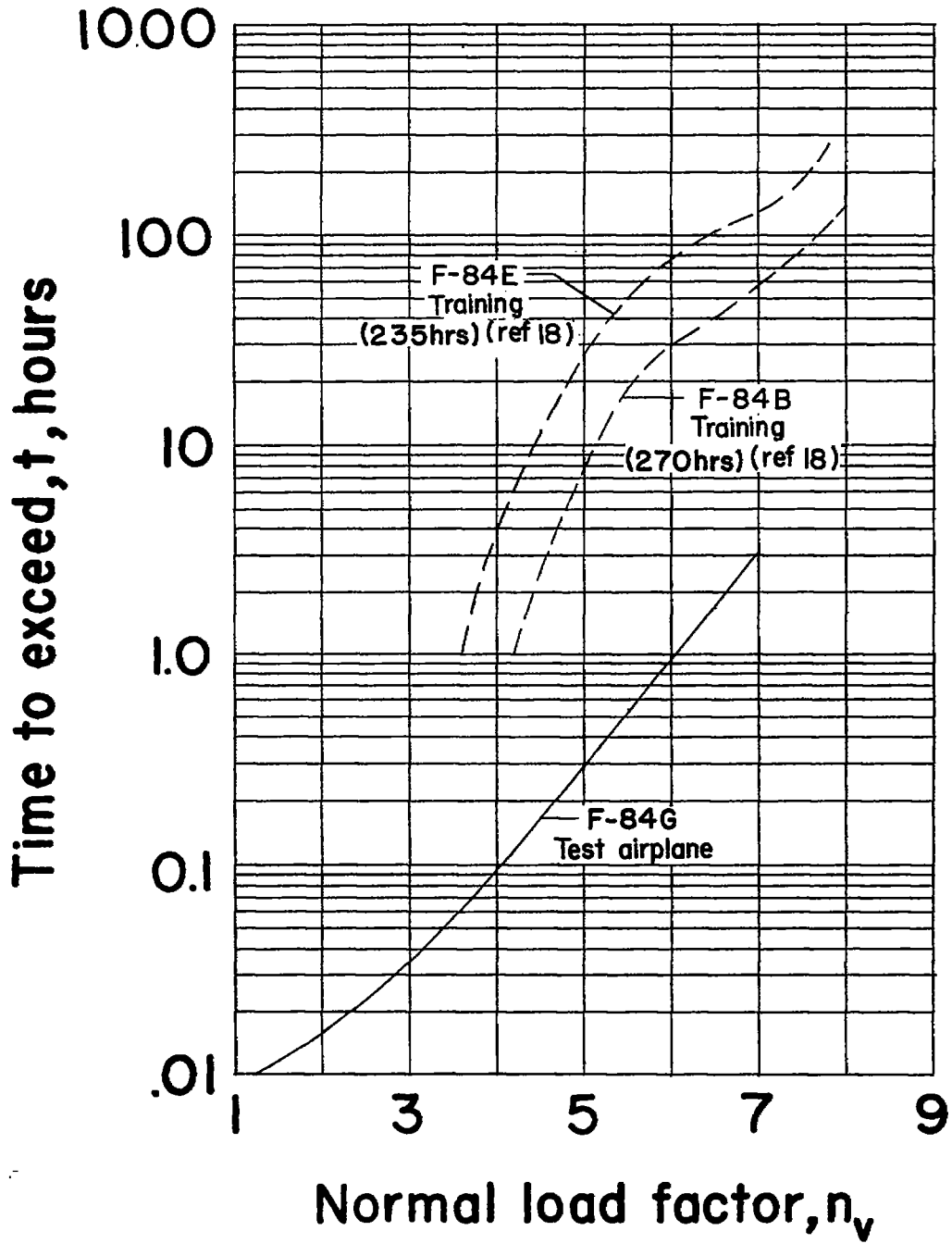

Figure 64.- Comparison of the average flight time required to equal or exceed a given normal load factor obtained for the F-84G test airplane with that obtained for F-84B and F-84E airplanes during training operations.

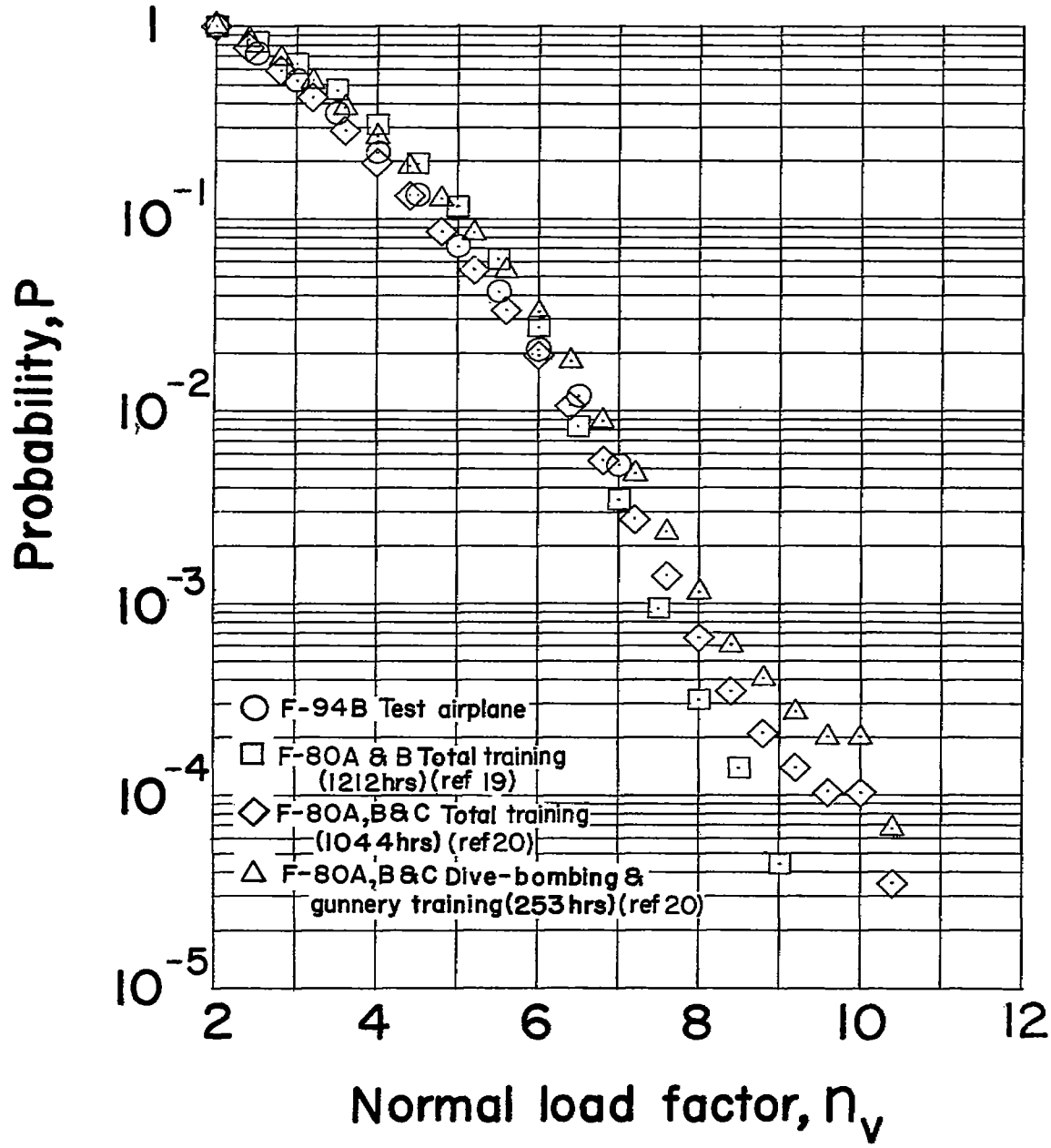

Figure 65.- Comparison of the probability of equaling or exceeding a given normal load factor obtained for the F-94B test airplane with that obtained for F-80 airplanes during training operations.

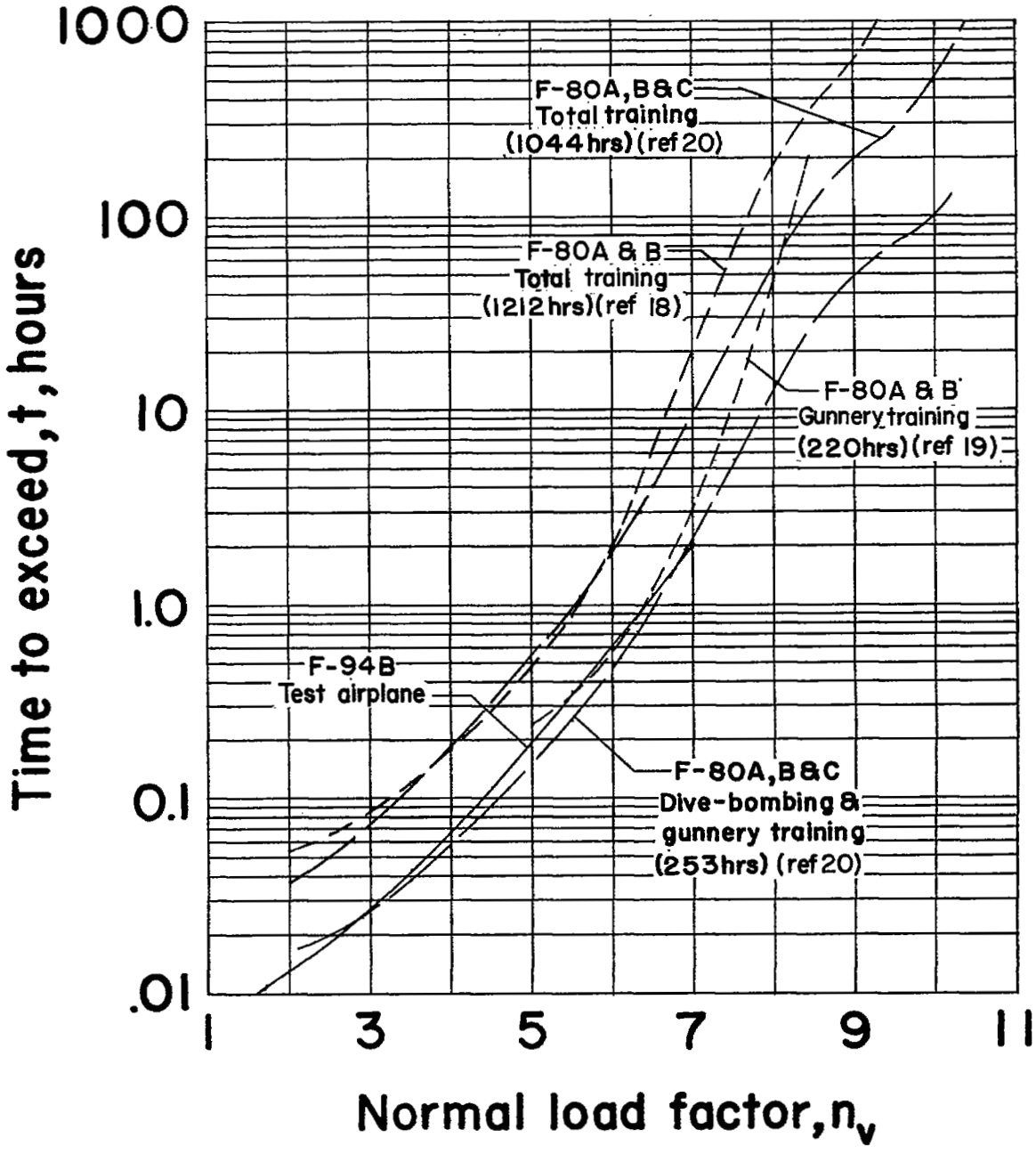

Figure 66.- Comparison of the average flight time required to equal or exceed a given normal load factor obtained for the F-94B test airplane with that obtained for F-80 airplanes during training operations.

[redacted]

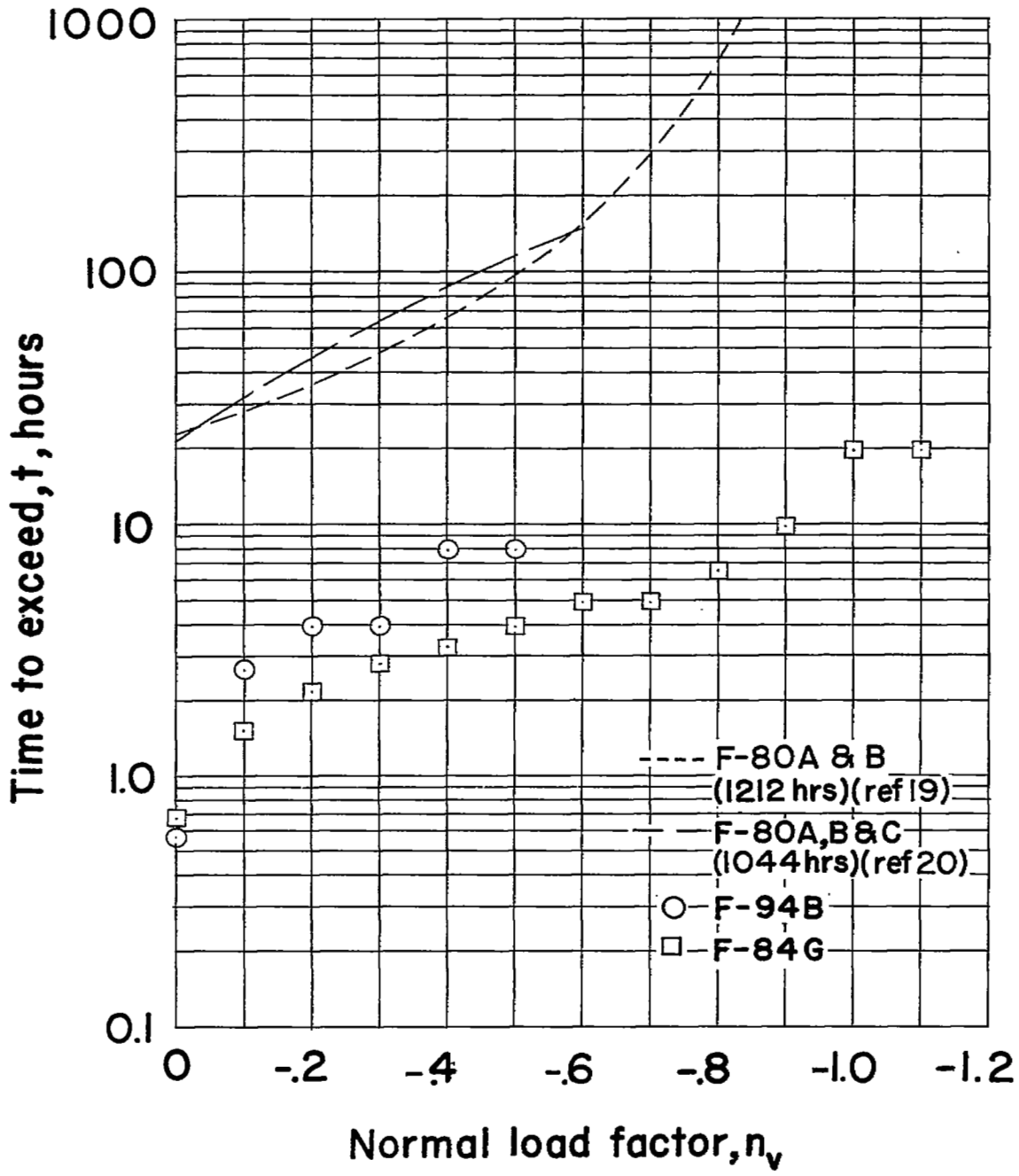

Figure 67.- Comparison of the average flight time required to equal or exceed a given negative normal load factor obtained for the F-94B and the F-84G test airplanes with that obtained for F-80A and F-80B airplanes during training operations.

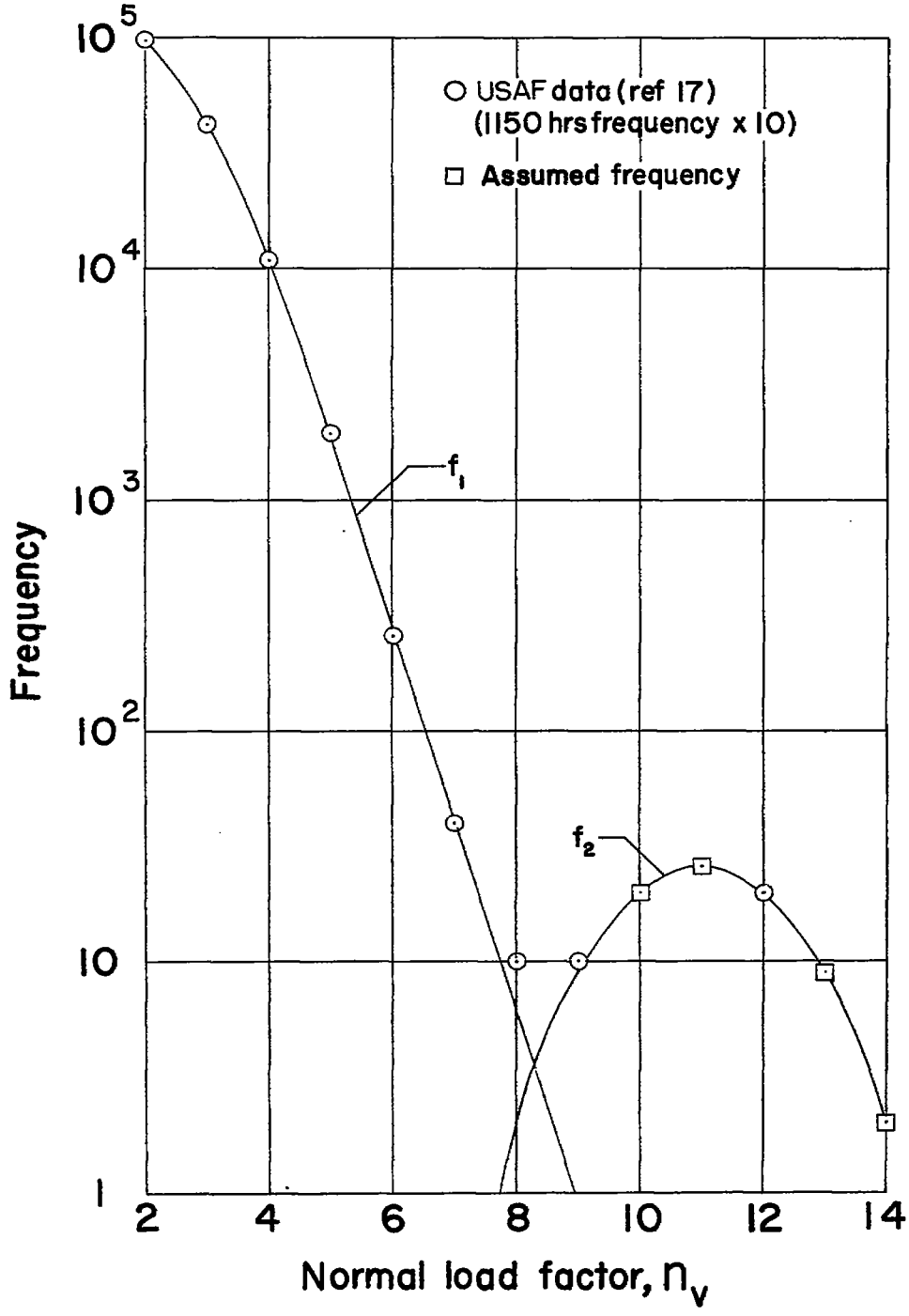

Figure 68.- Assumed frequency distributions of normal load factor for hypothetical case illustrating reversal of probability curve at high normal load factors.

[redacted]

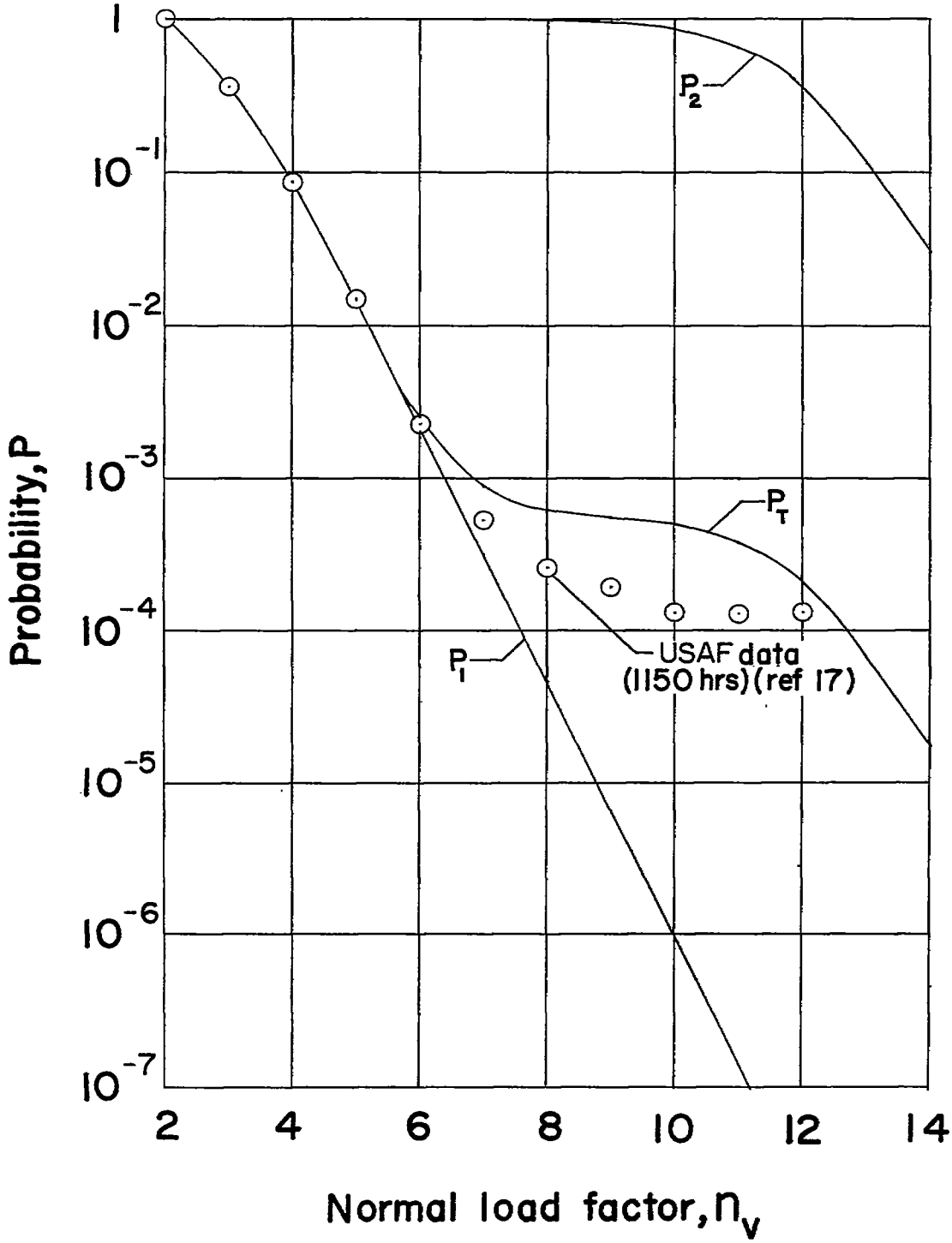

Figure 69.- Probability curves for hypothetical case illustrating reversal of probability curve at high normal load factors.

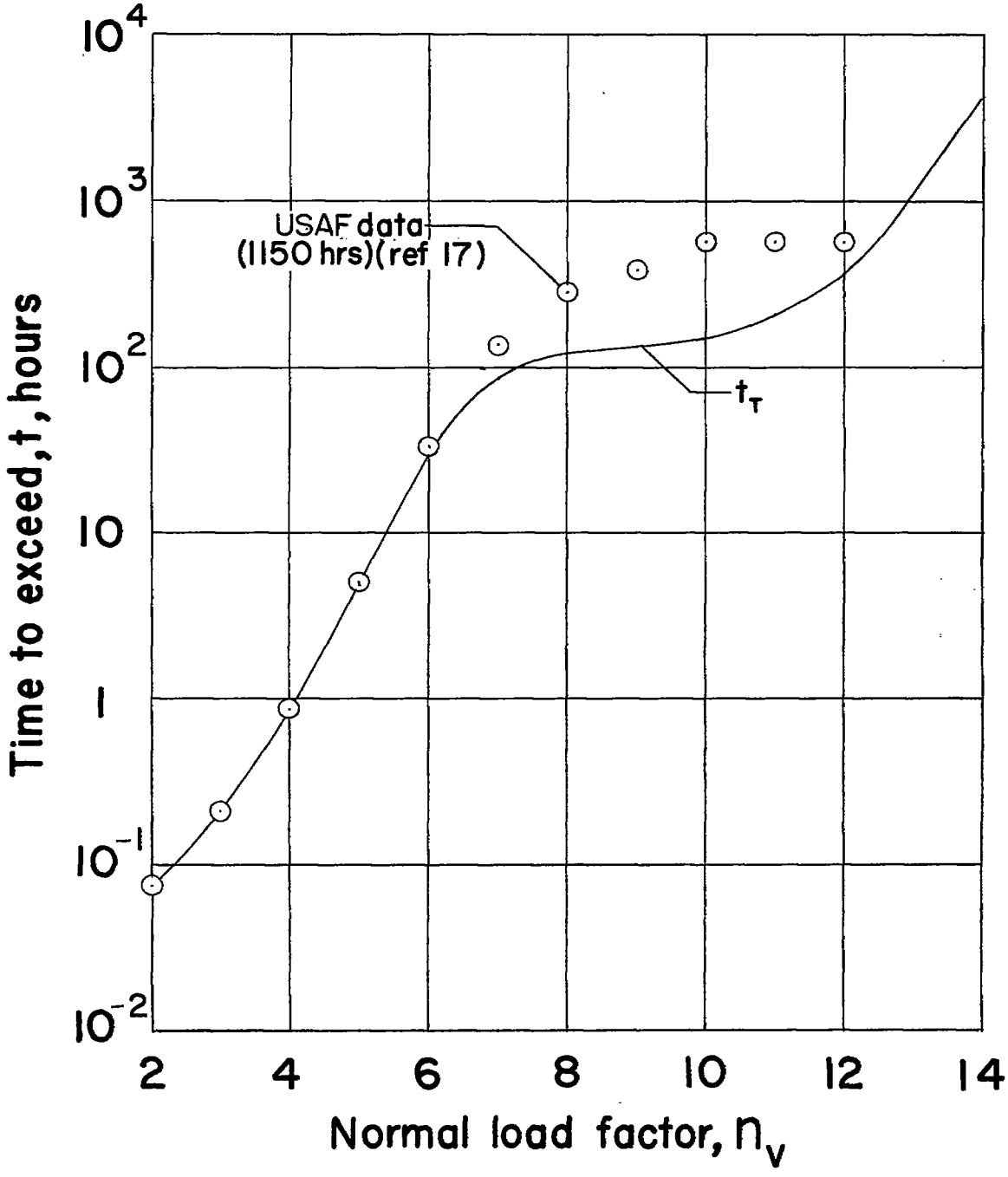

Figure 70.- Time to exceed curve for hypothetical case illustrating reversal of probability curve at high normal load factors.

[redacted]

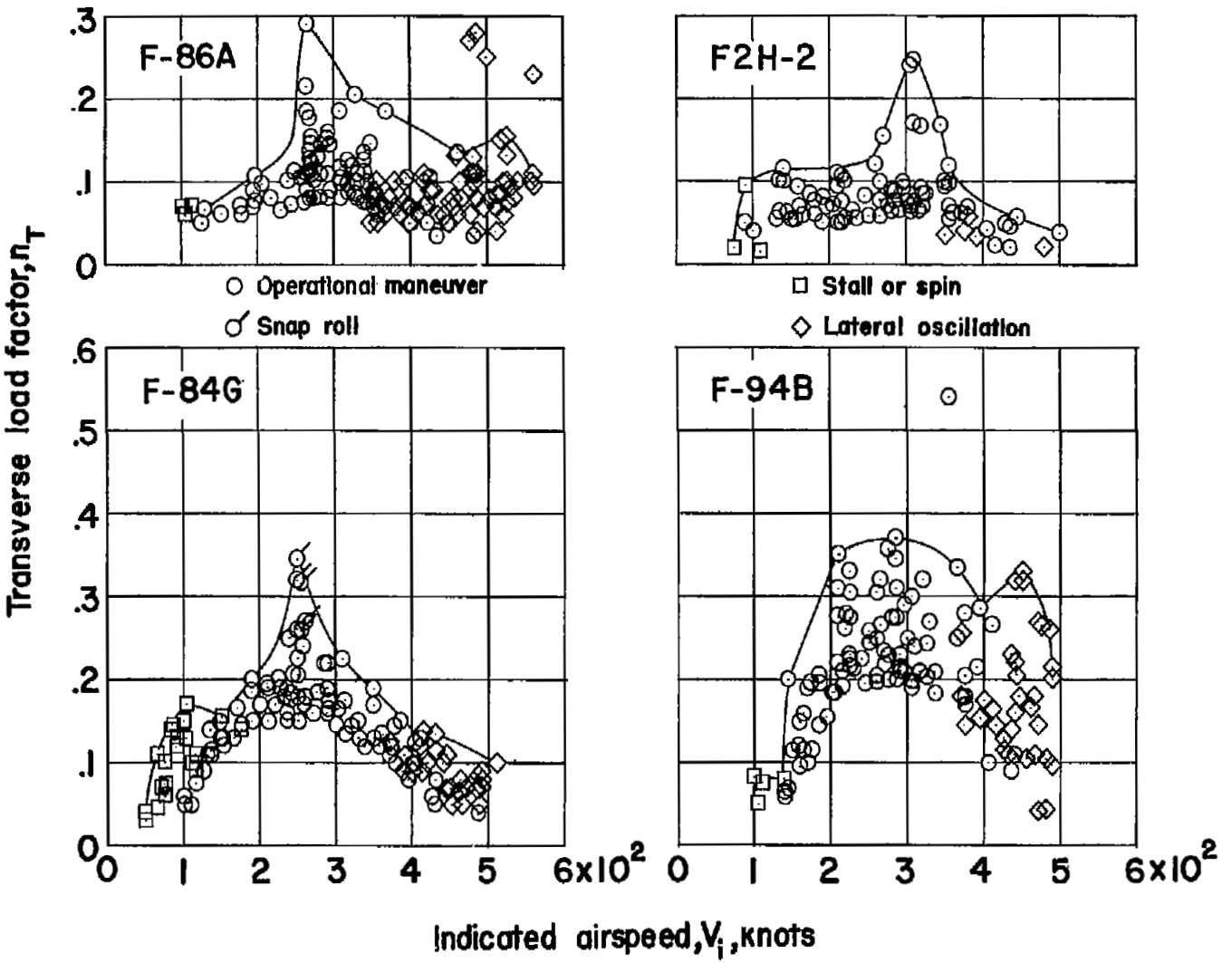

Figure 71.- Maximum corrected transverse load factors plotted against indicated airspeed.

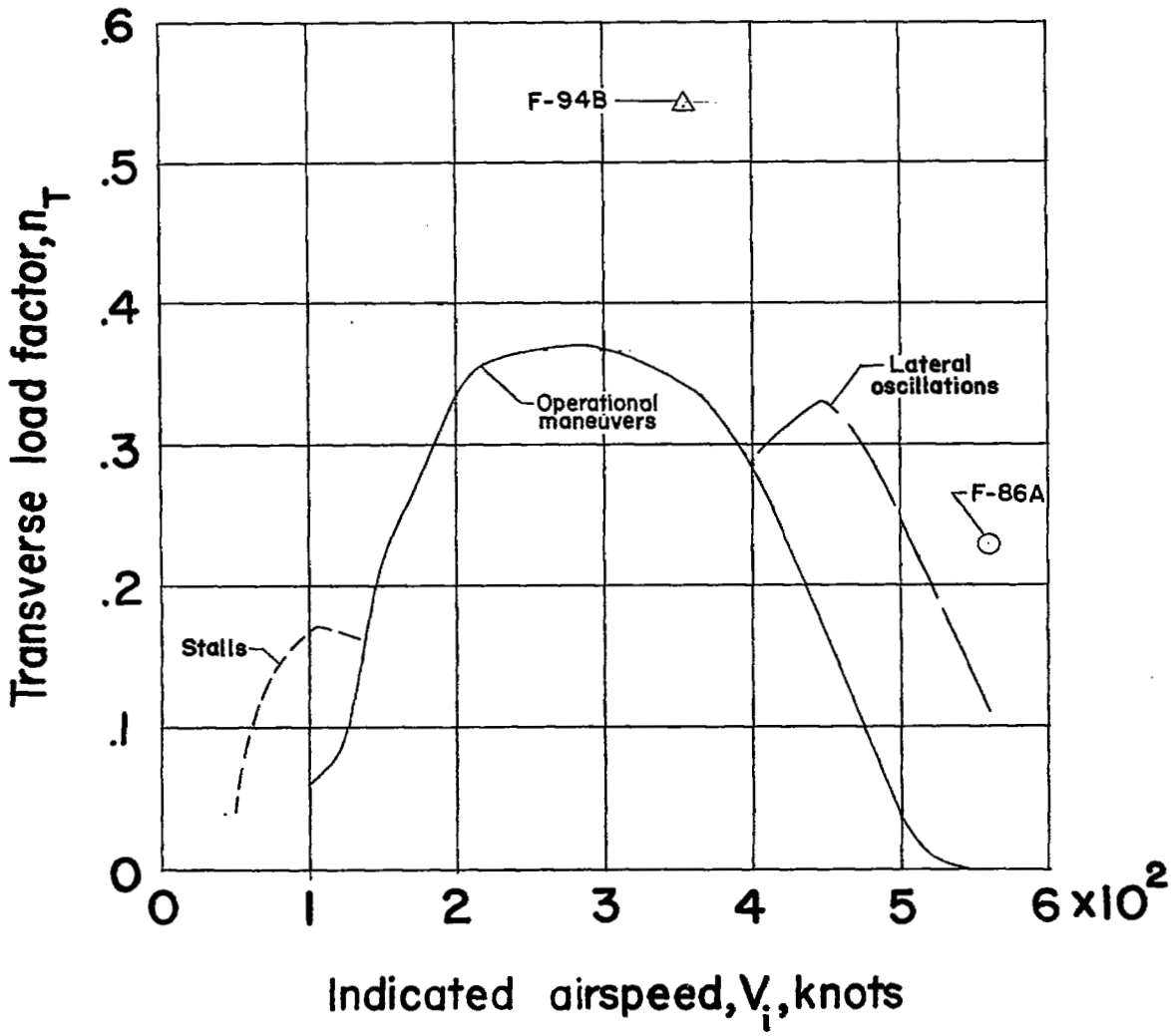

Figure 72.- Envelope of maximum corrected transverse load factor and indicated airspeed.

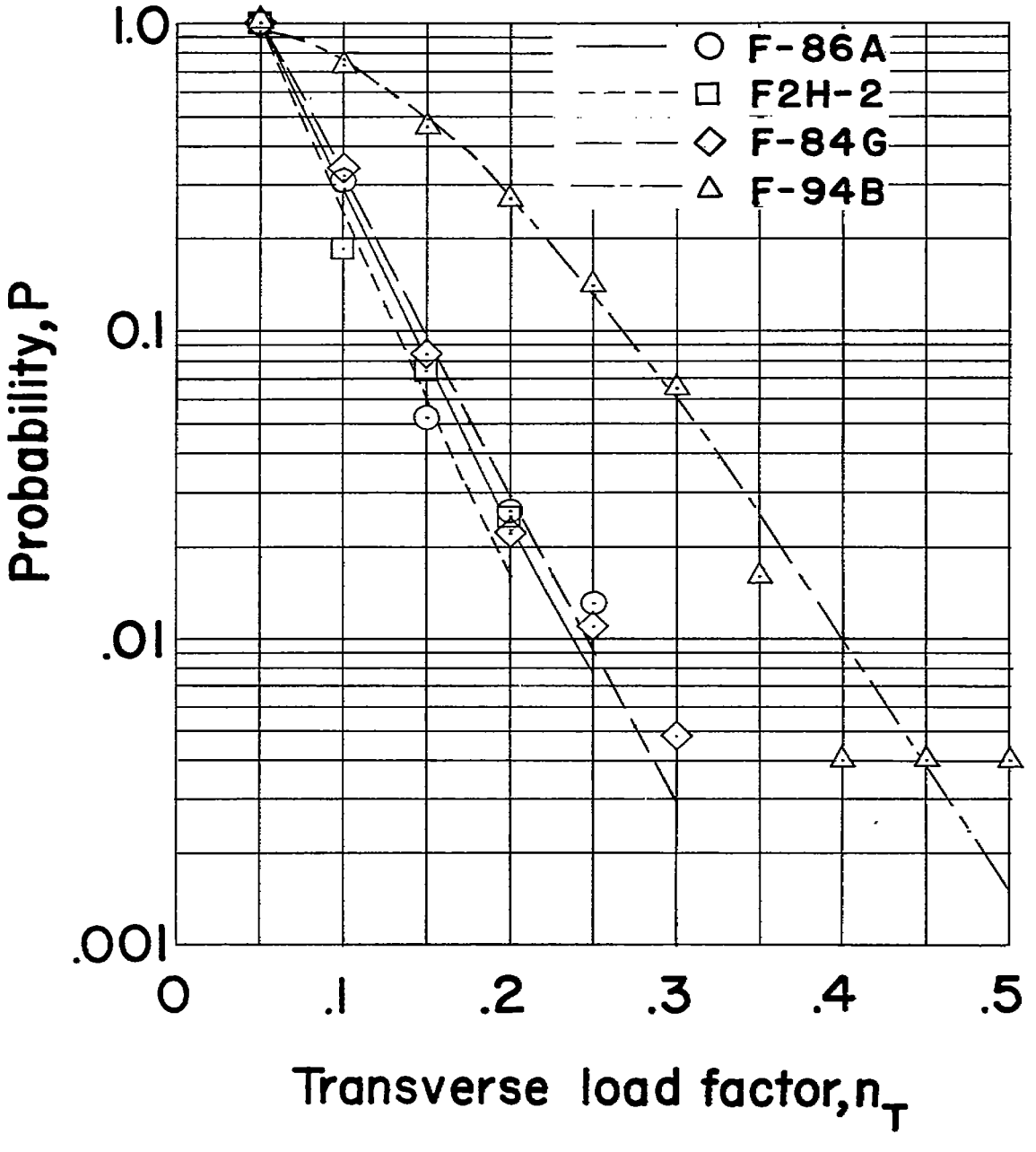

Figure 73.- Probability of equaling or exceeding a given transverse load factor.

[redacted]

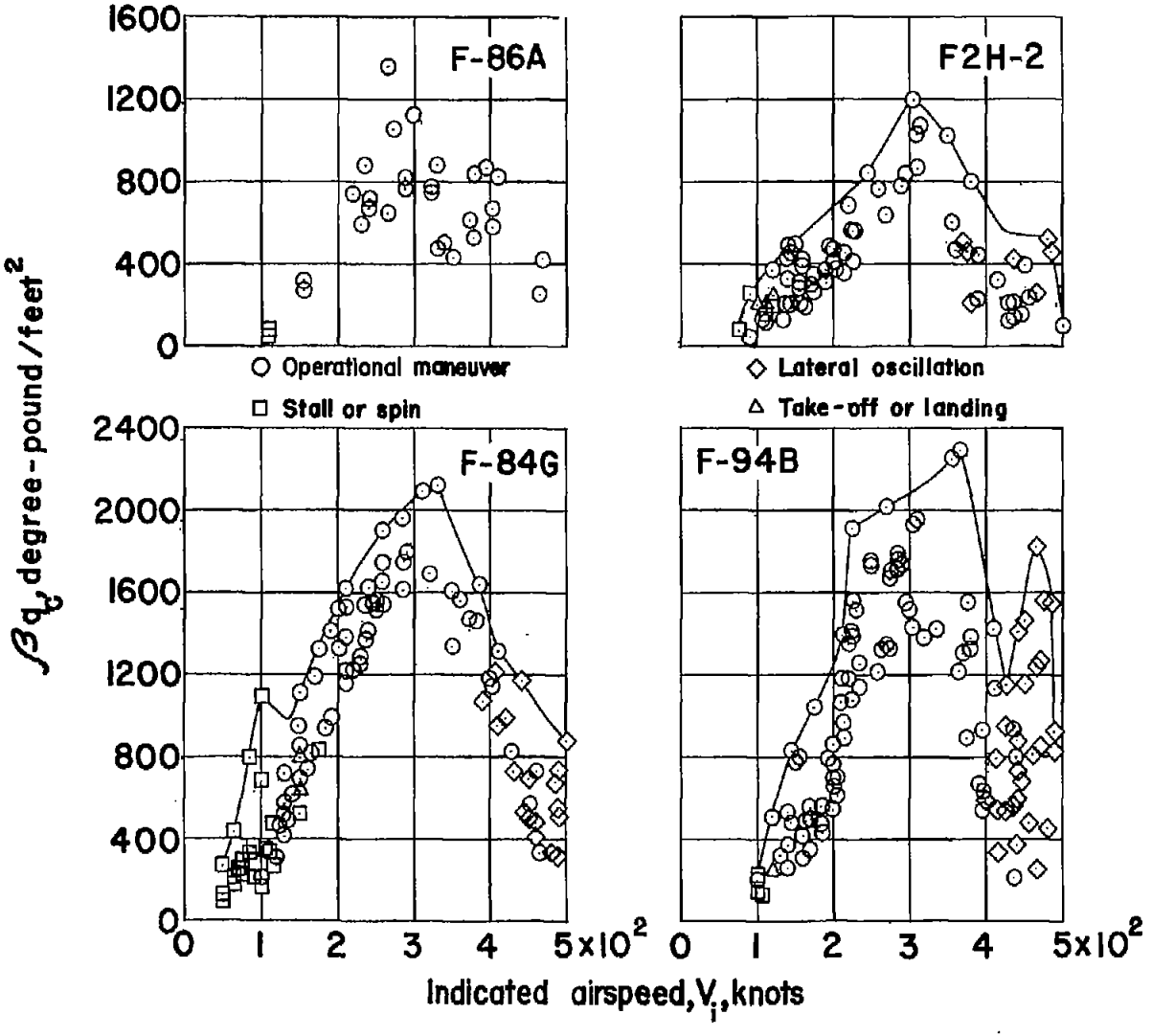

Figure 74.- Maximum values of vertical-tail load parameter βq_c plotted against indicated airspeed.

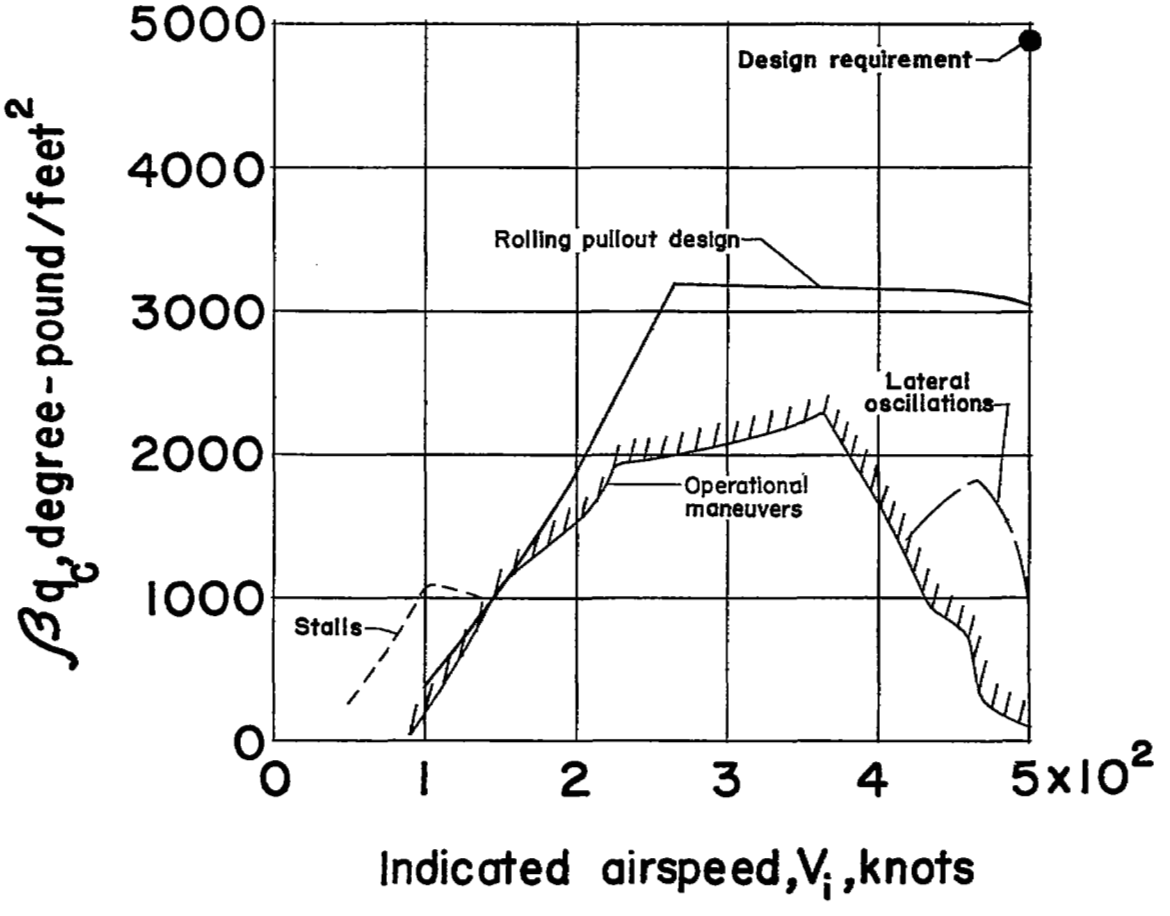

Figure 75.- Comparison of test results with two design requirements for vertical-tail load parameter βq_c.

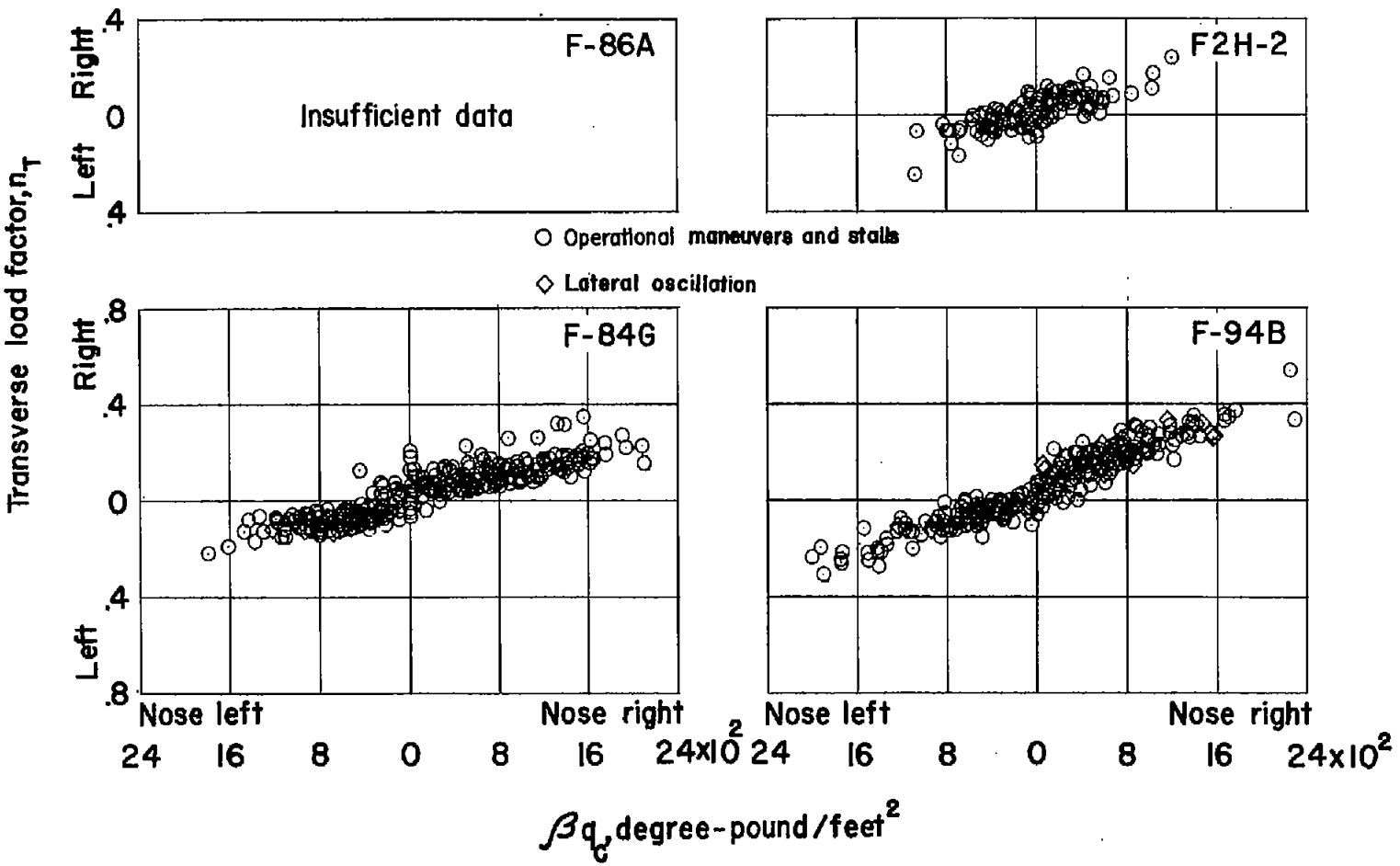

Figure 76.- Maximum corrected transverse load factors plotted against vertical-tail load parameter βq_c.

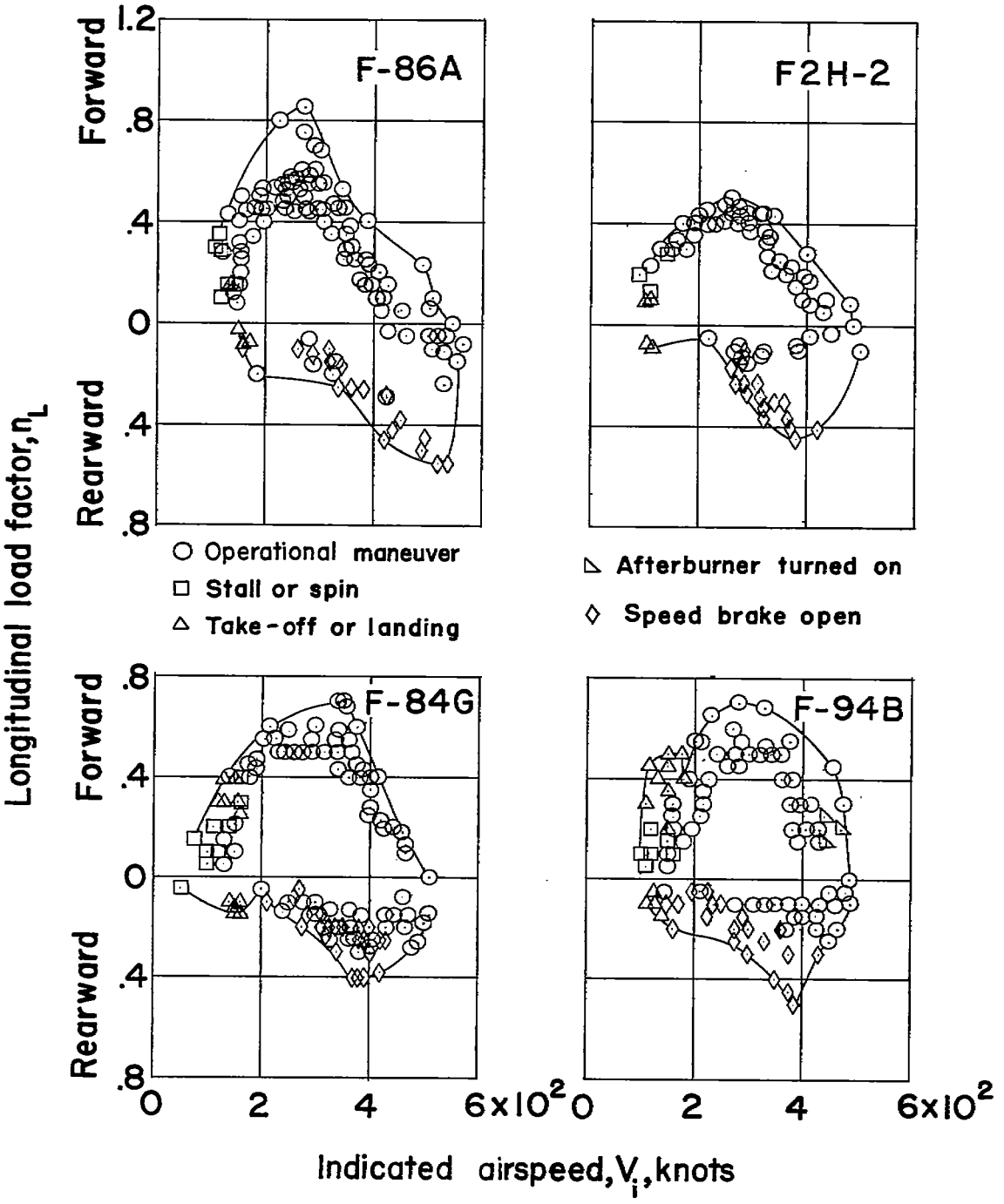

Figure 77.- Maximum longitudinal load factors plotted against indicated airspeed.

[redacted]

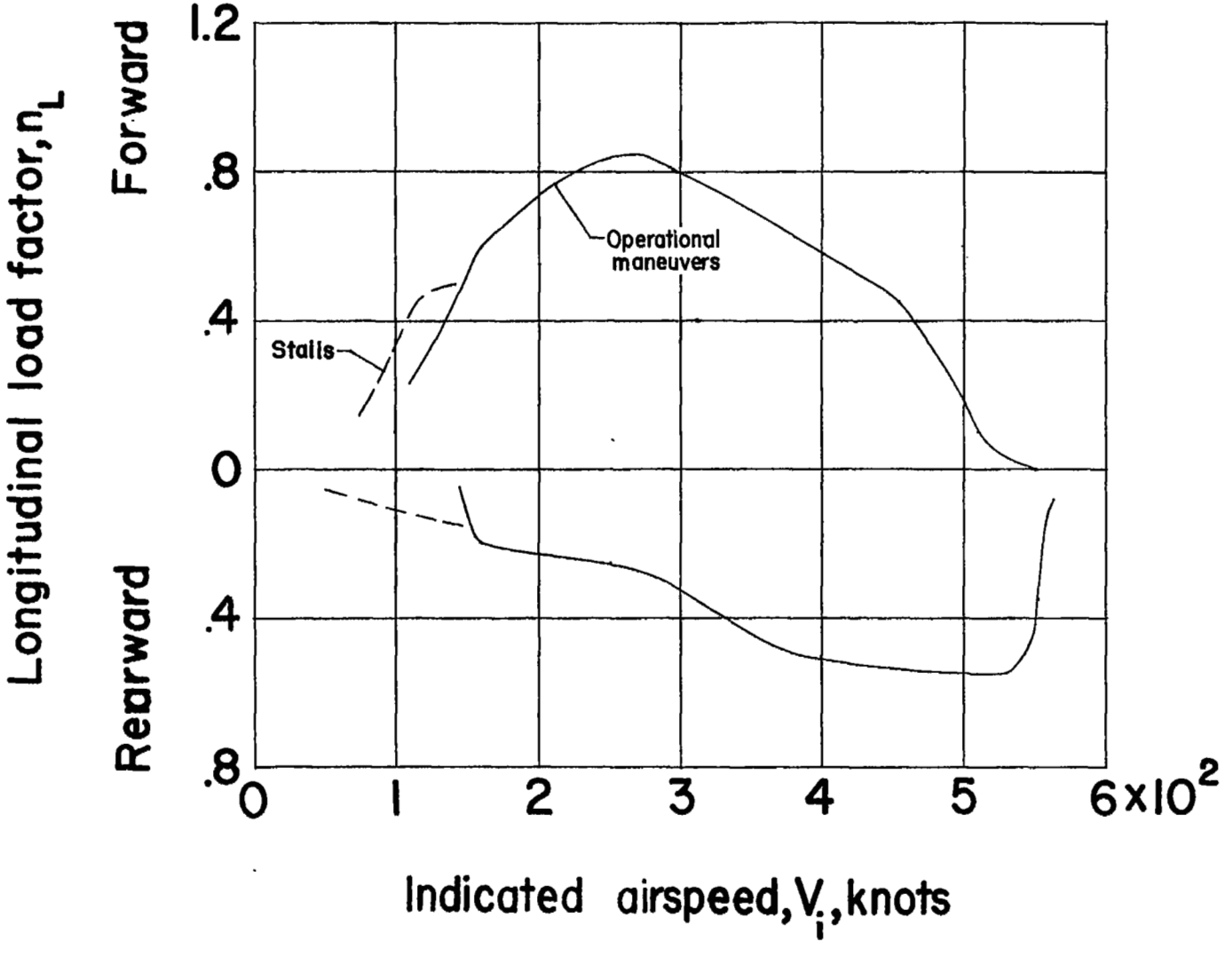

Figure 78.- Envelope of maximum longitudinal load factor and indicated airspeed.

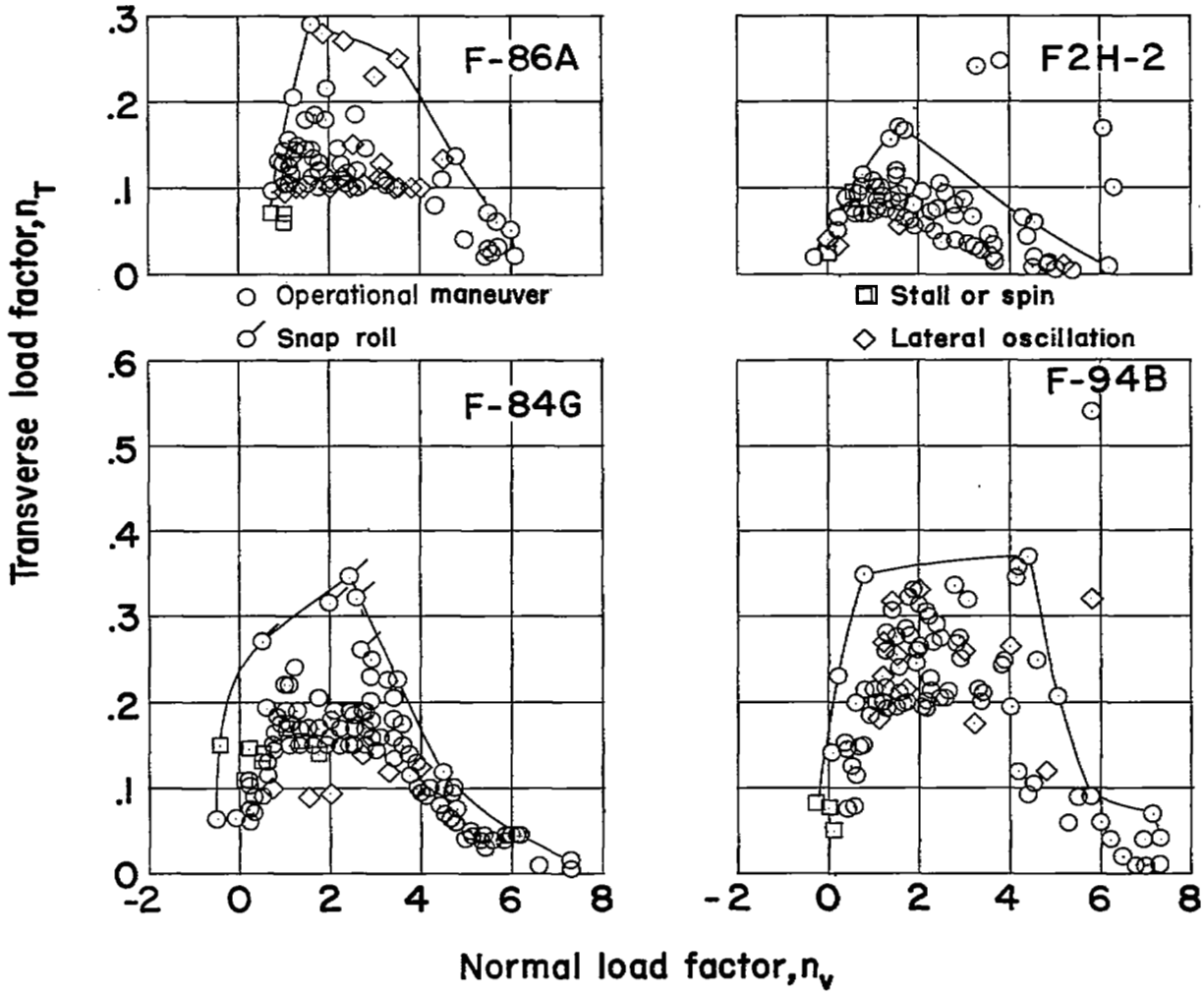

Figure 79.- Maximum corrected transverse load factors plotted against normal load factor.

[redacted]

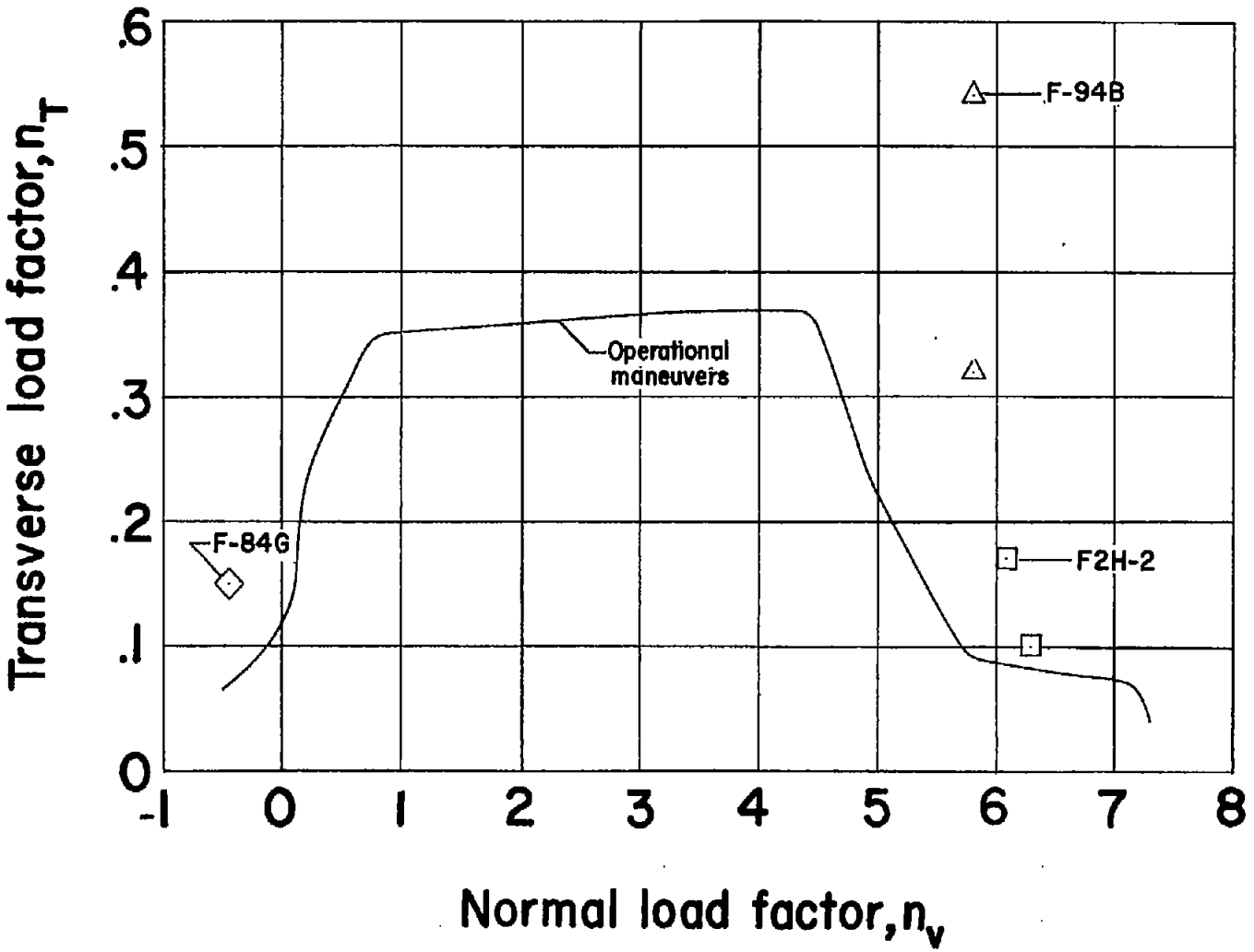

Figure 80.- Envelope of maximum corrected transverse load factor and normal load factor.

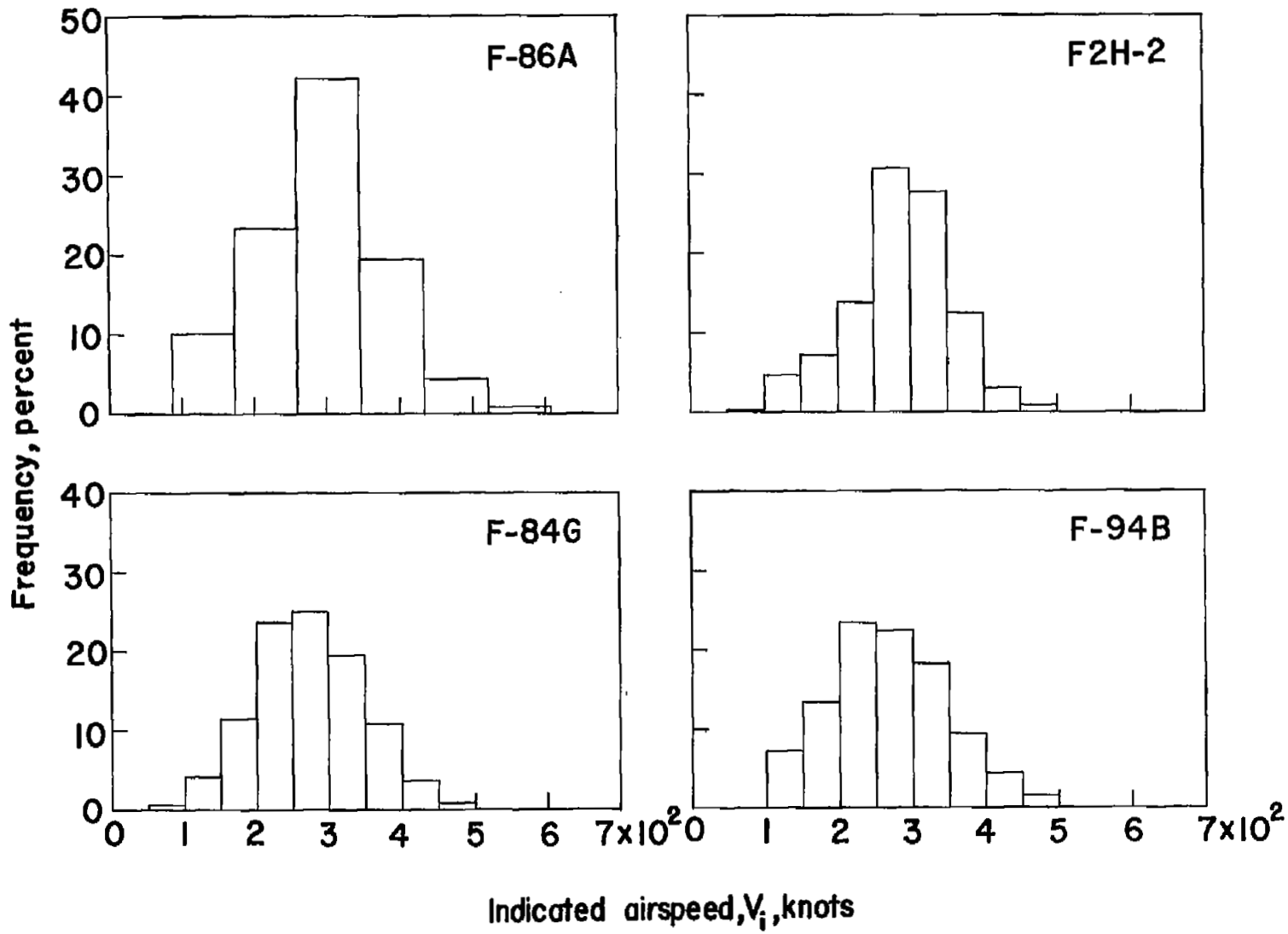

Figure 81.- Frequency distribution of indicated airspeeds.

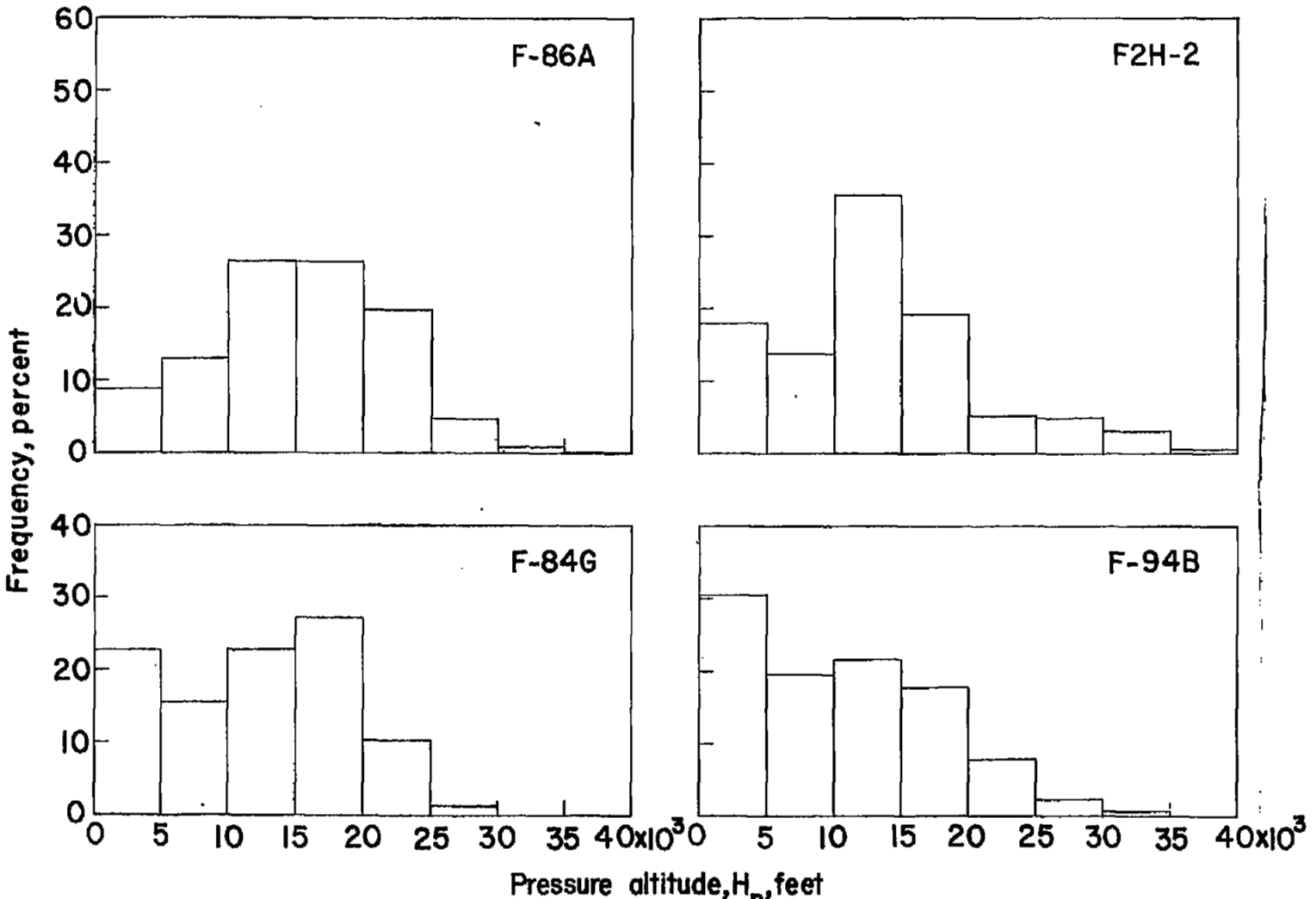

Figure 82.- Frequency distribution of pressure altitudes.

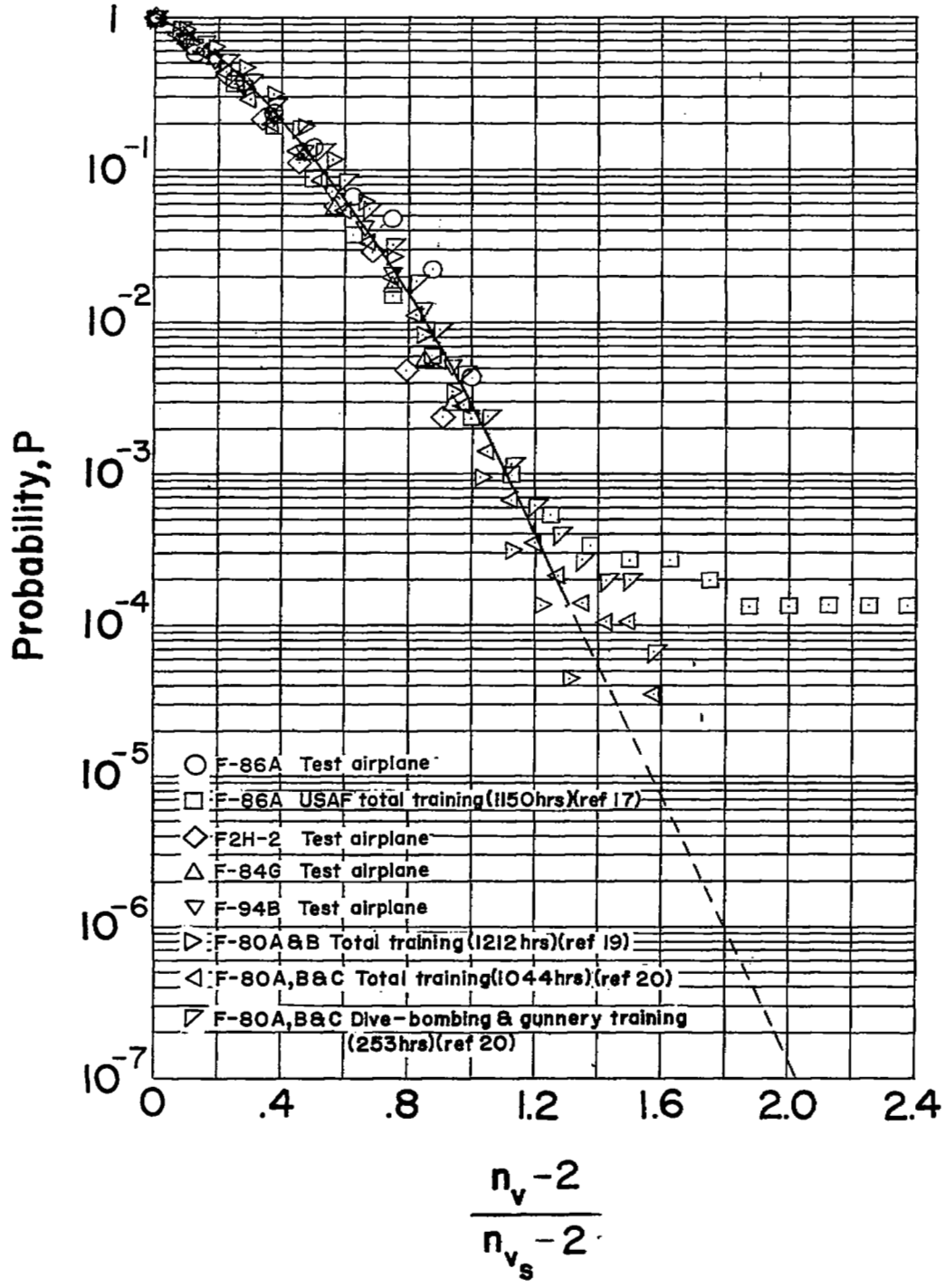

Figure 83.- Probability of equaling or exceeding a given fraction of the service limit normal load factor for load factors greater than 2.

[redacted]

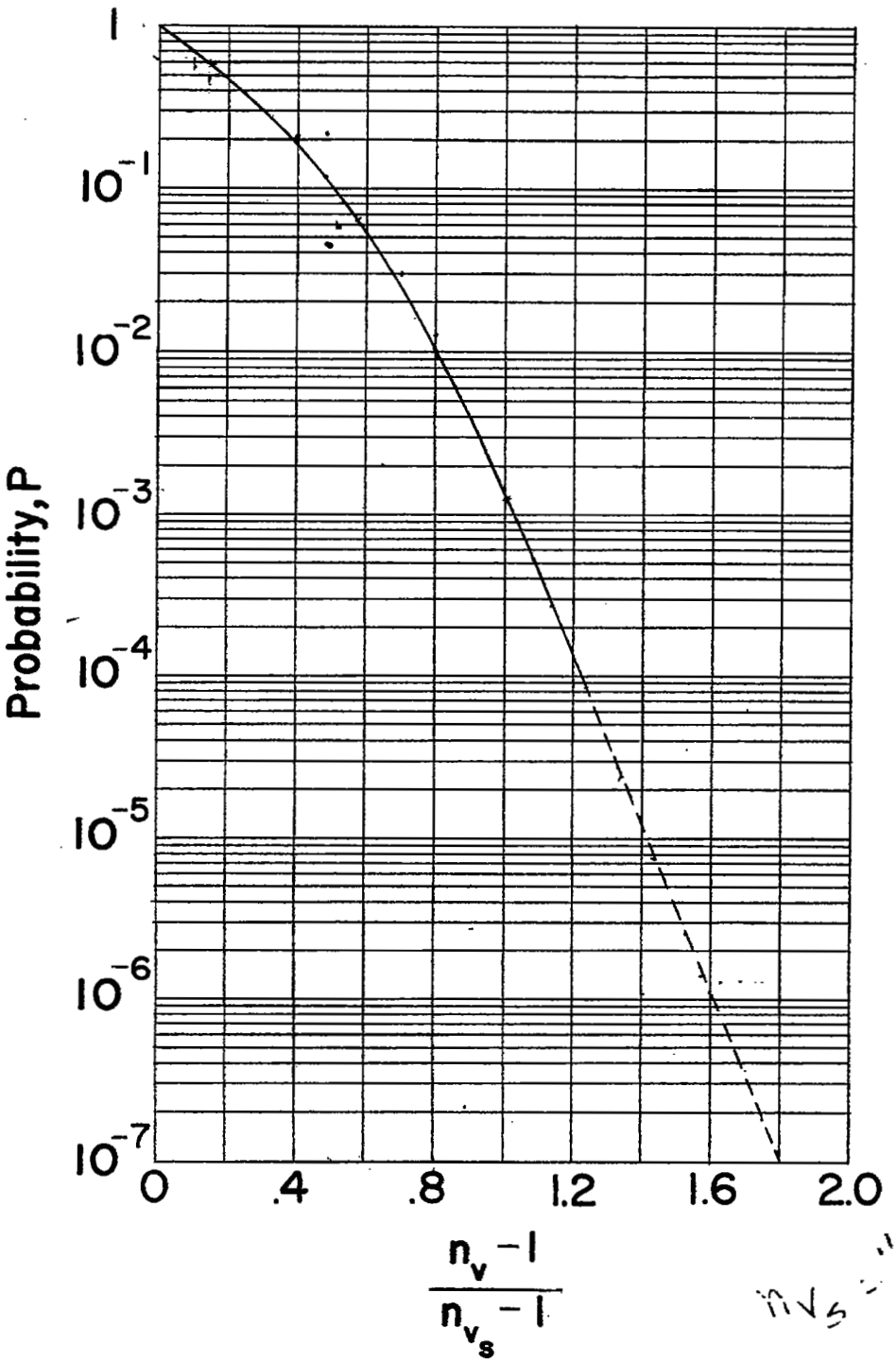

Figure 84.- Probability of equaling or exceeding a given fraction of the service limit normal load factor for load factors greater than 1.

[redacted]

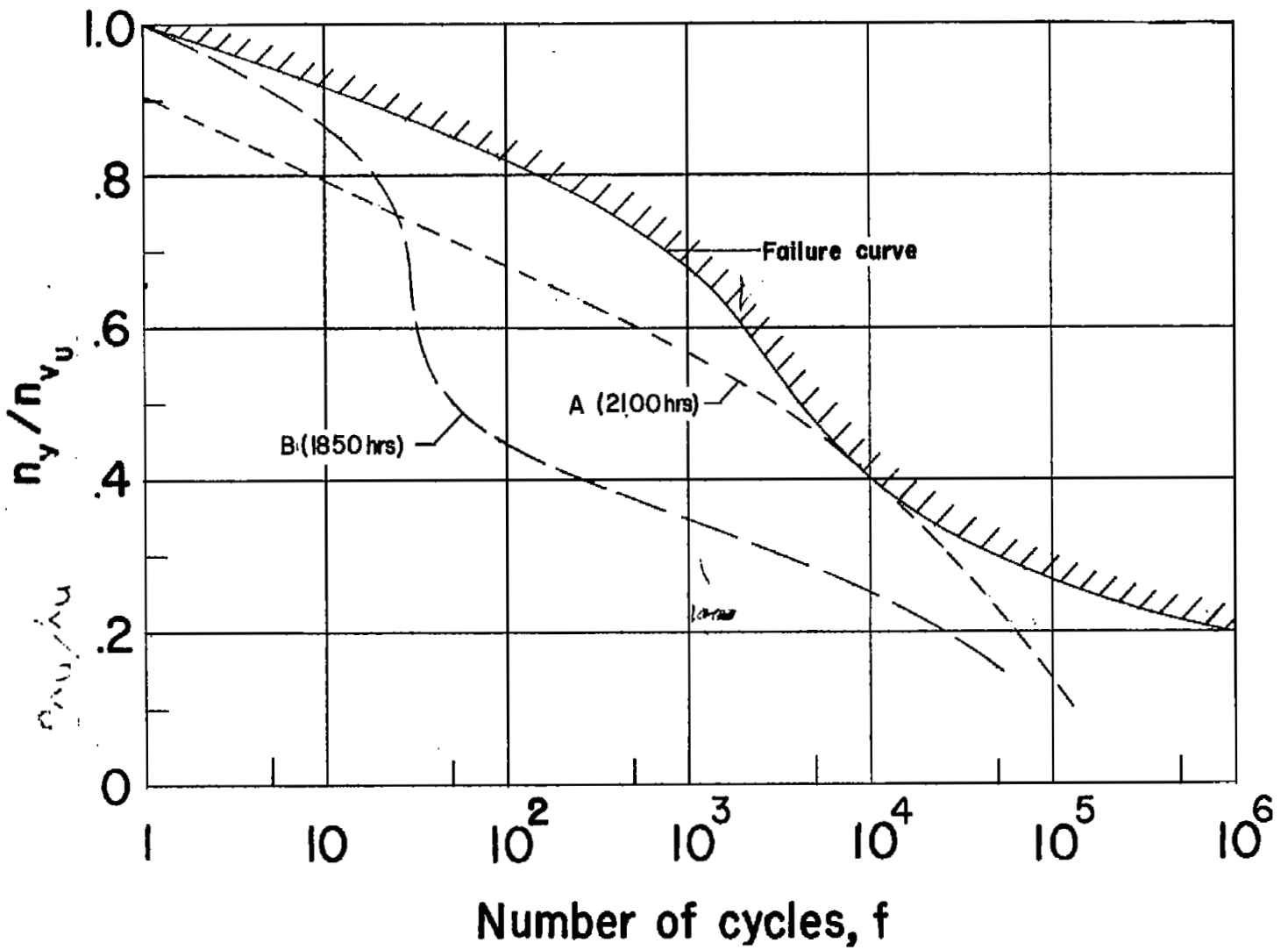

Figure 85.- Illustration of fatigue failures using two types of load-factor cumulative-frequency distributions.

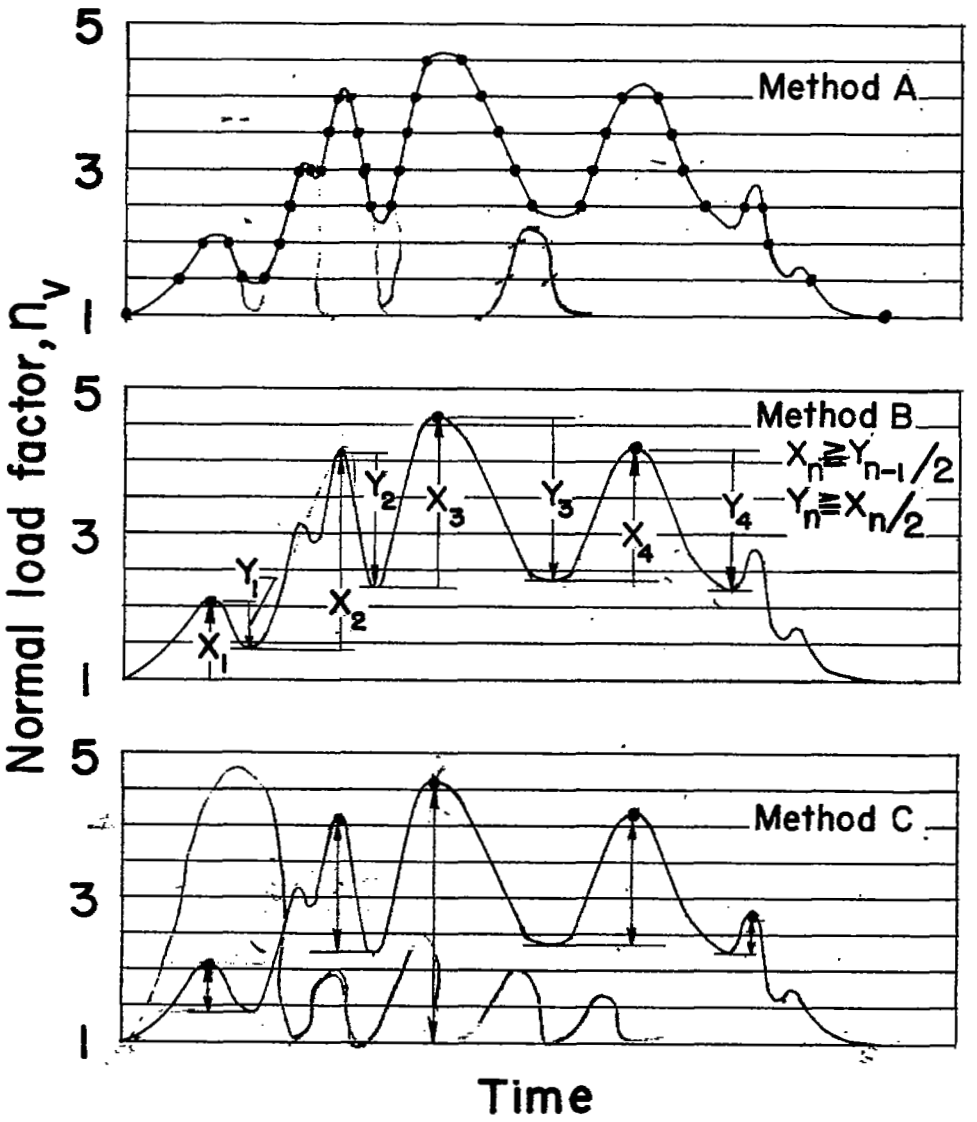

Normal load factor	1.0	1.5	2.0	2.5	3.0	3.5	4.0	4.5	5.0
Method A	2	4	4	8	8	6	6	2	---
Method B	---	---	1	---	---	---	2	1	---

Incremental normal load factor	0.5	1.0	1.5	2.0	2.5	3.0	3.5	4.0	4.5
Method C	2	---	2	---	---	---	1	---	---

Figure 86.- Diagram showing the three methods used for counting frequency distribution of normal load factors.

[redacted]

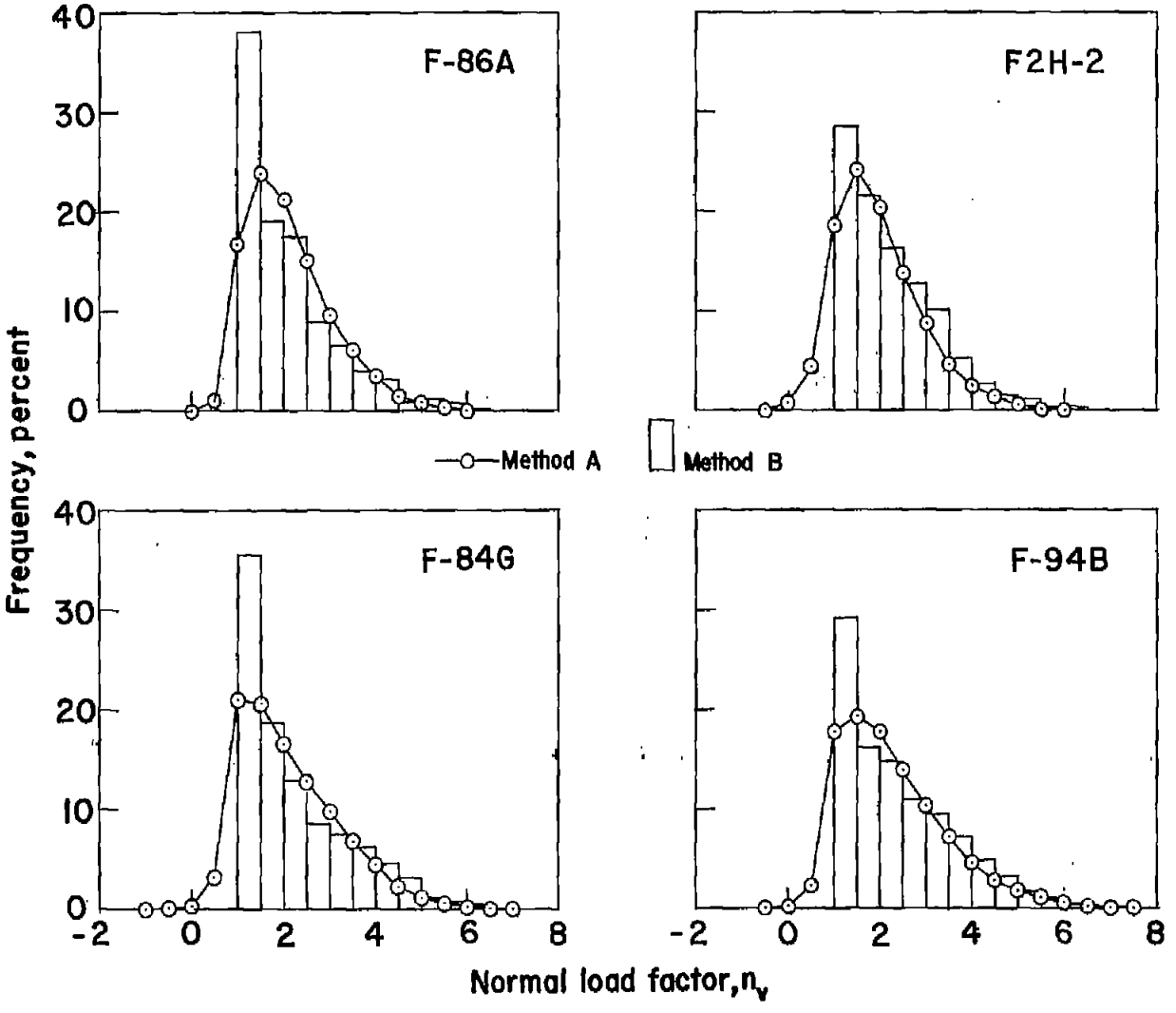

Figure 87.- Comparison of the normal-load-factor frequency distributions obtained by methods A and B.

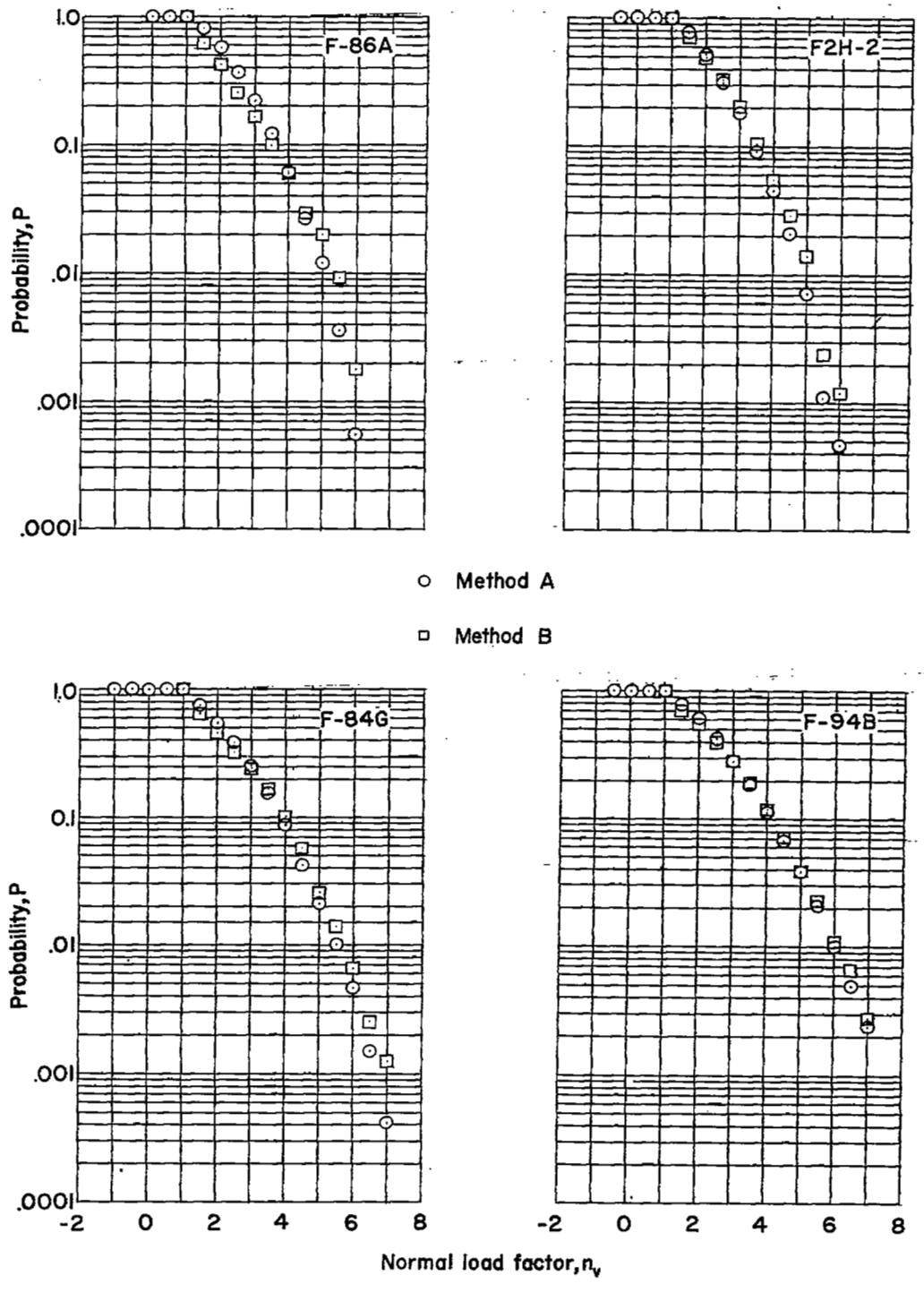

Figure 88.- Comparison of the probabilities of equaling or exceeding a given normal load factor obtained by methods A and B.

[redacted]

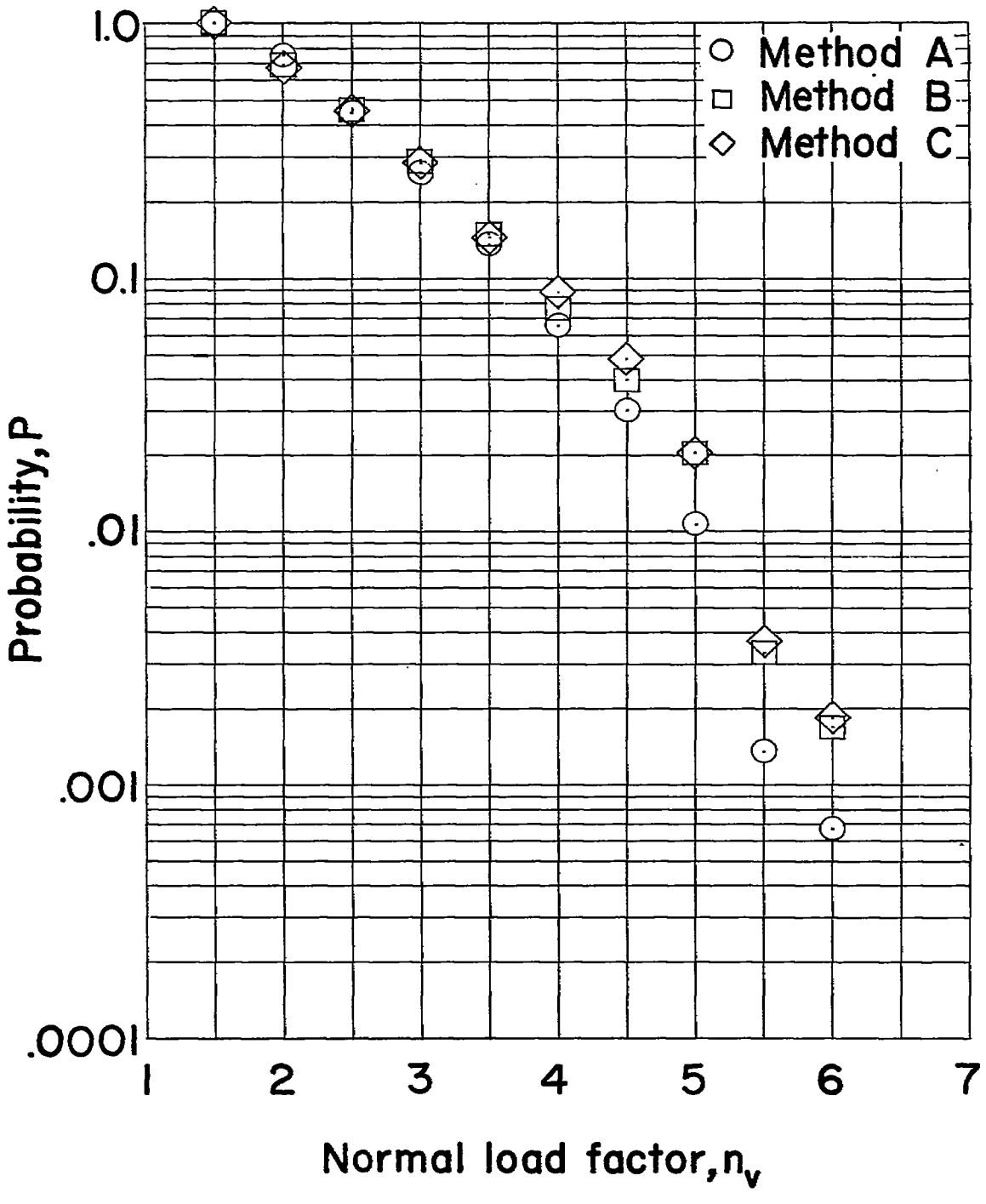

Figure 89.- Comparison of the probabilities of equaling or exceeding a given normal load factor for the F2H-2 airplane obtained by methods A, B, and C.